Karlsruhe Institute of Technology

Fakultät für Physik
Institut für Theoretische Festkörperphysik

Qubit Dekoheränz durch Quasiteilchen Tunneln

Diplomarbeit

von

Sebastian Zanker

11.10.2013

Referent:	Prof. Dr. Gerd Schön
Korreferent:	Prof. Dr. Alexander Shnirman

Hiermit erkläre ich, dass ich die vorliegende Diplomarbeit selbständig verfasst und gelieferte Datensätze und graphische Darstellungen selbständig erstellt habe. Ich habe keine anderen Quellen als die angegebenen benutzt und habe die Stellen der Arbeit, die anderen Werken entnommen sind in jedem einzelnen Fall unter Angabe der Quelle als Entlehnung kenntlich gemacht.

Sebastian Zanker,
Karlsruhe, den 11.10.2013

Deutsche Zusammenfassung

Klassische Computer basieren auf dem Bit, einer logischen Einheit, die entweder den Wert Null oder Eins repräsentiert. In modernen Systemen werden Bits durch sogenannte MOSFETs (Metal Oxide Fieldeffect Transistor) realisiert, wobei jeder Transistor entweder leitend (Eins) oder nichtleitend (Null) ist. Während der letzten Jahrzehnte konnte die Leistung von Computern durch eine immer noch andauernde Miniaturisierung ihrer Architektur stetig verbessert werden. Dennoch stoßen selbst moderne Computer rasch an ihre Grenzen, wenn sie komplexe mathematische Probleme lösen oder gar größere Quantensysteme simulieren sollen. Dies liegt daran, dass der Hilbertraum in dem ein quantenmechanisches System "lebt" mit der Anzahl der zu simulierenden Teilchen exponentiell größer wird. Betrachten wir beispielsweise ein System bestehend aus N miteinander wechselwirkenden Zweizustandssystemen. Um ein solches System vollständig darzustellen, muss ein klassischer Computer 2^N komplexe Koeffizienten speichern, einen für jeden Basiszustand des gekoppelten Systems. Dadurch "explodiert" die Anzahl der benötigten Bits mit steigender Anzahl der zu simulierenden Teilchen förmlich. Dies brachte Richard Feynman 1982 auf die Idee, diese besondere Eigenschaft eines quantenmechanischen Systems auszunutzen. Durch die Projektion von mathematischen Problemen oder Quantensystemen auf den Hilbertraum eines Systems aus gekoppelten Zweizustandssystemen könnte ein gewaltiger Leistungssprung erreicht werden. In Analogie zum klassischen Fall werden die Zweizustandssysteme, die die Grundbausteine eines möglichen Quantencomputers sind, Quantenbits (Qubits) genant. Im Gegensatz zu seinem klassischen Pendant kann ein System aus N Qubits in einer beliebigen Superposition seiner Basiszustände sein. Dies ermöglicht Berechnungen, die auf einem klassischen System so nicht möglich sind. Allerdings benötigt man speziell auf den Quantencomputer zugeschnittene Algorithmen, die die besonderen Eigenschaften der Qubits ausnutzen, um tatsächlich von einem Register aus Quantenbits zu profitieren. Ein Beispiel für einen solchen Algorithmus ist der Shor-Algorithmus, welcher in der Lage ist, große zusammengesetzte Zahlen zu faktorisieren. Der quantenmechanische Algorithmus benötigt dabei eine Berechnungszeit, die lediglich polynomisch mit der Anzahl der Stellen ansteigt, während ein klassischer Algorithmus für die selbe Aufgabe mit einer exponentiell ansteigenden Berechnungsdauer zu kämpfen hat. Um für einen Quantencomputer verwendbar zu sein, muss ein Zweizustandssystem verschiedene Voraussetzungen erfüllen, die unter dem Namen "DiVincenzo Kriterien" bekannt sind. Zu diesen gehören unter anderem das Vorhandensein universeller Gates zur Kontrolle des Qubits, die Möglichkeit, den Zusatnd des Qubits auszuleseen oder auch Koheränzzeiten, die die Dauer mehrerer (tausend) Gateanwendungen übersteigt. Eine mögliche Realisierung von Quantenbits sind natürlich Spin-1/2 Systeme wie Elektronenspins in Atomen oder Molekülen. Tatsächlich wurden bereits organische Moleküle verwendet, um die Zahl 15 mit Hilfe eines Kernspinverfahrens in die Faktoren drei und fünf zu teilen. Atome und Moleküle besitzen zwar einen guten Schutz gegen ungewollte Einflüsse

der Umgebung, allerdings führt diese natürliche Abschirmung gleichzeitig dazu, dass das Steuern und Auslesen des Qubits sehr schwierig wird. Dieses Problem besteht in vielen Systemen: Entweder das Qubit ist gut geschützt gegen Dekoheränz oder es lässt sich einfach ansteuern.

Unter den vielen möglichen Kandidaten für ein Qubit spielen supraleitende Qubits eine vielversprechende Rolle. Sie basieren auf mikroelektronischen supraleitenden Schaltkreisen, welche ohne größere Schwierigkeiten mit modernen Litographieverfahren hergestellt werden können. Zusätlich können sie mittels elektrischer Schaltungen einfach miteinander gekoppelt werden und sind ebenso einfach anzusprechen. Andererseits führt jede Kopplung an externe elektronische Schaltungen unweigerlich zu Dekoheränz, welche bei supraleitenden Qubits besonders durch Ladungsrauschen und Rauschen des magnetischen Flusses verursacht wird. Zusätzlich zur Dekoheränz verursacht durch externe Störquellen existiert in supraleitenden Qubits noch ein weiterer, interner Störprozess: Die Kopplung der Qubit Freiheitsgrade an Freiheitsgrade der Quasiteilchen im Supraleiter.

Gemäß BCS Theorie lassen sich die besonderen Eigenschaften von supraleitenden Materialien auf gebundene Zustände zweier Elektronen, die sogenannten Cooper Paare, zurückführen. Diese zeigen auch ein kollektives Verhalten und sorgen damit dafür, dass sich supraleitendene Schaltkreise wie quantenmechanische Systeme ähnlich zu Atomen verhalten. Alle supraleitenden Qubits haben eines gemeinsam: sie basieren auf dem Josephson Effekt, dem koheränten Tunneln von Cooper Paaren durch eine dünne Barriere zwischen zwei supraleitenden Schichten. Im Gegensatz hierzu ist das Tunneln einzelner Quasiteilchen durch die Barriere kein koheränter Effekt und verursacht Dekoheränz. Glücklicherweise können Quasiteilchen im Supraleiter nur oberhalb einer Energielücke, dem Ordnungsparameter des Supraleiters, existieren, was einen gewissen Schutz des Qubits verspricht. Dennoch existieren neben thermisch angeregten Quasiteilchen im Gleichgewicht auch durch Prozesse wie Photoanregung oder Diffusion auftretende nicht Gleichgewichts Quasiteilchen in den supraleitenden Schichten. Das Tunneln einzelner Quasiteilchen durch eine Josephson Junction gibt daher eine universelle untere Grenze für Koheränzzeitden von supraleitenden Qubits vor. Daher ist Dekoheränz verursacht durch Einzelteilchentunneln auch Thema dieser Arbeit.

Generell kann man zwischen zwei verschiedenen Arten der Dekoheränz unterscheiden: Dephasierung und Relaxiation. Relaxiation beschreibt Prozesse, bei denen Energie zwischen dem Qubit und seiner Umgebung ausgetauscht wird, was letztendlich dazu führt, dass Qubit und Umgebung ins thermische Gleichgewicht kommen. Für das Qubit bedeutet dies für gewöhnlich eine Relaxiation in den Grundzustand. Dephasierung dagegen beschreibt Prozesse ohne Energietransfer. Lediglich die Phase zwischen den Basiszuständen des Qubits wird hierbei verändert, was aber dennoch zu einem Verlust von Information führt.

Relaxiation durch Quasiteilchentunneln lässt sich sehr gut mittels Fermis goldener Regel berechnen und ergibt einen exponentiellen Zerfall des Qubit Zustandes mit einer

Rate Γ_1. Die aus der goldenen Regel abgeleitete Relaxiationszeit $T_1 = \Gamma_1^{-1}$ wurde durch viele Experimente bestätigt und liefert sehr gute Ergebnisse. Anderst verhält es sich mit der Dephasierung. Hier führt eine Behandlung mit Fermis goldener Regel zu einer divergenten Dephasierungsrate, da die zu Grunde liegende Spektralfunktion der supraleitenden Reservoirs im niedrigen Frequenzbereich divergiert. Daher ist es ein Hauptanliegen vorliegenden Arbeit, einen nicht divergierenden Ausdruck führ die Dephasierungsrate zu finden.

In der Arbeit wird zunächst eine generelle Einführung zum Thema supraleitende Qubits und der zu Grunde liegenden Theorie gegeben, siehe Kapitel 1. Dabei gehen wir auch auf die Circuit Quantenelektrodynamik ein, welche einen systematischen Weg zur Bestimmung des Hamiltonoperators eines gegebenen Schaltkreises liefert. Im einleitenden Kapitel wird ebenfalls eine kurze Zusammenfassung der wichtigsten Schritte bei der Herleitung der BCS Theorie für Supraleiter gegeben. Anschließend diskutieren wir die mikroskopische Theorie, die dem Quasiteilchentunneln sowie dem Josephson Effekt zu Grunde liegt.

In Kapitel 2 entwickeln wir eine diagrammatische Technik, mit deren Hilfe sich sogenannte offene Quantensysteme behandeln lassen, d.h. Systeme, die an wesentlich größere Reservoirs gekoppelt sind, wobei man aber nur an der Dynamik des eigentlich Systems, in unserem Fall des Qubits, interessiert ist. Mit Hilfe dieser Technik ist es möglich, die Kopplung zwischen System und Reservoir in beliebigen Ordnungen einzubeziehen, um die Dynamik des Systems unter dem Einfluss der Kopplung an das Reservoir zu bestimmen.

Anschließend wird die zuvor entwickelte Technik in Kapitel 3 auf das eigentlich Problem angewandt: Ein Qubit, welches durch Quasiteilchentunneln an die Supraleiter gekoppelt ist. In diesem Kapitel werden zunächst Relaxiations- und Dephasierungsraten in der niedrigsten Ordnung im Tunnelhamiltonian berechnet. Da die Dephasierungsrate für bestimmte Qubitkonfigurationen divergiert, entwickeln wir anschließend eine Methode ähnlich zur selbskonsistenten Bornnäherung, mit deren Hilfe wir einen selbstkonsistenten Ausdruck für die Dephasierungsrate herleiten. Im letzten Abschnitt dieses Kapitels werden wir die Markovnäherung wegfallen lassen, welche wir bis zu diesem Punkt als gültig erachten. Die Markovnäherung geht von einem "erinnerungslosen Reservoir" aus, d.h., dass die Koheränzzeiten des Bades wesentlich kürzer sind als die Zeitskala, die von der entpsrechenden Zerfallsrate des Qubits vorgegeben wird. Eine Näherung die für Dephasierung nicht zwingend erfüllt ist. Mit einem alternativen Ansatz finden wir eine nicht markovsche Lösung des Problems mit einer Dephasierungsrate, welche keine Rate im eigentlichen Sinne ist. Statt eines Exponenten der linear in der Zeit ist, finden wir einen Zerfall mit einer komplizierteren Zeitabhängigkeit im Exponenten.

Im letzten Kapitel 4 wenden wir die zuvor berechneten generellen Raten auf ein Transmon an, einen speziellen Typ eines supraleitenden Qubits. Die berechneten Relaxiationsraten stimmen sehr gut mit den entsprechenden Experimenten überein. Mit

Hilfe verschiedener Quasiteilchen Verteilungsfunktionen berechnen wir die Temperaturabhängigkeit der Raten. Anschließend vergleichen wir die Dephasierungsraten miteinander, die sich aus den verschiedenen Methoden ergeben. Es zeigt sich, dass die verschiedenen Raten für ein Transmon dasselbe Ergebnis liefern: Eine Dephasierungszeit die wesentlich größer als die Relaxiationszeit ist.

Karlsruhe Institute of Technology

Fakultät für Physik
Institut für Theoretische Festkörperphysik

Qubit decoherence induced by quasiparticle tunneling

Diploma thesis

by

Sebastian Zanker

2013-10-11

Instructor: Prof. Dr. Gerd Schön
2nd Instructor: Prof. Dr. Alexander Shnirman

Introduction

The basic building block of a classical computer is a bit, a system that can be in either one of its two logical states zero or one. In modern computer architecture silicon based MOSFET transistors are the most common physical realization of bits. During the last decades classical computer performance has steadily increased due to a high degree of miniaturization of computer architecture. According to Moore's law the number of transistors per unit area doubles about every two years due to this miniaturization. However, even the fastest classical computer quickly reaches its limits solving complex mathematical problems or simulating large quantum systems. The reason for this is the exponentially growth of the Hilbert space of a quantum system with increasing particle number. For example, to represent the quantum state of a system containing N two-level systems a classical computer has to store 2^N complex coefficients, one for each base vector of the system. Hence the number of bits necessary to store and simulate a quantum system rapidly explodes to unreasonable high values.

In 1982 Richard Feynman suggested to use exactly this property of a quantum system to simulate quantum systems [1]. Mapping quantum systems or other mathematical problems onto the Hilbert space of coupled quantum mechanical two-state systems promises a huge increase in computational power. Similar to classical information processing these two-state systems form the basic building blocks of a quantum computer and are called quantum bits (qubits). Contrary to a classical N-bit system, the state of a system consisting of N qubits can be in an arbitrary superposition of its 2^N eigenstates. This feature allows for powerful computations not possible with conventional systems [2]. But only adapted algorithms that make use of these properties reap the benefits of a quantum computer. An example for such an algorithm is Shor's algorithm to factorize large integer numbers, a computation which requires exponential computation time in the number of digits on classical systems while the same result can be achieved in polynomial time with a quantum computer [3].

To be applicable as qubit a two-level system has to fulfill a set of requirements [4]. For example, we need a universal gate set, e.g. control over the qubit state, we must be able to read easily out and couple qubits. A qubit must also have coherence times longer than any timescale provided by gate operations. The simplest two level quantum systems fulfilling these requirements (at least partly) are natural spin-1/2 systems, for example nuclei or electron spins in atoms or molecules. Indeed, organic molecules have been used to factorize the number 15 into its prime factors three and five using a NMR implementation [5]. Although they exhibit good natural protection against noise and

environmental induced decoherence, atoms and other natural spin-1/2 systems suffer from their poor ability to be addressed from outside making control and read-out a difficult task. However this trade off has been observed in many systems. Either the qubits are well protected from decoherence or they can be easily controlled but seldom both.

Amongst several other alternative possible qubit realizations superconducting qubits play a promising role. They are based on superconducting microelectronic circuits which can be fabricated using state-of-the-art technology such as photo or electron lithography. Using transmission lines they can be easily coupled to each other as well as to read-out or control circuits. In contrary to microscopic systems as nuclei, molecules or atoms, superconducting qubits are macroscopic devices with a large number of degrees freedom. But despite their macroscopic nature superconducting circuits show quantum mechanical behavior such as discretized energy levels or superposition of different eigenstates, features arising due to the collective behavior of the Cooper pair condensate of the superconducting wires. In order to show quantum mechanical behavior superconducting qubits have to be protected against noise from the environment. This is a complicated task since on the one hand the qubit needs to be coupled to read-out and control lines while on the other hand every coupling to external devices is a possible source of noise and hence decoherence. In superconducting qubits there exist two major sources of decoherence due to the environment: charge and flux noise. In addition to these external sources of decoherence which can, theoretically, be reduced to very small values, superconducting qubits suffer from an additional internal sources of decoherence: the coupling between qubit degrees of freedom and superconducting quasiparticle degrees of freedom.

According to BCS theory of superconductivity the key features of a superconducting materials such as lossless electrical currents arise due to bound pairs of electrons, known as Cooper pairs. Also it is the Cooper pairs that give rise to the collective quantum mechanical behavior of superconducting circuits and hence create the possibility to build superconducting qubits. All superconducting qubits are based on the Josephson effect, coherent Cooper pair tunneling through a thin barrier sandwiched between two superconducting layers. In contrast to Cooper pair tunneling single quasiparticle tunneling through the Josephson junction gives rise to qubit decoherence. Although they can exist only at energies above the superconducting gap there are always single quasiparticles present in superconducting wires, partly thermally excited partly due to non-equilibrium processes, for example excitation from stray infrared light or in-diffusion from the electrical environment. The coupling between qubit and quasiparticles implys a fundamental limit to qubit coherence times. Single quasiparticle tunneling through a Josephson junction and the induced qubit limitations to coherence times are subject of this thesis.

In general one can distinguish between two types of decoherence: pure dephasing and qubit relaxation. The latter describes relaxation of the qubit into its ground state due

to energy exchange with the environment while the former describes interactions with the environment changing the qubits phase but not leading to relaxation since no energy is transfered. Relaxation due to quasiparticle tunneling is well understood and can be described with an exponential decay with relaxation time T_1, obtained from a first order (golden rule) approximation[6][7]. This theory is confirmed by many experiments demonstrating qubit relaxation due to equilibrium as well as non-equilibrium quasiparticles with relaxation times in good agreement with theoretical results. An interesting experiment from Lenander and Martinis uses an additional RF-Squid to inject quasiparticles into a supercondcuting circuit and measure corresponding lifetimes[8] while Barends et al. demonstrated the influence of stray infrared light on qubit lifetimes which they explained with non-equilibrium quasiparticles excited by the radiation[9]. In different experiments the temperature dependence of relaxation times was measured and can be traced back to quasiparticles [10][11][12].

Contrary to relaxation, dephasing due to quasiparticle tunneling is not that good understood because a golden rule calculation unfortunately does not (necessarily) yield a reasonable result when it comes to dephasing. Instead it yields rates that suffer from divergences such that one has to deal with dephasing more carefully than with relaxation. Hence, the main topic of this thesis is qubit dephasing due to quasiparticle tunneling. We use a diagrammatic approach and find a self-consistent dephasing rate in the Markov approximation ('memoryless superconductor'). The rate we calculate in this section reproduces the result obtained from G. Catelani et al. published in a recent publication using a different approach [13]. In a second step we do not use the Markov approximation and obtain a rate with a more complex time dependence. While we have a time dependence of form $exp(-t/T_{2^*})$ in the Markov approximation, we find a time dependence of the form $exp(-J_{2^*}(t))$ with J_{2^*} not linear in time in the non-Markovian case. We calculate dephasing times for a transmon, a specific type of superconducting qubit and that in this specific case both self consistently obtained dephasing time T_{2^*} as well as the non-Markovian exponential decay are way longer than the relaxation rate of the transmon and dephasing plays a minor role at the most. But this result might change for different types of qubits because in the specific case of a transmon the dephasing rate doesn't diverge from the beginning. Therefor further investigations for different qubits will be necessary to make a final statement about fundamental limits on dephasing times caused by quasiparticle tunneling.

Contents

List of Figures

Chapter 1

Basics

In this chapter we establish the basis for the entire thesis. We sum up basic information on superconducting qubits and the underlying theory. Superconducting electrical circuits, basis for superconducting qubits, are described in the framework of quantum electro dynamics (QED). Hence we will give a short introduction to this wide field with special focus on quantum bits. Furthermore we discuss different qubits design which are all based on the Josephson junction. Since this device plays a crucial role throughout the thesis we discuss both its voltage-current relations 1.1.2 and the corresponding microscopic theory 1.3.2. Besides circuit theory superconductivity proofs to be very important in this work. In 1.2 we sum up basic features of the microscopy BCS (Bardeen-Cooper-Schrieffer) theory of superconductivity before we describe quasiparticle tunneling through insulating barriers in section 1.3.

1.1 Superconducting Qubits

In this section we give a short introduction to quantum electro dynamics (QED) and superconducting qubits. We show how to describe a superconducting circuit with a Hamiltonian that can be derived for the corresponding classical circuit and depends on a 'position' variable, the flux ϕ and its canonical conjugate 'momentum', the charge q. The transition to a quantum circuit is performed by replacing the ordinary numbers ϕ and q with conjugate operators. Due to their linearity usual circuit elements as capacitors or inductances cannot be used to obtain two level quantum systems (equidistant energy levels). Hence, in order to build artificial atoms with tunable parameters and nonlinear energy spacing, we will find ourselves in need for a non-linear element. The non-linear element of choice is the Josephson junction, based on Cooper pair tunneling through a thin insulating (or normal conducting) barrier in between two superconducting leads. In sections 1.1.1 and 1.1.2 we will treat the Josephson junction simply as a non-linear lumped element for which we assume that its microscopic properties are

of no further interest, a more detailed look on Josephson junction properties can be found in section 1.3.2.

For interested readers, there are many good reviews on superconducting qubits [14][15][16]. A glance on the future of superconducting qubits is given by M. H. Devoret and R. J. Schoelkopf [2].

1.1.1 Circuit QED

In this section we will summarize the parts of the Les Houches course [17] on quantum fluctuations in electrical circuits, that we need for our purpose which is to find a Hamiltonian for a given electric circuit. In general, this course provides a good introduction into QED and dissipative circuits and is recommended to the interested reader.

We will treat the circuits in the 'lumped element' approximation, where each element of the circuit is assumed to have no spacial extend, valid as long as energy scales correspond to wavelengths $\lambda \sim \hbar c_0/E$ way larger than system scales (an extension to this model is straightforward and presented in section 4.2). As an example we take a look at the LC oscillator in figure 1.1a. For typical circuit parameters ($L \sim 10nF$, $C \sim 1pF$) it has a resonance frequency $\omega_0 = 1/\sqrt{LC}$ in the microwave spectrum, $\omega_0 \sim 1GHz$, with a corresponding wavelength $\lambda \sim 1cm$ [17] while the size of typical microelectronic circuits is in the μm range such that the circuits are well in the lumped element limit (later we will see, that superconducting qubits have transition frequencies in the range $5 - 20GHz$, fulfilling the requirements for the lumped element approximation). The circuits of interest consist of two terminal elements, such as inductors or capacitors. Each of theses elements represents a branch of the circuit described by two physical variables, the electrical current $I(t)$ through it and the voltage drop $V(t)$ across it. For our purpose to describe a superconducting circuit with Hamilton mechanics, it is favorable to introduce the branch flux $\phi = \int_{-\infty}^{t} V(t')dt'$ and charge $q(t) = \int_{-\infty}^{t} I(t')dt'$ instead of voltage and current, since the flux is related to the phase of the superconducting condensate and it will turn out, that we can describe an electrical circuit similar to a mechanical system where ϕ plays the role of a position and the charge q being the conjugate momentum. Kirchhoff's laws impose some constraints to branch fluxes and currents: all currents arriving/ leaving a node have to sum up to zero and all fluxes around an arbitrary loop contained in the circuit have to sum up to an external flux ϕ_{ext} penetrating the loop (to every branch is assigned a direction determining the sign of the variables):

$$\sum_{b \in node} s_b I_b(t) = 0 \tag{1.1}$$

$$\sum_{b \in loop} s_b \phi_b = \phi_{ext}\,, \tag{1.2}$$

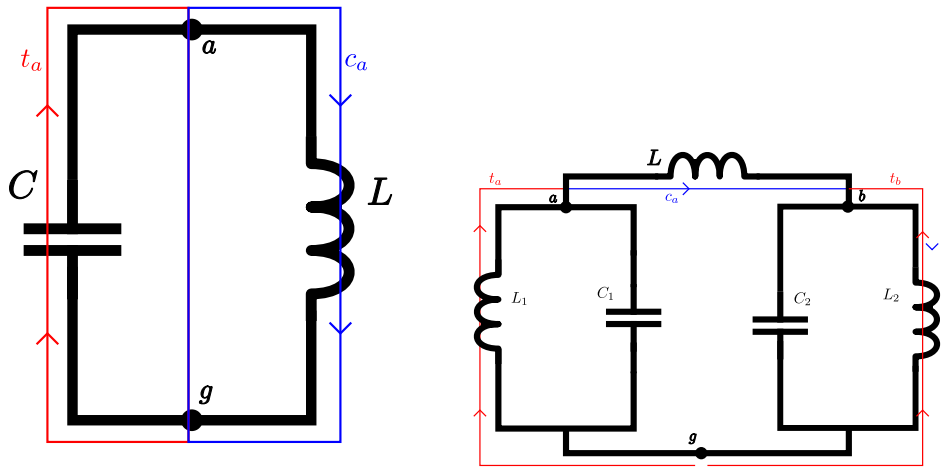

(a) LC oscillator **(b)** Inductive coupled LC oscillators

Figure 1.1: (a) A simple LC oscillator, that consists of two branches: inductance L and capacity C, and (b) two inductive coupled LC oscillators, each with two branches and one branch representing the coupling inductance L. Black dots represent nodes, tree and closure branches are color coded red and blue respectively with arrows fixing electrical current directions.

where $s_b = \pm 1$ depending on branch directions. To obey those constraint, it is natural to introduce node variables instead of branch variables. To be specific, one chooses one node as the reference or 'ground' node and introduces node fluxes ϕ_i for every additional node of the circuit. A node flux is nothing else but the time integral of the potential of the corresponding node with respect to the ground node, which itself has zero potential and zero flux. The next step is to choose a set of branches connecting every node with the ground node in such a way, that there only exists one path along these branches for every node. These branches form the so called 'spanning tree' (see figure 1.1 for examples). The remaining branches are closure branches, each creating a closed loop together with spanning branches. Depending on wether a branch belongs to the spanning or closure tree, one of the two following equations connecting branch flux ϕ_b with the two corresponding node fluxes ϕ_n hold:

$$\phi_{b\in T} = \phi_n - \phi'_n \tag{1.3}$$

$$\phi_{b\in C} = \phi_n - \phi'_n + \phi_{ext}\,, \tag{1.4}$$

where, again, ϕ_{ext} is an external flux penetrating the loop formed by the closure branch $b \in C$. Now, to obey Kirchhoff's laws (1.1) the sum of all the currents arriving at a

node and leaving a node must equal to zero. Together with the constitutive relations

$$I_{C,ii'}(t) = C(\ddot{\phi}_i - \ddot{\phi}_{i'})\,, \tag{1.5}$$

$$I_{L,ii'}(t) = \frac{\phi_i - \phi_{i'}}{L}\,, \tag{1.6}$$

$$I_{J,ii'}(t) = I_0 \sin(\frac{\phi_i - \phi_{i'}}{\Phi_0}) \tag{1.7}$$

for the different elements one finds the equations of motion (eof) for the given circuit. From these equations one than derives the systems Lagrangian and finally the corresponding Hamiltonian. We will show these steps on some examples below. In equations (1.5-1.7) I_C and I_L are currents through a linear capacitive and a linear inductive element respectively. The last relation represents a pure Josephson element, a highly non-linear inductance, which is explained in more detail in sections 1.1.2 and 1.3.2.

A simple example for which we want to use previous recipe is the LC circuit in figure 1.1a, where one has only one active node (a) with an incoming current from the capacity C and one leaving the node into the inductance L. One easily obtains the well known equation of motion for the LC circuit

$$C\ddot{\phi}_a - \frac{\phi_a}{L} = 0 \tag{1.8}$$

It's easy to check that the Lagrangian yielding this eof is

$$\mathcal{L} = \frac{C}{2}\dot{\phi}_a - \frac{1}{2L}\phi_a^2\,, \tag{1.9}$$

which is the difference between the energy of the capacitor and the inductive energy, so that we may interpret the capacities as masses, inductances as spring constants, the flux ϕ_a as a position, capacitative energies as kinetic energy and inductive energies as potential energies in a mechanical harmonic oscillator. The charge q_a is defined as the canonical momentum of the node flux ϕ_a:

$$q_a = \frac{\partial \mathcal{L}}{\partial \phi_a} \tag{1.10}$$

and is nothing else but the sum of all charges on the capacities connected to the node, which can be easily shown for the simple case of the harmonic LC oscillator, $q_a = C\dot{\phi}_a = CV_a = Q_a$. The Hamiltonian for this simple system is, as in the mechanical case, the sum of kinetic and potential energy

$$\mathcal{H} = \frac{1}{2C}q_a^2 + \frac{1}{2L}\phi_a^2\,. \tag{1.11}$$

As a second illustrating example we take two LC circuits coupled via an inductance, figure 1.1b, and ask again what the Hamiltonian looks like. We have two active nodes, a and b. Node a has incoming currents from the left LC circuit and an outgoing current into inductance L while the latter current is incoming at node b and the current into the right LC circuit is leaving nod b. Therefore, the eof for both node fluxes is found to be

$$C_1\ddot{\phi}_a + \frac{\phi_a}{L_1} - \frac{\phi_b - \phi_a + \phi_{ext}}{L} = 0 \tag{1.12}$$

$$C_1\ddot{\phi}_b + \frac{\phi_b}{L_1} - \frac{\phi_b - \phi_a + \phi_{ext}}{L} = 0 \tag{1.13}$$

The Lagrangian, as for the previous example, is achieved by subtracting the potential energy due to inductances from kinetic (capacitive) energies:

$$\mathcal{L} = \frac{C_1}{2}\dot{\phi}_a^2 + \frac{C_2}{2}\dot{\phi}_b^2 - \frac{1}{2L_1}\phi_a^2 - \frac{1}{2L_2}\phi_b^2 - \frac{1}{2L}(\phi_a - \phi_b - \phi_{ext})^2 \,. \tag{1.14}$$

The corresponding Hamiltonian is the sum of the electrostatic energy stored on the capacitors and the magnetic energy stored in the inductive elements:

$$H = \left(\frac{1}{2C_1}q_a^2 + \frac{1}{2L_1}\phi_a^2\right) + \left(\frac{1}{2C_2}q_b^2 + \frac{1}{2L_2}\phi_b^2\right) + \frac{1}{2L}(\phi_a - \phi_b - \phi_{ext})^2 \,. \tag{1.15}$$

We can identify three parts in the Hamiltonian, both uncoupled LC circuits (first two terms) and a coupling term due to the inductance L.

The formal transition from a classical description as above to a quantum mechanical one is straightforward. As in the mechanical analogy the classical variables ϕ_i and q_i are replaced by operators obeying the commutator relations for conjugate variables,

$$\phi_i \to \hat{\phi}_i \tag{1.16}$$

$$q_i \to \hat{q}_i \tag{1.17}$$

$$[\hat{\phi}_i, \hat{q}_j] = i\hbar\delta_{ij} \,, \quad [\hat{\phi}_i, \hat{\phi}_j] = [\hat{q}_i, \hat{q}_j] = 0 \,. \tag{1.18}$$

Again, we see that ϕ_i corresponds to a position variable x while q_i corresponds to the conjugate momentum p_x. Due to this transition from a classical to a quantum mechanical treatment the flux and the charge cannot be at the same time measured with arbitrary accuracy. Contrary they are represented with quantum mechanical wavefunctions and are determined only up to a certain threshold. In most QED systems one of the variables is strongly confined while the second variable is has a large uncertainty.

At the end of this section, we want to discuss shortly, why we cannot use a simple harmonic oscillator to build qubits. The Hamiltonian (1.11) for the LC circuit is a

simple harmonic oscillator that can be written in terms of creation and annihilation operators $a\,, a^\dagger$

$$H = \hbar\omega_0(a^\dagger a + \frac{1}{2})\,, \quad \omega_0 = 1/\sqrt{LC}\,, \tag{1.19}$$

with eigenenergies $E_n = \hbar\omega_0(n + 1/2)$, yielding equal energy splitting $\hbar\omega_0$ between all neighboring energy states. This prevents one from truncating the system to an effective two level system. Assume one chooses the two lowest energies as basis states for a qubit than every manipulation of the qubit, e.g. stimulated relaxation from $|1\rangle$ to $|0\rangle$, requires pulses with resonance frequency ω_0, which in our example could not only cause the transition $|1\rangle \rightarrow |0\rangle$, but also the excitation $|1\rangle \rightarrow |2\rangle$. Therefore it's not possible to truncate the harmonic oscillators Hilbert space to two dimension only but it will always be of infinite size. The only possible way to bypass this issues is by integrating non linear elements into the circuit which will provide the required non degenerate energy spacing. The non linear element of choice is the Josephson junction, because it is dissipation less but still non linear.

1.1.2 The Josephson Junction

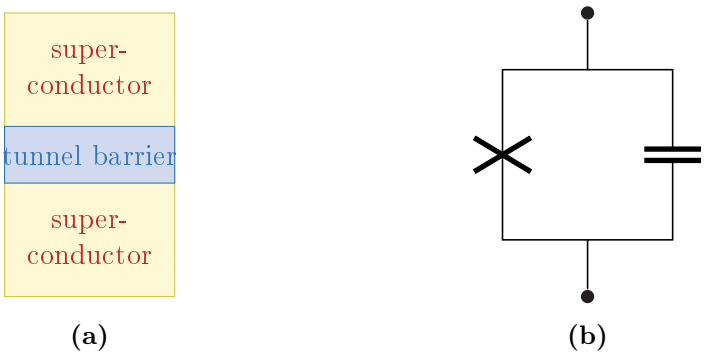

Figure 1.2: (a) Schematic setup of a Josephson junction with two superconductors and a weak link. (b) A Josephson junction can be modeled as a capacity in parallel with a pure Josephson tunneling element (cross).

In this section we want to discuss the governing equations of a Josephson junction as element of an electrical circuit, which we need to include Josephson junctions into the framework developed in section 1.1.1. A microscopic derivation of these equations will be given in section 1.3.2.

A Josephson (tunnel) junction consists of two superconducting layers coupled via a weak link, usually a thin oxide layer between the two superconducting layers (usually aluminum, see figure 1.2a). The barrier is thin enough to allow electron tunneling between the superconductors. Since, at absolute zero of temperature, all electrons

in the superconductors are part of the Cooper pair condensate[1] (see section 1.2.1 for details), there are no single electrons available to serve as charge carriers and Cooper pair tunneling is the only possible contribution to a current through the junction. Unfortunately, Cooper pair tunneling is a second order process requiring two electrons to tunnel through the junction simultaneously. Therefore, it was long expected, that at most a weak current could flow through the junction unless the applied voltage exceeds a value of $2\Delta/e$, providing enough energy to break Cooper pairs and generate single electron excitations above the gap Δ. Due to thermal excitations above the gap, a small quasi particle current would flow through the barrier even if a smaller voltage is applied, but at temperatures well below Δ/k_B this current is weak. In contrary B. D. Josephson proposed in 1962, that tunneling of Cooper pairs through the barrier gives rise to a significant current with outstanding current- flux characterisitcs through the junction, even if no voltage is applied to the junction (and even at $T = 0K$) [18]. In the following years, different experiments (e.g. [19]) confirmed Josephson's proposal resulting in the Nobel prize for Josephson in 1973.

Due to Cooper pair tunneling, a highly non linear relation between the current I through the junction, the voltage V across it and the phase difference φ between the superconductors[2] governs the behavior of a Josephson junction as part of an electrical circuit:

$$I = I_0 \sin(\varphi) \tag{1.20}$$

$$\frac{d\varphi}{dt} = \frac{V}{\Phi_0}\,, \tag{1.21}$$

Here, I_0 is the junction's critical current and depends on junction parameters, e.g. junction geometry, and $\Phi_0 = \frac{\hbar}{2e}$ is the reduced flux quantum. One consequence of above equations is the so called DC-Josephson effect: Even if no voltage is applied to the junction, yet a constant, phase dependent current with $|I| \leq I_0$ will flow. Another interesting effect occurs if one applies a DC voltage to the junction. A constant voltage, according to equation 1.20 and 1.21, yields an AC current $I(t) \sim \sin(\frac{V}{\Phi_0}t + \varphi_0)$ through the junction. This is known as the AC-Josephson effect.

Equations (1.20) - (1.21) describe a 'pure' Josephson element, represented as a cross (see figure 1.2b) in a circuit diagram. A pure Josephson element can be interpreted as a highly non linear inductive element. This can be shown by differentiating eq. (1.20) with respect to time and replacing $\dot{\varphi}$ with equation (1.21), yielding the conventional relation

$$\dot{I}(t) = \frac{V}{L_J}\,, \tag{1.22}$$

[1] In superconductors, two electrons can be in a bound state due to small attractive forces, so called Cooper pairs. At $T = 0K$, all electrons are in these bound state and the Cooper pair condensate forms a new ground state. The energy gap between a Cooper pair bound state and the quasi particle continuum is Δ, the superconducting order parameter.

[2] The condensate can be described with only one wavefunction having a phase $e^{i\varphi(r,t)}$

where we introduced the Josephson inductance [20]

$$L_J = \phi_0/(I_0 \cos(\varphi)) \,. \tag{1.23}$$

According to electro dynamics, an inductance is non dissipative and the energy stored in an inductive element can be calculated as

$$E(\varphi) = \int dt' P(t') = \int dt' V(t') I(t') = I_0 \Phi_0 \int dt' V(t') \frac{d\varphi}{dt'} = -E_J \cos(\varphi) \,, \tag{1.24}$$

with the Josephson coupling energy $E_J = I_0 \Phi_0$ (for a linear inductance we have $E(\phi) = \frac{1}{2L}\phi^2$). Having the energy (and current phase relations) of pure Josephson elements, they can easily be included in the Hamiltonian circuit theory from preceding section, where it's convenient to use 'node phases' instead of node fluxes. Flux and phase at a given position are connected via

$$\varphi_i = \frac{\phi_i}{\Phi_0} \mathrm{mod} 2\pi \,. \tag{1.25}$$

In addition to Cooper pair tunneling resulting in the Josephson effect, a Josephson junction serves as a capacity, since the leads separated by an insulating layer form a plate-capacitor with its capacity C_J depending on junction parameters. Therefore, a Josephson junction is always modeled as a pure Josephson inductive element in parallel with a capacity C_J, see figure 1.2b.

1.1.3 Superconducting Qubits

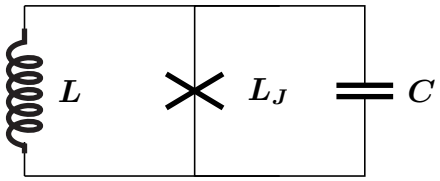

Figure 1.3: General circuit for a superconducting qubit, where C and L are an effective capacity and inductance due to circuit the Josephson junction is embedded in.

Now, with the highly non linear Josephson inductance (1.23), we have the last element for actually building a qubit using superconducting circuits. The general circuit of a simple superconducting qubit is sketched in figure 1.3, where L is for example the inductance of a superconducting loop connecting the junction sides or due to e.g. two more large Josephson junctions which can be modeled as linear inductances. There exist, in general, three basic types of qubits, namely charge, flux and phase qubit, and a lot of derivatives based on those three. The names are chosen to describe the variable

that can be controlled externally for qubit operations and read-out. All qubits have in common that they use at least one Josephson junction as non linear element, but they differ in circuit design, coupling to external circuit parts and in the parameter range for L, C and E_J. To understand, why we need different qubit designs, we first have a look on the bare Josephson junction and the issues one has to overcome.

If we do not connect the junction leads with a circuit (see 1.2a), the Hamiltonian takes the form

$$\mathcal{H} = 4E_C(\hat{n} - \frac{q_r}{2e})^2 - E_J \cos(\varphi)\,. \tag{1.26}$$

Here, $E_C = \frac{e^2}{2C}$ is the Cooper pair charging energy of the junction, $\hat{n}$ is the operator counting the Cooper pairs tunneled through the junction and q_r is a residual charge that always exists on the junction, e.g. due to production, and usually is way larger than the charge corresponding to n [21]. This offset charge cannot be controlled during (or prior to) qubit operation, such that it is impossible to measure the influence of one Cooper pair on energies of the entire system making it impossible to operate this pure junction as a qubit. The different qubit designs have different strategies to overcome the difficulties due to the uncontrollable but large residual charge by providing control over charge on the junction or flux through it. As an example we take a look on the Cooper pair box (CPB), the simplest form of a charge qubit, and the transmon[22], a derivate from the CPB. Both qubits are described with the same Hamiltonian (1.27) but operate in entirely different parameter regimes. Both, the CPB and the transmon, consist of a

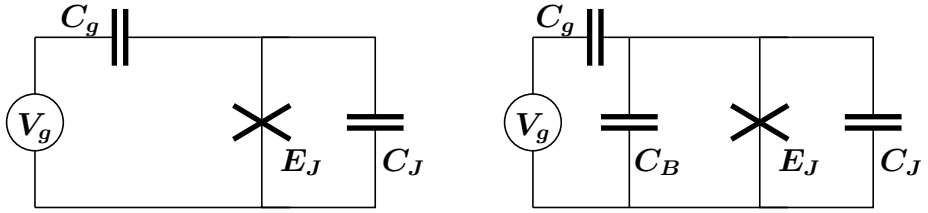

(a) Cooper pair box **(b)** Transmon

Figure 1.4: Circuit diagrams for the CPB a and the Transmon b

superconducting island confined by a Josephson junction and a gate capacitor used to apply a voltage V_g to the island. This additional voltage allows for tuning the charge on the island to negate the uncontrollable offset charge q_r. In case of the transmon, the Josephson junction is shunted with an additional capacity C_B, allowing the transmon to be operated in the opposite parameter regime ($E_J \gg E_C$) as the CPB ($E_C \simeq E_J$). Circuit diagrams for both, transmon and CPB are shown in figure 1.4. Both circuits yield the same Hamiltonian:

$$\mathcal{H} = 4E_C(\hat{n} - n_g)^2 - E_J \cos(\hat{\varphi})\,, \tag{1.27}$$

where $n_g = C_g V_g/(2e)$ is an offset charged due to the gate voltage and E_C is the charging energy, which is $E_C = e^2/(C_j + C_g)$ or $E_C = (2e)^2/(C_j + C_g + C_b)$ for CPB and transmon respectively. $\hat{n}$ is the number operator of excess Cooper pairs on the island which, by its nature, has discrete eigenvalues $\hat{n}|n\rangle = n|n\rangle$, where n is an integer number. This restricts its canonical conjugate variable, the phase difference φ across the junction ($[\hat{\varphi}, \hat{n}] = i$), to values on a circle, $\varphi \in [0, 2\pi)$, yielding $\Psi(\varphi + 2\pi) = \Psi(\varphi)$ in the phase basis. The Hamiltonian 1.27 can either be written in the charge basis with

$$\hat{n} = |n\rangle n \langle n| \tag{1.28}$$

$$cos(\hat{\varphi}) = \frac{1}{2} \sum_n (|n+1\rangle\langle n| + |n\rangle\langle n+1|) \tag{1.29}$$

or in the phase basis

$$\hat{n} = -i\partial_\varphi \hat{\varphi} = \varphi\,. \tag{1.30}$$

Using the phase basis, where we can interpret the Hamiltonian as a particle with position φ and momentum $\hat{n}$, we want to compare CPB and transmon. The additional capacity C_B in the transmon design can be used to drastically increase the ratio E_J/E_C which scales with $1/C$. While for the CPB the ratio $E_J/E_C \simeq 1$ is fixed by junction parameters, this value can be orders of magnitude larger for the transmon due to C_B, drastically changing qubit behavior. As long as E_J and E_C are in the same order of magnitude, the attractive potential, described by $V = -E_J \cos(\hat{\varphi})$, is weak resulting in wave functions in the φ-basis with a large width and spreading over a large range of the cosine potential. Therefore, the particle feels the strong anharmonicity due to the cosine potential, yielding strong anharmonicity in the eigen energies of the qubit as well. On the other hand, the charge on the island is sharp defined in these eigenstates and the CPB is sensitive to short time charge noise as well as long time shifts in n_g. Contrary, for the transmon with $E_J \gg E_c$ the particle will be trapped in the first minimum of the cosine potential with a narrow peaked wave function. In this case it is appropriate to approximate the potential for the lowest lying energy levels as a harmonic potential while anharmonicity can be introduced with a quartic perturbation:

$$\mathcal{H}_{transmon} \approx 4E_C(\hat{n} - n_g)^2 + \frac{E_J}{2}\hat{\varphi}^2 \quad \left(-\frac{E_j}{4!}\hat{\varphi}^4\right). \tag{1.31}$$

In figure 1.5 we compare the absolute value of exact wave functions and those obtained with the harmonic approximation. The approximation becomes good for the ground state as well as the first excited state at values for $E_J/E_C \gtrsim 10$ and is almost exact if increasing the ratio by one order of magnitude. Therefore, we will use the harmonic approximation later on to calculate different matrix elements between qubit states for the transmon, which we will need to calculate dephasing and relaxation rates.

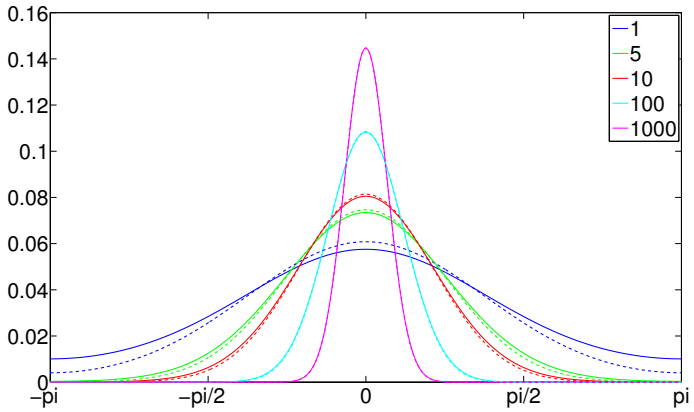

(a)

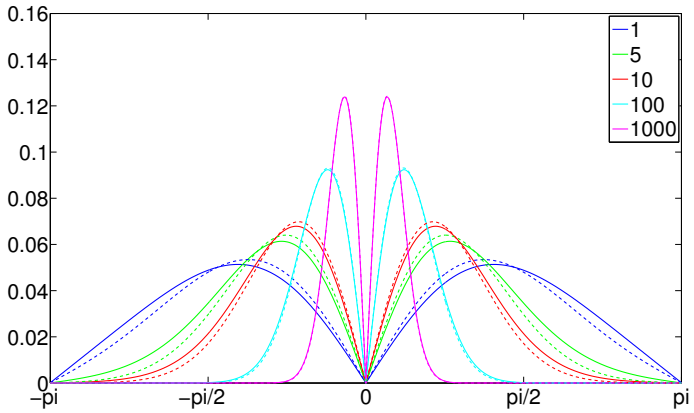

(b)

Figure 1.5: We plot the absolute value $|\Psi(\varphi)|^2$ of the wave function for a the ground state and b the first excited state of the Hamiltonian (1.27), for different ratios of E_J/E_C (see legend). Solid lines correspond to exact solutions, while dashed lines are obtained using the harmonic oscillator Hamiltonian. The approximate wave functions coincidence with the exact solutions at relative small ratios ($E_J/E_C \simeq 10$), and we can use the harmonic oscillator wave functions to calculate matrix elements for a transmon.

At the end of this section we want to emphasize that, no matter how it actually is realized, every superconducting qubit uses at least one Josephson junction which is sensitive to the dissipative process of single electron tunneling processes which we are going to investigate in this work. The qubit Hamiltonian we will use does not depend on the actual realization of the qubit. Since a qubit is a two level system, it can also be represented with spin-1/2 notation. The Hamiltonian of a qubit than reads

$$H_q = \frac{\delta E}{2}\sigma_z\,, \tag{1.32}$$

where δE is the qubit energy splitting and σ_z is the Pauli matrix in z direction. Throughout this work we will use this Hamiltonian for qubits and only use the actual realization (e.g. transmon) if we need to calculate matrix elements.

1.1.4 Qubit Decoherence

A generic qubit state can be written as

$$|\Psi\rangle = \cos\frac{\Theta}{2}|0\rangle + \sin\frac{\Theta}{2}e^{i\phi}|1\rangle \tag{1.33}$$

with $0 \leq \Theta \leq \pi$ and $0 \leq \phi \leq 2\pi$. We interpret Θ as polar and ϕ as azimuthal angel of spherical coordinates and the qubit state as a vector pointing on a unit sphere called Bloch sphere. For a perfect qubit, coupled to the environment only during gate operations, the free time evolution of the state is unitary and the phase ϕ between the two states oscillates with the qubits Larmor frequency, $\phi(t) = \phi(0) + i\delta E t$ while the polar coordinate remains constant. Due to undesired coupling with the environment two types of error occur: relaxation and pure dephasing. The first one corresponds to a change of the polar angel. For example, if the environment is at lower temperature than the qubit it will drain energy from the qubit and the tip of the Bloch vector will diffuse to the south pole (ground state) of the sphere. The second process, pure dephasing, describes undesired changes in the azimuth angel which can, for example, arise from low-frequency fluctuations of the qubits energy splitting δE. Due to the interaction with its environment the qubit will eventually reach its thermal equilibrium state $\vec{\Psi} = \tanh(\delta E/k_B T)\hat{e}_z$[21]. Assuming that the decay due to both processes is exponential we can define the relaxation rate Γ_1 and the pure dephasing rate Γ_{2^*}. These rates are related to the relaxation time T_1 and decoherence time T_2 as [21]

$$T_1 = \Gamma_1^{-1} \tag{1.34}$$

$$T_2 = (\Gamma_{2^*} + \Gamma_1/2)^{-1} \tag{1.35}$$

1.2 Superconductivity and Josephson Junctions

Superconductivity, due to its remarkable features, is the crucial ingredient to qubits based on electrical circuits because without dissipation free current flow QED could never be realized. Nowadays, most superconducting circuits are based on aluminum, a conventional superconductor with an s-wave order-parameter. The theory was established in 1957 by Bardeen, Cooper and Schrieffer and hence is called BCS-theory. Since a basic understanding of BCS theory and the corresponding quasiparticle excitations is crucial for work with tunnel junctions and superconducting qubits, we will give a short introduction to BCS theory in the following section. BCS theory provides the tools we need to discuss electron tunneling and the Josephson junction in the succeeding sections 1.3.2 and 1.3.

1.2.1 Superconductivity - BCS Theory

Superconductivity arises due to an instability of the Fermi surface to a small attractive interaction between electrons, as demonstrated by Neil Cooper in 1956 [23]. This instability was the foundation to a microscopic theory of superconductivity published in 1957 by J. Bardeen, N. Cooper and R. Schrieffer [24],[25], nowadays known as the BCS theory of superconductivity. According to BCS theory, the instability of the Fermi sea to the small attractive interaction between electrons gives rises to a condensate of electron pairs, the so called Cooper pairs. In conventional superconductivity this attractive interaction is mediated by phonons and Cooper pairs are bound states of two electron with vanishing total momentum, total angular momentum and in a spin singlet (s=0). Therefore this type of superconductivity also is called s-wave superconductivity. For this work we are not interested in the details of the attractive interaction and will assume conventional superconductivity with a local interaction yielding a constant attractive potential $V_{qq'} = -V$ $(V > 0)$ in momentum space between electrons of opposite momentum and spin. In this case the Hamiltonian can be written using second-quantization:

$$\mathcal{H} = \sum_{k,\sigma} \xi_k c^\dagger_{k\sigma} c_{k\sigma} - V \sum_{k,k'} c^\dagger_{k\uparrow} c^\dagger_{-k\downarrow} c_{-k'\downarrow} c_{k'\uparrow} \tag{1.36}$$

Here $c^{(\dagger)}_{k\sigma}$ is an annihilation (creation) operator for an electron with momentum k and spin σ. The first term is the kinetic energy of the system (free particle Hamiltonian) with energy ξ_k measured from the chemical potential μ and the second term is the interaction between electrons, where we made use of the fact that in a conventional superconductor only electrons with opposite spins and momentua couple to each other. We can interpret $c^\dagger_{k\uparrow} c^\dagger_{-k\downarrow}$ and $c_{-k'\downarrow} c_{k'\uparrow}$ as creation and annihilation operator for a Cooper pair respectively. For BCS theory a mean field approach to the Hamiltonian

1.36 is good enough to yield the important features of superconductivity. Since superconductivity arises due to Cooper pairs, we expand the Hamiltonian in the deviation of the Cooper pair operator $c_{-k\downarrow}c_{k\uparrow}$ from its (thermal) expectation value $b_k \equiv \langle c_{-k\downarrow}c_{k\uparrow}\rangle$:

$$c_{-k\downarrow}c_{k\uparrow} = b_k + \left[c_{-k\downarrow}c_{k\uparrow} - b_k\right] , \tag{1.37}$$

where we assume $\langle[\dots]\rangle \ll b_k$ and neglect terms of quadratic and higher orders in $[\dots]$. This yields the BCS mean field Hamiltonian

$$\mathcal{H} = \sum_{k,\sigma} \xi_k c^\dagger_{k\sigma}c_{k\sigma} - \sum_k \left(\Delta^* c_{-k\downarrow}c_{k\uparrow} + \Delta c^\dagger_{k\uparrow}c^\dagger_{-k\downarrow}\right) - \Delta^* b_k \,, \tag{1.38}$$

with the order parameter $\Delta = V\sum_k b_k$. The mean field Hamiltonian is an effective one particle Hamiltonian and we can diagonalize it in a straightforward way. Therefore we introduce the Nambu spinor

$$\Psi_k = \begin{pmatrix} c_{k\uparrow} \\ c^\dagger_{-k\downarrow} \end{pmatrix} \tag{1.39}$$

and express the BCS Hamiltonian in terms of Nambu spinors, yielding

$$\mathcal{H} = \sum_k \Psi^\dagger_k \begin{pmatrix} \xi_k & \Delta \\ \Delta^* & -\xi_k \end{pmatrix} \Psi_k - \sum_k \left(\Delta^* b_k + \xi_k\right) \equiv \sum_k \Psi^\dagger_k \underline{H}_k \Psi_k - \sum_k \left(\Delta^* b_k + \xi_k\right) . \tag{1.40}$$

The 2×2 matrix $\underline{H}_k$, with eigenvalues $E_k = \sqrt{\xi_k^2 + |\Delta|^2}$, can be diagonalized with a Bogolioubov transformation yielding a new set of fermionic operators defined as $\Phi_k = U^\dagger_k \Psi_k$:

$$\begin{pmatrix} \gamma_{k0} \\ \gamma^\dagger_{k1} \end{pmatrix} = \begin{pmatrix} u^*_k & -v_k \\ v^*_k & u_k \end{pmatrix} \begin{pmatrix} c_{k\uparrow} \\ c^\dagger_{-k\downarrow} \end{pmatrix} \tag{1.41}$$

with $|u_k|^2 + |v_k|^2 = 1$. A proper choice for u_k and v_k is

$$u_k = \sqrt{\frac{1}{2}(1 + \frac{\xi_k}{E_k})} \tag{1.42}$$

$$v_k = e^{i\phi}\sqrt{\frac{1}{2}(1 - \frac{\xi_k}{E_k})} \tag{1.43}$$

where ϕ is the phase of the order parameter Δ. In their original approach, BCS started from a variational ground state defined as $|\Psi\rangle = \prod_k (u_k + v_k c^\dagger_{k\uparrow}c^\dagger_{-k\downarrow})|0\rangle$ instead of the mean field approach we present here. The parameters u_k and v_k in the variational

ground state turn out to be identical with the parameters from the mean field approach. From the variational ground state we can find a physical meaning for u_k and v_k. While latter measures the probability of Cooper pair state to be filled, first measures the probability to have an empty pair state. For the new quasiparticles γ_{k0} and γ_{k1} the Hamiltonian 1.38 is diagonal and reads

$$\mathcal{H} = -\sum_k \left(\Delta^* b_k + \xi_k + E_k\right) + \sum_{k\alpha} E_k \gamma^\dagger_{k\alpha}\gamma_{k\alpha}\,. \tag{1.44}$$

Here, the first term is the energy gain of the Cooper pair condensate compared to the Fermi sea, the second term is the quasiparticle spectrum with excitation energies $E_k = \pm\sqrt{\xi_k^2 + |\Delta|^2}$. The quasiparticle spectrum has an energy gap of 2Δ between hole like ($E_k \leq -|\Delta|$) and electron like ($E_k \geq |\Delta|$) quasiparticles. The energy gap is temperature dependent only and obeys the self-consistency equation

$$\Delta = V\sum_k b_k = V\sum_k u_k^* v_k[1 - f(E_k)] = V\sum_k \frac{\Delta}{2E_k}\tanh(\frac{E_k}{k_B T}) \tag{1.45}$$

with the Fermi distribution $f(x) = 1/(1+e^{x/k_B T})$. As usual, we evaluate the sum over all k-vectors with an integral over quasiparticle energies:

$$\sum_k \to \int_{-\infty}^{\infty} d\xi N_{el}(\xi) \to \int_{-\infty}^{\infty} dE N(E) \tag{1.46}$$

where $N_{el}(\xi)$ is the electron density of states (dos) and $N(E) = N_{el}(\xi)d\xi/dE$ is the BCS density of states. The attractive interaction has a characteristic energy scale which is small compared to the Fermi energy, limiting integrals over electronic energies to a narrow region around the Fermi energy such that we have to introduce a cutoff energy for energy integration. For example, considering conventional superconductors with phonon mediated electron-electron interaction, this cutoff energy is the Debye energy of the phonons. In the case of a small cutoff-energy we can approximate the electronic density of states with its value N_0 at the Fermi surface and can evaluate the BCS density of states

$$N(E) = N_0 \frac{E}{\sqrt{E^2 - |\Delta|^2}}\Theta(E^2 - |\Delta|^2)\,, \tag{1.47}$$

which has a square root singularity at the gap. We also introduce the density of states normalized to the electron density at the fermi surface and denote it with a lower case letter, $n(E) = N(E)/N_=$. With the diagonalized Hamiltonian 1.44, the corresponding quasiparticles $\gamma_{k\alpha}$ and the BCS density of states we have all tools that we need to deal with electron tunneling occurring in a Josephson junction. Before we introduce the formalism for quasiparticle tunneling processes we will present a different approach to superconductivity, that we will use later to calculate dephasing rates. The formalism is based on Nambu spinors and the so called Nambu-Gorkov Greens functions.

1.2.2 BCS Theory- Greens Function Formalism

In this section we present a slightly different approach to the BCS theory of superconductivity based on Greens functions. To begin with, we recap the BCS mean field Hamiltonian 1.38 from previous section, neglecting constant energy offsets:

$$\mathcal{H} = \sum_k \Psi_k^\dagger \begin{pmatrix} \xi_k & \Delta \\ \Delta^* & -\xi_k \end{pmatrix} \Psi_k \,. \tag{1.48}$$

We now introduce the Nambu-Gorkov (Matsubara) Greens function as

$$G(k\sigma, k'\sigma', \tau) = -\langle T_\tau \Psi_k(\tau) \Psi_{k'}^\dagger \rangle = - \begin{pmatrix} \langle T_\tau c_{k\uparrow}(\tau) c_{k'\uparrow}^\dagger \rangle & \langle T_\tau c_{k\uparrow}(\tau) c_{-k'\downarrow,i} \rangle \\ \langle T_\tau c_{-k\downarrow}^\dagger(\tau) c_{k'\uparrow}^\dagger \rangle & \langle T_\tau c_{-k\downarrow}^\dagger(\tau) c_{-k'\downarrow} \rangle \end{pmatrix} , \tag{1.49}$$

where $\tau = it$ is the imaginary time and T_τ the time ordering operator with respect to τ. With the Heisenberg equation of motion for an operator $\hat{A}(\tau)$

$$\partial_\tau \hat{A}(\tau) = [\mathcal{H}, \hat{A}(\tau)] \tag{1.50}$$

we find the equation of motion for the Nambu-Gorkov Greens function:

$$(-\partial_\tau - \xi_k \tau_3 + \Delta\tau_+ + \Delta^*\tau_-) G(k, k', \tau) = \delta(\tau)\delta_{kk'} \,, \tag{1.51}$$

with τ_i the ith Pauli matrix. We Fourier transform above eof yielding

$$(i\omega_n - \xi_k \tau_3 + \Delta\tau_+ + \Delta^*\tau_-) G(k, k', i\omega_n) = \delta_{kk'} \,, \tag{1.52}$$

where we have fermionic Matsubara frequencies $\omega_n = (2n+1)\pi/\beta$ with the inverse temperature $\beta = 1/k_B T$. This yields the Greens function of the BCS superconductor

$$G(k, k', i\omega_n) = \frac{i\omega_n + \xi_k \tau_3 - \Delta\tau_+ - \Delta^*\tau_-}{(i\omega_n)^2 - \xi_k^2 - |\Delta|^2} \tag{1.53}$$

which has poles exactly at the excitation energies $E_k^2 = \xi_k^2 + |\Delta|^2$, yielding the same quasiparticle spectrum as in previous section. The density of states of the BCS superconductor can be calculated using

$$\mathcal{N}(\omega) = -\frac{1}{\pi} \mathrm{Im} \sum_{kk'} G(k, k', i\omega_n \to \omega + i\eta) = N_0 \frac{\omega - \Delta\tau_1}{\sqrt{\omega^2 + |\Delta|^2}} \,, \tag{1.54}$$

The Nambu-Gorkove Green's function's diagonal elements produce the BCS quasiparticle density of states $N(\omega)$ while off diagonal elements give rise to the pair density of states, $P(\omega) = N(\omega)\Delta/\omega$. Again we remind of the normalized densities, $p(\omega) = P(\omega)/N_0$ and $n(\omega) = N(\omega)/\Delta$. Since we don't find any additional insight from the Greens function method at this point, we won't discuss the formalism in details at this point. We will refer to this section in 3.3.

1.3 Quasiparticle Tunneling

In this section we will analyze two superconductors coupled via a weak link, e.g. a Josephson junction. We will motivate a Hamiltonian for the system and give a microscopic derivation of the Josephson effect and show the connection to superconducting qubits. We will see, that in addition to the coherent pair tunneling single quasiparticles present above the gap can tunnel through the weak link. This single particle processes are dissipative and induce qubit decoherence, e.g. relaxation and dephasing. We will find ourselves in the need for a framework dealing with the qubit coupled to the single particle part of the Hamiltonian, which is not included in the qubit Hamiltonian. Such a framework will be provided in chapter 2. We analyze the dynamics of the qubit coupled to the single particle part of the tunneling Hamiltonian in chapter 3.

1.3.1 Foundation

In this section we want to give the foundations for the upcoming sections about the Josephson effect and single quasiparticle tunneling. Therefore we have to introduce the Hamiltonian describing the different subsystems building the Josephson junction. As presented in section 1.1.2, the Josephson junction consists of two superconducting leads separated by a thin insulating barrier or another weak link suppressing the super current, see figure 1.2a. For a usual Josephson junction with aluminum leads, we can describe both superconducting sides with bulk BCS Hamiltonians

$$\mathcal{H}_i = \sum_{k,\sigma} \xi_k c^\dagger_{k\sigma,i} c_{k\sigma,i} - \Delta_i \sum_k \left(c_{-k\downarrow,i} c_{k\uparrow,i} + c^\dagger_{k\uparrow,i} c^\dagger_{-k\downarrow,i} \right) = \sum_{k\alpha} E_{k,i} \gamma^\dagger_{k\alpha,i} \gamma_{k\alpha,i} \,, \quad i = l, r \tag{1.55}$$

where l, r stands for the left and right lead respectively. We neglect the constant energy gain of the condensate which means nothing else than measuring the systems energy with reference energy $\epsilon_0 = \epsilon_{FermiSea} - \epsilon_{condensate}$. Additionally we take the as a real constant, which is possible due to a gauge transformation absorbing the gaps phase $\varphi_{l/r}$ into the definition of creation and annihilation operators. The weak link between both leads allows electrons to tunnel from one lead to the other giving rise to a finite overlap of electron wave functions belonging to different sides. We describe the coupling between both sides due to this final overlap with the tunneling Hamiltonian

$$H_T = \sum_{kk'\sigma} g_{kk'} e^{i\varphi/2} c_{k\sigma,l} c^\dagger_{k'\sigma,r} + h.c. \,, \tag{1.56}$$

where the phase $\varphi = \varphi_r - \varphi_l$ is the phase difference between the condensates. The tunneling matrix element $g_{kk'}$ describes the overlap of wavefunctions for electrons with

momenta k and k' on the left and right side respectively. For conventional tunnel junctions the coupling is not magnetic and no spin flip occurs for an electron tunneling from one side to the other. Since we do not know details about the tunnel matrix element, we will assume it to be a constant not depending on momenta k and k'. This is a common assumption for the tunneling matrix element and yields results fin good agreement with experimental data. As we will see, the constant tunnel element g is connected to the normal state resistance of the junction as [20]

$$R_N = \frac{\hbar g^2 N_{0,l} N_{0,r}}{4\pi e^2}\,, \tag{1.57}$$

with the electron density of state (dos) at the Fermi surface for the left and right lead $N_{0,l/r}$. The first part of the tunneling Hamiltonian represents a tunneling process from left to right while the harmonic conjugate *h.c.* represents a tunneling process in the other direction. Since the BCS Hamiltonians on either side are diagonal in the γ operators, we express the tunneling Hamiltonian in these operators. Therefore we have to invert relation 1.41, yielding

$$\begin{pmatrix} c_{k\uparrow,i} \\ c^\dagger_{-k\downarrow,i} \end{pmatrix} = \begin{pmatrix} u_{k,i} & v_{k,i} \\ -v_{k,i} & u_{k,i} \end{pmatrix} \begin{pmatrix} \gamma_{k0,i} \\ \gamma^\dagger_{k1,i} \end{pmatrix} \tag{1.58}$$

The parameters $u_{k,i}$ and $v_{k,i}$ are real for our definition of the BCS Hamiltonian and the tunnel Hamiltonian. The Hamiltonian expressed in terms of γ particles can be split into two fundamental differet parts. On the one hand, we find terms proportional to $\gamma_{k\alpha,i}\gamma_{k'\beta,j}$ $(\gamma^\dagger_{k\alpha,i}\gamma^\dagger_{k'\beta,j})$, on the other hand the second class of terms has the normal tunneling form proportional to $\gamma_{k\alpha,i}\gamma^\dagger_{k'\alpha,j}$. While latter class gives rise to single particle tunneling first class is pair tunneling and gives rise to the Josephson effect. Therefore, we split the tunnel Hamiltonian into two parts, namely the pair tunneling Hamiltonian H_p and the single quasiparticle tunneling H_{qp}:

$$H_T = H_{qp} + H_p \tag{1.59}$$

$$H_{qp} = g \sum_{kk'\alpha} A_{kk'} \gamma_{k\alpha,l} \gamma^\dagger_{k'\alpha,r} + h.c. \tag{1.60}$$

$$H_p = g \sum_{kk'\alpha} B_{kk'} \epsilon_\alpha \gamma_{k\beta,l} \gamma_{k'\alpha} + h.c.\,. \tag{1.61}$$

Here, we defined the coherence factors A_{kq} for quasi particle tunneling and B_{kq} for pair tunneling respectively:

$$A_{kk'} = e^{i\varphi/2} u_{k,l} u_{k',r} - e^{-i\varphi/2} v_{k,l} v_{k',r} \tag{1.62}$$

$$B_{kk'} = e^{i\varphi/2} u_{k,l} v_{k',r} + e^{-i\varphi/2} v_{k,l} u_{k',r} \tag{1.63}$$

while $\epsilon_\alpha = +1$ for $\alpha = 1$ and $\epsilon_\alpha = -1$ for $\alpha = 0$ and $\beta \neq \alpha$.

1.3.2 Pair Tunneling & Josephson Effect

In this section we will calculate the change in energy due to the coupling between the superconducting leads. We will find, that the coupling gives rise to a constant energy shift and an additional shift proportional to $\cos(\varphi)$ where φ is the phase difference between the superconductors. To clarify why we separated the tunneling Hamiltonian into a 'pair' and a quasiparticle term claiming that the pair Hamiltonian gives rise, we will first calculate the energy shift

$$\langle \delta H \rangle = \langle H_T \rangle \tag{1.64}$$

at zero temperature with simple second order perturbation theory (since H_T is linear in creation/ annihilation operators for each side the first order in H_T vanishes). At zero temperature the unperturbed supercondcutors are in their ground states $|0\rangle_i$ with $\gamma_{k\alpha,i}|0\rangle_i = 0$ yielding the ground state $|0\rangle \equiv |0\rangle_1 \otimes |0\rangle_r$. The second order energy shift due to tunneling reads

$$\langle \delta H \rangle = \sum_m \frac{\langle 0|H_T|m\rangle\langle m|H_T|0\rangle}{-\epsilon_m} = -\sum_m \frac{\langle 0|H_p|m\rangle\langle m|H_p|0\rangle}{\epsilon_m} - \sum_m \frac{\langle 0|H_{qp}|m\rangle\langle m|H_{qp}|0\rangle}{\epsilon_m}\,, \tag{1.65}$$

where ϵ_m is the energy of the intermediate state $|m\rangle$. In the quasiparticle Hamiltonian H_{qp} only combinations of a creation operator for one side with a annihilation operator for the other side occur. Therefore everytime the quasiparticle part acts on the ground state, we have a anihilation operator acting on the ground state yielding $H_{qp}|0\rangle = H_{qp}^\dagger|0\rangle = 0$ so that the quasi particle part vanishes at zero temperature. Using the symmetry of the Hamiltonian under spin rotation we evaluate the pair contribution to be

$$\langle \delta H_p \rangle \;=\; -2g^2 \sum_m \sum_{kk'} |B_{kk'}|^2 \frac{\langle 0|\gamma_{k1,l}\gamma_{k'0}|m\rangle\langle m|\gamma_{k'0}^\dagger\gamma_{k1,l}^\dagger|0\rangle}{\epsilon_m} \;=\; -2g^2 \sum_{kk'} \frac{|B_{kk'}|^2}{E_k + E_{k'}}\,. \tag{1.66}$$

We evaluate the squared norm $|B_{kk'}|^2$ with relations 1.42 and 1.43 for real v_k. We find

$$|B_{kk'}|^2 = \frac{1}{2}\left[1 - \frac{\xi_k\xi_{k'}}{E_kE_{k'}} + \cos(\varphi)\frac{\Delta^2}{E_kE_{k'}}\right]. \tag{1.67}$$

The linear part in electron energies vanishes during summation over all possible k vectors and the zero temperature energy shift due to pair tunneling is

$$\langle \delta H_p \rangle = -2\frac{g^2}{2}\sum_{kk'}\frac{1}{E_k + E_{k'}} - 2\cos(\varphi)\frac{g^2}{2}\sum_{kk'}\frac{\Delta^2}{E_kE_{k'}}\frac{1}{E_k + E_{k'}} \tag{1.68}$$

The first expression is a constant energy shift we are not interested in and therefore won't analyze any further. The second expression proportional to the cosine of the phase difference is exactly the energy shift $-E_J\cos(\varphi)$ we used in the section on superconducting qubits. With our approach we can calculate the the Josephson energy E_J based on a microscopic model. Evaluating the sums in previous expression yields

$$E_J = 2\frac{g^2}{2}N_{0,l}N_{0,r}\int\int d\xi_l d\xi_r \frac{\Delta^2}{E_l E_r}\frac{1}{E_l+E_r}\,. \tag{1.69}$$

with the substitution $\sinh\Theta_l = \xi_i/\Delta$ we find

$$E_J = 2\frac{g^2}{2}\Delta N_{0,l}N_{0,r}\int\int d\Theta_l d\Theta_r \frac{1}{\cosh(\Theta_l)+\cosh(\Theta_r)} = g^2\pi^2\Delta N_{0,l}N_{0,r} \tag{1.70}$$

the well known Ambegaokar-Baratoff relation for the Josephson energy E_J at zero temperature.

Calculating the effect at elevated temperatures is a little more tricky but since we will apply the same technique to calculate dephasing rates, we will give a derivation at this point. To begin with, we define the combined right-left Greens function

$$G_{rl}(k,k',\tau) = -\langle T_\tau \Psi_{k,r}(\tau)\Psi^\dagger_{k',l}\rangle = -\begin{pmatrix} \langle T_\tau c_{k\uparrow,r}(\tau)c^\dagger_{k'\uparrow,l}\rangle & \langle T_\tau c_{k\uparrow,r}(\tau)c_{-k'\downarrow,l}\rangle \\ \langle T_\tau c^\dagger_{-k\downarrow,r}(\tau)c^\dagger_{k'\uparrow,l}\rangle & \langle T_\tau c^\dagger_{-k\downarrow,r}(\tau)c_{-k'\downarrow,l}\rangle \end{pmatrix}, \tag{1.71}$$

and note that the thermal expectation value for the tunneling Hamiltonian can be expressed in terms of the diagonal elements of the right-left Greens function:

$$\begin{aligned}\langle \delta H_T\rangle &= g\sum_{kk'\sigma} e^{i\varphi/2}\langle c_{k\sigma,l}c^\dagger_{k'\sigma,r}\rangle + e^{-i\varphi/2}\langle c_{k'\sigma,r}c^\dagger_{k\sigma,l}\rangle = g\sum_{kk'\sigma} e^{i\varphi/2}\langle c_{-k'\uparrow,r}c^\dagger_{-k\uparrow,l}\rangle \\ &+ e^{i\varphi/2}\langle c_{k\downarrow,l}c^\dagger_{k'\downarrow,r}\rangle = 2\sum_{kk'} e^{-i\varphi/2}G_{rl,22}(k,k',0^-) - e^{-i\varphi/2}G_{rl,11}(k,k',0^-)\,. \end{aligned} \tag{1.72}$$

We now proceed as in section 1.2.2 by finding the eof for the left-right as well as the left-left Greens function G_l since those differential equations are coupled due to the tunneling. In Fourier space we find

$$(i\omega_n - \xi_k\tau_3 + \Delta\tau_1)G_l(k,k',i\omega_n) = \delta_{kk'} + g\sum_q \begin{pmatrix} e^{i\varphi/2} & 0 \\ 0 & -e^{-i\varphi/2}\end{pmatrix} G_{rl}(q,k',\tau) \tag{1.73}$$

$$(i\omega_n - \xi_k\tau_3 + \Delta\tau_1)G_{rl}(k,k',i\omega_n) = g\sum_q \begin{pmatrix} e^{-i\varphi/2} & 0 \\ 0 & -e^{i\varphi/2}\end{pmatrix} G_l(q,k',\tau) \tag{1.74}$$

where we identify the BCS Greens function $G_o(k,i\omega_n) = (i\omega_n - \xi_k\tau_3 + \Delta\tau_1)^{-1}$. Since we want to calculate the Josephson effect up to second order in g, we need the Greens

function only linear in g and can solve for the right-left Greens function by taking the left side function only up to zeroth order in g. Therefore we insert G_0 in the eof for the right-left Greens function and obtain

$$G_{rl}(k,k',i\omega_n) = gG_0(k,i\omega_n)\begin{pmatrix} e^{-i\varphi/2} & 0 \\ 0 & -e^{i\varphi/2} \end{pmatrix} G_p(k',i\omega_n)\,. \tag{1.75}$$

With the free BCS Greens function

$$G_0(k,i\omega_n) = \frac{-1}{\omega_n^2+\xi_k^2+\Delta^2}\begin{pmatrix} i\omega_n+\xi_k & -\Delta \\ -\Delta & i\omega_n-\xi_k \end{pmatrix} \tag{1.76}$$

we find the right-left function to be

$$G_{rl}(k,k',i\omega_n) = g\frac{\begin{pmatrix} (i\omega_n+\xi_k)(i\omega_n+\xi_{k'})e^{-i\varphi/2}-\Delta^2 e^{i\varphi/2} & -\Delta(i\omega_n+\xi_k)e^{-i\varphi/2}+\Delta(i\omega_n-\xi_{k'})e^{i\varphi/2} \\ -\Delta(i\omega_n+\xi_{k'})e^{-i\varphi/2}+\Delta(i\omega_n-\xi_k)e^{-i\varphi/2} & -(i\omega_n-\xi_{k'})(i\omega_n--\xi_k)e^{i\varphi/2}+\Delta^2 e^{-i\varphi/2} \end{pmatrix}}{(\omega_n^2+\xi_k^2+\Delta^2)(\omega_n^2+\xi_{k'}^2+\Delta^2)} \tag{1.77}$$

We insert the expression for G_{rl} into equation 1.72 for the energy shift due to tunneling. This yields

$$\langle\delta H_T\rangle = 4g^2\sum_n(\omega_n^2+\Delta^2\cos\varphi)\left(\sum_k\frac{1}{\omega_n^2+\xi_k^2+\Delta^2}\right)^2 \tag{1.78}$$

As in the previous paragraph we neglect the constant energy shift and take into account the term proportional to the cosine only. We evaluate the sum in the k space with integration in energy space and find the Josephson energy at elevated temperatures

$$E_J = 4g^2\pi^2\Delta^2 N_{0,l}N_{0,r}\frac{1}{\beta}\sum_n\frac{1}{\omega_n^2+\Delta^2} \tag{1.79}$$

The sum over Matsubara frequencies can be evaluated as contour integral in the usual way yielding

$$E_J = -2g^2\pi^2\Delta^2 N_{0,l}N_{0,r}\frac{n_F(\Delta)-n_F(-\Delta)}{\Delta} = 2g^2\pi^2\Delta N_{0,l}N_{0,r}\tanh\frac{\beta\Delta}{2} \tag{1.80}$$

which converges to the value obtained for zero temperature for β goes to infinity ($T\to 0$). Obviously, we did not distinguish between pair and single quasiparticle tunneling in the derivation of the temperature dependent Josephson energy. On one hand this makes sense since at elevated temperatures we always have thermally excited quasiparticles above the gap, which explains the factor $\tanh\frac{\beta\Delta}{2}?1-2n_F(\Delta)$ in equilibrium. For non-equilibrium cases we can substitute the Fermi function n_F with a general distribution function $f(E)$ and the hyperbolic tangent is replaced with $1-2f(\Delta)$. On the other

hand, we associate dissipation with single quasiparticle effects since they are joint with real excitations in the superconductors. However, we have a dissipation free process here, thermally influenced by quasi particle excitations but it seems like we have only contributions from Cooper pairs in our derivation. This difficulties in separating single particle from pair effects are already revealing the problems one has in distinguishing between these effects when analyzing qubit decoherence due to tunneling processes since the pair tunneling is included in the qubit Hamiltonian already and one has to avoid double counting.

1.3.3 Quasiparticle tunneling and Qubit (de-)coherence

To analyze the influence of single particle tunneling on a superconducting qubit, we start from the Hamiltonian of Josephson junction in a superconducting circuit which in its microscopic form is

$$H = E_c\hat{n}^2 + H_{0,l} + H_{0,r} + H_T\,. \tag{1.81}$$

We explicitely write every Hamiltonian of interest into above Hamiltonian: The charging energy E_C of the junction, the BCS Hamiltonians of both leads and the tunneling Hamiltonian for the junction. As we've seen in previous section, pair tunneling effects are dominant at low temperatures and we make use of this fact by explicitly pulling out the energy shift due to pair tunneling. The Hamiltonian now reads

$$H = E_c\hat{n}^2 - E_J\cos\varphi + H_{0,l} + H_{0,r} + \tilde{H}_T\,. \tag{1.82}$$

Here, we identify the Josephson junction Hamiltonian we used in the QED section, $H_J = E_C\hat{n}^2 - E_j\cos\varphi$. The new tunneling Hamiltonian $\tilde{H}_T$ should only include single particle effect. The last statement is difficult to quantize or base on a solid mathematical foundation, e.g. we could define $\tilde{H}_T = H_T + E_J\cos\varphi$, which still is hard to handle as we will see. Nevertheless, from this point we will take φ as a quantum mechanical operator and treat the Josephson junction in the way described in section 1.1. Therefore, we can express the system Hamiltonian for a superconducting qubit coupled to the single particle tunneling Hamiltonian as

$$H = H_S + H_R + H_T\,, \tag{1.83}$$

where from now on we will simply use the tunneling Hamiltonian 1.56 in our calculations and keep in mind that we have to be careful with which terms to actually use. H_R is the reservoir Hamiltonian, in this case the BCS leads. This Hamiltonian belongs to the general class of Hamiltonians describing the coupling of a microscopic system, in our case the qubit, to very large reservoirs, the two superconductor in our case, with a coupling Hamiltonian H_C, the tunneling in our case. Therefore, we need a theoretical framework capable of dealing with these kind of systems, so called open

quantum systems. We will develop such a framework in the following chapter allowing us to calculate the time evolution of the microscopic system, without the exact time evolution of the large reservoirs which anyway are more or less undisturbed by the small system.

Chapter 2

2 Open Quantum Systems and the Master Equation

In this chapter we introduce a systematic expansion of the non-unitary time evolution of a quantum system coupled to two (or more) large reservoirs. Therefore we expand the time evolution of the systems density matrix on a Keldysh contour and find a diagrammatic expansion. With this diagrammatic language we are able to describe the time evolution with a propagator Π *obeying a Dyson like equation. With the diagrammatic approach and the Dyson equation we obtain the tools to finally tackle the time evolution of a qubit coupled to quasiparticle degrees of freedom.*

2.1 The Master Equation

In this thesis we want to discuss decoherence of superconducting qubits due to tunneling of single quasiparticles through a Josephson junction, a problem that involves a small system, the qubit, with a limited number of eigenstates coupled to larger systems, the reservoirs. In the specific case of quasiparticle tunneling the reservoirs are two superconducting leads. Throughout this section we will refer to the microscopic system simply as 'system' and talk about the 'full system' if both, reservoirs and microscopic system, are considered. Because we are not interested in the exact time evolution of the reservoirs, we need a systematic way to get rid of uninteresting reservoir degrees of freedom, a step referred to as 'tracing out the environment'. Since their exists an energy transfer between the small system and the connected reservoirs, the time evolution of the system can not be described in closed form without taking into account reservoir degrees of freedom in some way. Hence this kind of system is known as an "open quantum system".

The starting point for our calculation is the equation of motion for the full density

matrix (system and reservoirs), known as the Von Neumann equation:

$$\dot{\rho} = -i\left[H, \rho\right] \tag{2.1}$$

where H is the full system Hamiltonian, which consists of three different parts, namely the system part H_S, the reservoir Hamiltonian H_R and the coupling between reservoir and system H_C:

$$H = H_S + H_R + H_C\,. \tag{2.2}$$

We emphasize that the reservoirs can either provide energy to the system or take energy away from it but will, in general, remain undisturbed due to their large size compared to the small system of interest. This allows us to 'trace out the environment' and introduce the reduced density matrix describing the microscopic systems dynamics:

$$\rho_S(t) = \mathrm{Tr}_R\left\{\rho(t)\right\}\,. \tag{2.3}$$

In this expression, the trace is only taken with respect to the reservoir degrees of freedom. The reduced density matrix contains the relevant information of the system of interest: the behavior of the small system while it is coupled to the large reservoirs. The entire problem is reduced to find the time evolution of the reduced density matrix. In a standard approach one uses the Born-Markov approximation to find a Lindblad form master equation which describes the system dynamics [26]. However, this approach lacks the possibility to make statements about higher order contributions from the coupling Hamiltonian. But exactly this kind of contributions will prove important when it comes to qubit dephasing where first order approximations fail. To overcome the issue with the standard Lindblad approach, we will introduce an alternative approach to the problem. In the following sections we will expand the reduced density matrix time evolution on a Keldysh contour and introduce a diagrammatic language to solve the given problem.

2.1.1 Expansion on Keldysh Contour

This section closely follows the derivation of a diagrammatic expansion from Michael Marthaler [27]. The starting point for our calculation is the thermal average of a general operator $\hat{A}$ which is taken with respect to the full density matrix ρ:

$$\langle\hat{A}(t)\rangle = \mathrm{Tr}\left[\rho(t_0)U^\dagger(t,t_0)\hat{A}U(t,t_0)\right] \tag{2.4}$$

where $U(t,t_0) = T\exp(-i\int_{t_0}^{t} H(t')dt')$ is the full time evolution operator from start time t_0 when the coupling between reservoir and system is switched on to time t and T is the time ordering operator. For a time independent Hamiltonian, the time evolution operator reduces to the well known form $U(t,t_0) = e^{-iH(t-t_0)}$. The trace has to be taken with respect to all states, including reservoir as well as system states. To

simplify our calculations we will assume that the density matrix factorizes at time t_0, $\rho_0 = \rho(t_0) = \rho_S(t_0) \otimes \rho_R(t_0)$, a reasonable assumption hence the coupling is switched off at previous times and without coupling the density matrix factorizes. In addition the initial density matrix becomes less important for long time dynamics in which we are more interested than in short time dynamics. Defining a reduced density matrix for the system implies, that the change of the system due to the coupling is not too large such that the systems eigenstates are still good quantum numbers which can be used to describe the system. Therefore we can assume that the energy scale due to coupling is much weaker than the system and reservoir Hamiltonians. To take into account this smallness, it is convenient to change from the Schrödinger to the interaction picture with respect to H_C

$$\begin{aligned} \tilde{A}(t) &= U_0^\dagger(t,t_0) A U_0(t,t_0)\,, \\ U_0(t,t_0) &= e^{-iH_0(t-t_0)}\,, \\ H_0 &= H_S + H_R\,. \end{aligned} \tag{2.5}$$

Here, $\tilde{A}(t)$ denotes an operator in the interaction picture, $U_0(t,t_0)$ is the time evolution operator of the free system and reservoirs, which, because system and reservoir Hamiltonians commute, factorizes into the product of the free system time evolution $U_S(t,t) = e^{-iH_S(t-t_0)}$ and the reservoir time evolution $U_R(t,t_0) = e^{-iH_R(t-t_0)}$. Using $\tilde{A}(t)$ we can rewrite equation 2.4

$$\langle \hat{A}(t) \rangle = \mathrm{Tr}\left[\rho_0 U_I^\dagger(t,t_0)\tilde{A}(t)U_I(t,t_o)\right] \tag{2.6}$$

with the interaction picture time evolution operator $U_I(t,t_0)$ and its conjugate defined as time ordered exponentials

$$U_I(t,t_0) = T\mathrm{exp}\left\{-i\int_{t_0}^{t}\tilde{H}_C(t')dt'\right\} \tag{2.7}$$

$$U_I^\dagger(t,t_0) = \bar{T}\mathrm{exp}\left\{i\int_{t_0}^{t}\tilde{H}_C(t')dt'\right\}\,. \tag{2.8}$$

T ($\bar{T}$) denotes the (anti-) time ordering operator. The time ordering operator acting on a set of time dependent operators at different time will always re-arrange their sequence in ascending order with respect to their time arguments (anti time ordering: descending order). Now, with a clever choice of $\hat{A}$, we are able to derive the equation of motion for the reduced density matrix directly from eq. (2.6). To accomplish this, we chose the operator $\hat{A}$ to be $\hat{A} = \hat{P}_{ss'} = |s\rangle\langle s'|$, where $|s\rangle$ and $|s'\rangle$ are system eigenstates fulfilling $H_S|s\rangle = E_s|s\rangle$. Now we want to show that the thermal average $\langle \hat{P}_{ss'}(t)\rangle$ equals the matrix element $\rho_{s's}(t) = \langle s'|\rho_S(t)|s\rangle$ of the reduced density matrix. To do this we

start with the matrix element $\rho_{s's}(t)$, explicitly carry out the trace over system states and use the invariance of the trace under cyclic permutation to show this equivalence:

$$\begin{aligned}
\rho_{s's}(t) &= \langle s'|\mathrm{Tr}_R\{\rho(t)\}|s\rangle = \langle s'|\mathrm{Tr}_R\{U\rho_0 U^\dagger\}|s\rangle \\
&= \langle s'|\mathrm{Tr}_R\{U\rho_{R,0}\sum_{qq'}|q\rangle\rho_{qq'}\langle q'|U^\dagger\}|s\rangle = \sum_{qq'}\mathrm{Tr}_R\{\langle s'|U|q\rangle\rho_{R,0}\rho_{qq'}\langle q'|U^\dagger|s\rangle\} \\
&= \sum_{qq'}\mathrm{Tr}_R\{\rho_{R,0}\rho_{qq'}\langle q'|U^\dagger|s\rangle\langle s'|U|q\rangle\} = \mathrm{Tr}\sum_{r,qq'}\rho_{R,0}\rho_{qq'}\langle q'|r\rangle\langle r|U^\dagger\hat{P}_{ss'}U|q\rangle \\
&= \mathrm{Tr}_R\sum_r\langle r|\rho_{R,0}U_I^\dagger\hat{P}_{ss',I}U_I\sum_{qq'}(|q\rangle\rho_{qq'}\langle q'|)|r\rangle = \mathrm{Tr}\{\rho_0 U_I^\dagger\hat{P}_{ss',I}U_I\} \\
&= \langle\hat{P}_{ss'}(t)\rangle \qquad (2.9)
\end{aligned}$$

With the identity 2.9 we are able to derive the time evolution of the density matrix element $\rho_{ss'}(t)$ by use of equation 2.4 for the operator $\hat{P}_{s's}$

$$\rho_{ss'}(t) = \sum_{qq'}\rho_{qq'}(t_0)\langle q'|\mathrm{Tr}_R\left\{\rho_R(t_0)U_I^\dagger(t,t_0)\hat{P}_{s's,I}(t)U_I(t,t_0)\right\}|q\rangle\,, \qquad (2.10)$$

where $\mathrm{Tr}_R\{\dots\}$ is the trace with respect to the reservoirs. We can interpret equation 2.10 as a rate equation for the scattering from a matrix element $\rho_{qq'}$ at a time t_0 into the matrix element $\rho_{ss'}$ at a later time t. We identify this scattering rates with a time evolution operator $\Pi_{qq'\to ss'} = \langle q'|\mathrm{Tr}_R\left\{\rho_R(t_0)U_I^\dagger(t,t_0)\hat{P}_{s's,I}(t)U_I(t,t_0)\right\}|q\rangle$. This evolution operator or propagator propagates the density matrix element $\rho_{qq'}(t_0)$ to the element $\rho_{ss'}(t)$. We will analyze it in more detail in the following sections. Unfortunately equation (2.10) in the current form is unpractical for calculations because of the time ordered exponentials hidden in the time evolution operators. To overcome the issues with the time evolution operators, we expand them into Taylor series and sort the resulting sums into products with the same order in the coupling Hamiltonian H_C. From that expansion we are able to find a diagrammatic expansion for $\rho_{ss'}$ which we can exploit to calculate $\rho_{ss'}$ up to arbitrary orders in H_C. After expanding the

exponentials the interaction time evolution operators read

$$\begin{aligned} U_I(t,t_0) &= T\exp\left\{-i\int_{t_0}^{t} H_C(t')dt'\right\} \\ &= \sum_{n=0}^{\infty}(-i)^n \int_{t_0}^{t} dt_1 \int_{t_0}^{t_1} dt_2 \cdots \int_{t_0}^{t_{n-1}} dt_n [H_C(t_1)H_C(t_2)\cdots H_C(t_n)] \\ U_I^\dagger(t,t_0) &= \bar{T}\exp\left\{i\int_{t_0}^{t} H_C(t')dt'\right\} \\ &= \sum_{n=0}^{\infty}(i)^n \int_{t_0}^{t} dt_1 \int_{t_0}^{t_1} dt_2 \cdots \int_{t_0}^{t_{n-1}} dt_n [H_C(t_n)H_C(t_{n-1})\cdots H_C(t_1)]\,, \end{aligned} \tag{2.11}$$

where we absorbed time ordering operators into integral limits. Inserting above equations in the time evolution for $\rho_{ss'}$ yields

$$\begin{aligned} \rho_{ss'}(t) = \sum_{qq'} \rho_{qq'}(t_0)\langle q'|\mathrm{Tr}_R\{\rho_R(t_0) \sum_{n=0}^{\infty}\sum_{m=0}^{\infty} i^n(-i)^m \int_{t_0}^{t} dt_1 \int_{t_0}^{t_1} dt_2 \cdots \int_{t_0}^{t_{n-1}} dt_n \times \\ \int_{t_0}^{t} dt'_1 \int_{t_0}^{t'_1} dt'_2 \cdots \int_{t_0}^{t'_{m-1}} dt'_m [H_C(t_n)H_C(t_{n-1})\cdots H_C(t_1)] \\ \times \hat{P}_{s's,I}(t)[H_C(t'_1)H_C(t'_2)\cdots H_C(t'_m)]\}|q\rangle\,. \end{aligned} \tag{2.12}$$

This expression is still rather complicated and we further simplify it by introducing a closed Keldysh time contour, see figure 2.1. The contour starts at time t_0 following the upper branch until it reaches the operator $\hat{P}_{s's}$ at time t from where it returns to the initial time following the lower branch. Every vertex at time t_i on the contour represents a coupling Hamiltonian $\tilde{H}_C(t_i)$. The operators are ordered according to their appearence on the contour, such that operators on the upper branch are anti time ordered and always to the left of the operator $\tilde{P}_{s's}(t)$ while operators on the lower branch are automatically time ordered and appear after $\tilde{P}_{s's}(t)$. We introduce the Keldysh time ordering operator T_γ which automatically orders operators according to their position on the Keldysh contour, beginning with the operator most left on the upper branch and ending most left on the lower branch. In addition it applys a minus sign for every vertex on the lower branch, taking care of the minus sign in the time evolution operator U_I. With the Keldysh time ordering we rewrite the time evolution

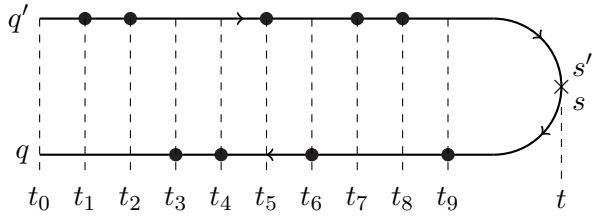

Figure 2.1: Expansion on Keldysh contour: The time evolution from $\rho_{qq'}$ to $\rho_{ss'}$ can be represented as a anti-time ordered evolution from $q' \to s'$, upper branch, and a time ordered evolution from $s \to q$, lower branch. The whole evolution is described with the Keldysh contour starting at t_0 and q', ending at t_0 and q after taking it's way to time t and s, s'. Each vertex on the branches represents a coupling Hamiltonian at time t_i. Operator sequence is determined by position on the contour.

into its final form which we will us as a basis for our diagrammatic technique:

$$\begin{aligned}\rho_{ss'}(t) = \sum_{qq'}\sum_{qq'} \rho_{qq'}(t_0)\langle q'|\mathrm{Tr}_R\{\rho_R(t_0)\sum_{n=0}^{\infty} i^n \int_{t_0}^{t} dt_1 \int_{t_0}^{t_1} dt_2 \cdots \\ \cdots \int_{t_0}^{t_{n-1}} dt_n T_\gamma[H_C(t_1)H_C(t_2)\cdots H_C(t_n)\hat{P}_{s's,I}(t)]\}|q\rangle\,.\end{aligned} \tag{2.13}$$

As an illustrative example on how a diagram translates into mathematical language, we take a look on the 9^{th} order diagram in figure 2.1. The corresponding mathematical expression for this diagram reads:

$$\begin{aligned}\sim (-1)^4 i^9 \langle q'|\mathrm{Tr}_R\{\rho_R(t_0)\int_{t_0}^{t} dt_9 \int_{t_0}^{t_9} dt_8 \cdots \int_{t_0}^{t_2} dt_1 [H_C(t_1)H_C(t_2)H_C(t_5)H_C(t_7)H_C(t_8) \\ \hat{P}_{s's,I}(t)H_C(t_9)H_C(t_6)H_C(t_4)H_C(t_3)]\}|q\rangle\,,\end{aligned} \tag{2.14}$$

where the factors i^9 and $(-1)^4$ arise due to the 9^{th} order and the four vertices on the lower branch respectively. The coupling Hamiltonians in front of $P_{s's}$ are anti time ordered and belong to the upper branch while the remaining time ordered Hamiltonians belong to the lower branch. Integral limits are determined by the position of time t_i on the real time axis, which spans from left to right.

In the next section we will introduce a specific form for the coupling Hamiltonian H_C and derive a set of diagrammatic rules for this form of H_C.

2.1.2 Coupling with N Reservoirs

In this section we will choose a specific but still rather general form for the coupling Hamiltonian and take a closer look on how we can derive diagrammatic rules from this type of coupling. Assume we have N reservoirs with operators $R_{k,\alpha}$, $k = 1, \ldots, N$ in the coupling Hamiltonian (Greek subscripts count different operators acting on the same Hilbert space). In this case we can write the general form of the coupling Hamiltonian as

$$H_C = \sum_i \sum_{\alpha,\ldots,\nu} g_{i,\alpha,\ldots,\nu} \hat{S}_i \hat{R}_{1,\alpha} \hat{R}_{2,\beta} \ldots \hat{R}_{N,\nu} = \sum_i \sum_{\{\alpha\}} g_{i,\{\alpha\}} \hat{S}_i \hat{R}_{\{\alpha\}} = \sum_i \sum_{\{\alpha\}} H_{i,\{\alpha\}} \tag{2.15}$$

where $\hat{S}_i$ is an operator acting in the system Hilbert space, $\hat{R}_{i,\gamma}$ is an operator acting in the Hilbert space of reservoir i and $g_{i,\alpha,\ldots,\nu}$ is a coupling constant. For convenience we defined the "super reservoir" operator $R_{\{\alpha\}} = R_{1,\alpha} R_{2,\beta} \ldots R_{N,\nu}$, where $\{\alpha\}$ is a multi index taking into account the different combinations of reservoir operators. The definition for $H_{i,\{\alpha\}}$ is self-explanatory. Now, in order to derive a set of diagrammatic rules, we take a closer look on the diagram in figure 2.2a, where we labeled the vertices with coupling Hamiltonian indices. This diagram reads ($\langle \ldots \rangle_R = \mathrm{Tr}_R\{\ldots\}$)

$$D = (-1)^2 i^4 \int_{t_0}^{t} dt_4 \int_{t_0}^{t_4} dt_3 \int_{t_0}^{t_3} dt_2 \int_{t_0}^{t_2} dt_1 \times \left\langle \langle q' | \tilde{H}_{i,\{\alpha_1\}}(t_2) \tilde{H}_{j,\{\alpha_2\}}(t_3) \tilde{H}_{k,\{\alpha_3\}}(t_4) \tilde{H}_{l,\{\alpha_4\}}(t_1) | q \rangle \right\rangle_R \tag{2.16}$$

To simplify this expression we make use of the time dependence of the coupling

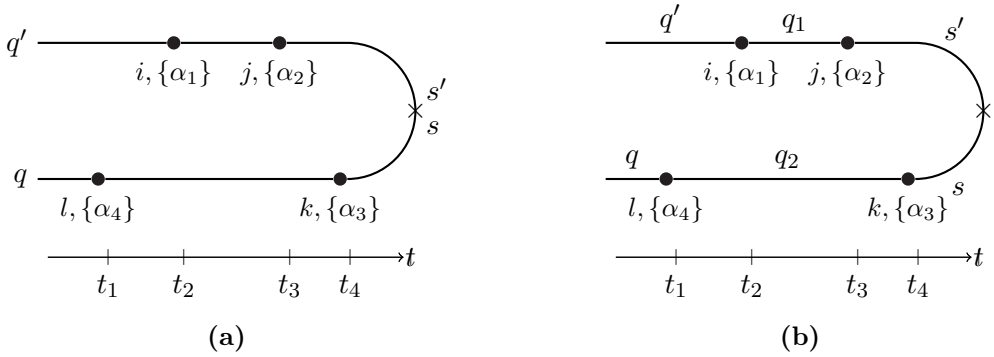

Figure 2.2: Exemplary fourth order diagram with (b) and without (a) internal system indices.

Hamiltonian in the interaction picture, $\tilde{H}_C(t) = U_0(t, t_0) H_C U_0^\dagger(t, t_0)$, which is only determined by the free system and reservoir Hamiltonians. Since the free time evolution

operator factorizes into a system and a reservoir operator according to

$$U_0(t,t_0) = U_{0,S}(t,t_0)U_{0,R}(t,t_0) \tag{2.17}$$

where $U_{0,S}$ acts on system states while $U_{0,R}$ describes the time evolution of the unperturbed reservoirs, the coupling Hamiltonian 2.15 simplifies to

$$\begin{aligned}\tilde{H}_{i,\{\alpha\}}(t) &= g_{i,\{\alpha\}}U_{0,S}(t,t_0)\hat{S}_i U_{0,S}^\dagger U_{0,R}(t,t_0)\hat{R}_{\{\alpha\}}U_{0,R}^\dagger(t,t_0) \\ &= g_{i,\{\alpha\}}\tilde{S}_i(t)\tilde{R}_{\{\alpha\}}(t)\,,\end{aligned} \tag{2.18}$$

and the integrand in equation 2.16 factorizes into a system part and a reservoir part as well, yielding

$$\begin{aligned}D =&(-1)^2 i^4 g_{i,\{\alpha_1\}}g_{j,\{\alpha_2\}}g_{k,\{\alpha_3\}}g_{l,\{\alpha_4\}}\int_{t_0}^{t}dt_4\int_{t_0}^{t_4}dt_3\int_{t_0}^{t_3}dt_2\int_{t_0}^{t_2}dt_1 \\ &\times\langle q'|\tilde{S}_i(t_2)\tilde{S}_j(t_3)\tilde{P}_{s's}(t)\tilde{S}_k(t_4)\tilde{S}_l(t_1)|q\rangle\langle\tilde{R}_{\{\alpha_1\}}(t_2)\tilde{R}_{\{\alpha_2\}}(t_3)\tilde{R}_{\{\alpha_3\}}(t_4)\tilde{R}_{\{\alpha_4\}}(t_1)\rangle_R\,.\end{aligned} \tag{2.19}$$

To evaluate last expression, we take a look on the system and reservoir part of the integrand separately. First, to get rid of the time dependence in the operators $\tilde{S}_i(t)$, we insert a one ($1 = \left\{\sum_q |q\rangle\langle q|\right\}$) in between every pair of system operators and explicitly write the time dependence of each operator with free evolution operators:

$$\begin{aligned}&\langle q'|\tilde{S}_i(t_2)\tilde{S}_j(t_3)\tilde{P}_{s's}(t)\tilde{S}_k(t_4)\tilde{S}_l(t_1)|q\rangle \\ &\quad= \langle q'|U_S(t_2,t_0)\hat{S}_i U_S^\dagger(t_2,t_0)\left\{\sum_{q_1}|q_1\rangle\langle q_1|\right\}U_S(t_3,t_0)\hat{S}_j U_S^\dagger(t_3,t_0)U_S(t,t_0)|s'\rangle \\ &\quad\times\langle s|U_s^\dagger(t,t_o)U_S(t_4,t_0)\hat{S}_k U_S^\dagger(t_4,t_0)\left\{\sum_{q_2}|q_2\rangle\langle q_2|\right\}U_S(t_1,t_0)\hat{S}_l U_S^\dagger(t_1,t_0)|q\rangle\,.\end{aligned} \tag{2.20}$$

Since $U_S(t,t_o)$ is a free time evolution, products of the form $U_S(t,t_0))|q\rangle$ yield a simple oscillatory time dependence with frequency determined by the energy E_q of state q:

$$U_S(t,t_0)|q\rangle = e^{-iE_q(t-t_0)}|q\rangle\,, \tag{2.21}$$

such that the entire time dependence of the system part can be absorbed in oscillatory factors. Equation 2.20 simplifies to its final form

$$\begin{aligned}\langle q'|\tilde{S}_i(t_2)\tilde{S}_j(t_3)\tilde{P}_{s's}(t)\tilde{S}_k(t_4)\tilde{S}_l(t_1)|q\rangle &= \sum_{q_1,q_2}\langle q'|S_i|q_1\rangle\langle q_1|S_j|s'\rangle\langle s|S_k|q_2\rangle\langle q_2|S_l|q\rangle \\ &\times e^{i(E_{q_1}-E_{q'})(t_2-t_0)}e^{i(E_{s'}-E_{q_1})(t_3-t_0)}e^{i(E_s-E_{s'})(t-t_0)}e^{i(E_{q_2}-E_s)(t_4-t_0)}e^{i(E_q-E_{q_2})(t_1-t_0)}\end{aligned} \tag{2.22}$$

At this point, we can identify a couple of diagrammatic rules dealing with 'free time evolution' lines and the system part of a diagram. Every line segment of the Keldysh contour connecting two vertices represents a free time evolution of the system. To every such line segment we assign a system state $|q_i\rangle$ (see 2.2b) and the line reaching from vertex i to vertex j contributes a factor $e^{-iE_{q_i}(t_j-t_i)}$, where $|q_i\rangle$ is the state assigned to the line. In addition, every vertex contributes a factor $\langle q_{in}|\hat{S}_i|q_{out}\rangle$, where $|q_{in}\rangle$ and $|q_{out}\rangle$ are the in- and outgoing state at the vertex respectively. Finally we have to sum over all internal states assigned to the lines.

Compared to the rather simple system part, dealing with the reservoir part of equation 2.19 is more complicated. We have a closer look on the reservoir part and expand the compact notation into full notation:

$$\begin{aligned}&\left\langle \tilde{R}_{\{\alpha_1\}}(t_2)\tilde{R}_{\{\alpha_2\}}(t_3)\tilde{R}_{\{\alpha_3\}}(t_4)\tilde{R}_{\{\alpha_4\}}(t_1)\right\rangle_R \\ &\quad= \left\langle \{R_{1,\alpha_1}(t_2)R_{2,\beta_2}(t_2)\cdots R_{N,\nu_1}(t_2)\}\{R_{1,\alpha_2}(t_3)\cdots R_{N,\nu_2}(t_3)\}\cdots R_{N,\nu_4}(t_1)\}\right\rangle_R .\end{aligned} \tag{2.23}$$

Since the trace is taken with respect to the density matrix at time t_0 which by definition factorizes, we can factorize the trace into traces over each reservoir separately. Therefore, we have to bring the operators for each reservoir close to each other. Hence we have to commute operators belonging to different reservoirs under the trace yielding a minus sign for every pair of commuted fermionic operators. The final sign of the expectation value therefore depends on the number p of fermionic permutations necessary to factorize the trace. After all permutations are performed, the trace over the reservoir states reads

$$\begin{aligned}\left\langle \tilde{R}_{\{\alpha_1\}}(t_2)\tilde{R}_{\{\alpha_2\}}(t_3)\tilde{R}_{\{\alpha_3\}}(t_4)\tilde{R}_{\{\alpha_4\}}(t_1)\right\rangle_R &= \left\langle \tilde{R}_{1,\alpha_1}(t_2)\tilde{R}_{1,\alpha_2}(t_3)\tilde{R}_{1,\alpha_3}(t_4)\tilde{R}_{1,\alpha_4}(t_1)\right\rangle_{R_1} \\ &\times\cdots\times \left\langle \tilde{R}_{N,\nu_1}(t_2)\tilde{R}_{N,\nu_2}(t_3)\tilde{R}_{N,\nu_3}(t_4)\tilde{R}_{N,\nu_4}(t_1)\right\rangle_{R_N}\cdot(-)^p .\end{aligned} \tag{2.24}$$

We reduced the problem of calculating the trace over all reservoir operators to individual traces for each reservoir. These traces can be performed using Wicks theorem, telling us, that a thermal average over a product of fermionic/ bosonic operators can be split into products of two operator thermal averages e.g.:

$$\begin{aligned}&\left\langle \tilde{R}_{1,\alpha_1}(t_2)\tilde{R}_{1,\alpha_2}(t_3)\tilde{R}_{1,\alpha_3}(t_4)\tilde{R}_{1,\alpha_4}(t_1)\right\rangle = \left\langle \underbrace{\tilde{R}_{1,\alpha_1}(t_2)\tilde{R}_{1,\alpha_2}(t_3)}\underbrace{\tilde{R}_{1,\alpha_3}(t_4)\tilde{R}_{1,\alpha_4}(t_1)}\right\rangle \\ &+\left\langle \underbrace{\tilde{R}_{1,\alpha_1}(t_2)\underbrace{\tilde{R}_{1,\alpha_2}(t_3)\underbrace{\tilde{R}_{1,\alpha_3}(t_4)}\tilde{R}_{1,\alpha_4}(t_1)}}\right\rangle + \left\langle \underbrace{\tilde{R}_{1,\alpha_1}(t_2)\underbrace{\tilde{R}_{1,\alpha_2}(t_3)\tilde{R}_{1,\alpha_3}(t_4)}\tilde{R}_{1,\alpha_4}(t_1)}\right\rangle\end{aligned} \tag{2.25}$$

where $AB\cdots\overbrace{C\cdots D}\cdots$ is the contraction between C and D. To evaluate the contractions the pair of contracted operators has to be next to each other under the trace

yielding a minus sign for every necessary fermionic permutation to reach this ordering, e.g. the above example evaluates to

$$\left\langle \tilde{R}_{1,\alpha_1}(t_2)\tilde{R}_{1,\alpha_2}(t_3)\tilde{R}_{1,\alpha_3}(t_4)\tilde{R}_{1,\alpha_4}(t_1)\right\rangle = \left\langle \tilde{R}_{1,\alpha_1}(t_2)\tilde{R}_{1,\alpha_2}(t_3)\right\rangle \left\langle \tilde{R}_{1,\alpha_3}(t_4)\tilde{R}_{1,\alpha_4}(t_1)\right\rangle$$
$$\mp\left\langle \tilde{R}_{1,\alpha_1}(t_2)\tilde{R}_{1,\alpha_3}(t_4)\right\rangle \left\langle \tilde{R}_{1,\alpha_2}(t_2)\tilde{R}_{1,\alpha_4}(t_1)\right\rangle + \left\langle \tilde{R}_{1,\alpha_1}(t_2)\tilde{R}_{1,\alpha_4}(t_1)\right\rangle \left\langle \tilde{R}_{1,\alpha_2}(t_2)\tilde{R}_{1,\alpha_3}(t_4)\right\rangle \tag{2.26}$$

Here, the $-$ and $+$ sign apply for fermionic/ bosonic operators respectively due to the odd number of permutations necessary to connect contracted operators in the middle term.

Since we have to apply Wick's theorem to every reservoir average the number of terms for large numbers of reservoirs N and higher orders in H_C will explode. Therefore, we will restrict ourselves to the case with two reservoirs, which indeed is the case for quasiparticle tunneling in superconducting qubits. In the next section we will find the final set of diagrammatic rules for this case. With this rules we will be able to calculate dephasing and relaxation rates in the next chapter.

2.1.3 Coupling with 2 Reservoirs - Diagrammatic Rules

In this section we analyze the reservoir part of the diagrammatic rules. Therefore we restrict ourselves to a case of two reservoirs coupled to the system. Additionally we will assume both reservoirs to be fermionic and the reservoir operators to be fermionic annihilation/ creation operators $\gamma^{(\dagger)}_{i,k\sigma}$, σ a spin index and k the momentum. We analyze the following coupling Hamiltonian:

$$\begin{aligned} H_C &= \sum_i \sum_{kk'\sigma} g_{i,kk'}\gamma_{2,k'\sigma}\gamma^\dagger_{1,k\sigma}\hat{S}_i + g^*_{i,kk'\sigma}\gamma_{1,k\sigma}\gamma^\dagger_{2,k'\sigma}\hat{S}^\dagger_i \\ &+ \sum_i \sum_{kk'\sigma} \tilde{g}_{i,kk'}\gamma_{1,k\sigma}\gamma_{2,k'-\sigma}\hat{S}_i + \tilde{g}^*_{i,kk'}\gamma^\dagger_{2,k'-\sigma}\gamma^\dagger_{1,k\sigma}\hat{S}^\dagger_i \equiv \sum_i H_{i,qp}\hat{S}_i + H_{i,p}\hat{S}_i + h.c.. \end{aligned} \tag{2.27}$$

This Hamiltonian describes the coupling between two particle exchanging reservoirs and a system described by the operator $\hat{S}_i$. The coupling constant $g_{i,kk'}$ determines the strength of the perturbation. We explicitly split the Hamiltonian into two parts, the quasiparticle Hamiltonian H_{qp} and the pair Hamiltonian H_p. The quasiparticle Hamiltonian describes ordinary particle transfer with a particle transfered from one reservoir to the other while the pair Hamiltonian describes processes involving pairs of quasiparticles. For quasiparticle tunneling through a Josephson junction this distinction is crucial since the pair Hamiltonian contributes to the Josephson effect while the

quasiparticle part describes dissipative processes involving single particle tunneling. Quasiparticle and pair Hamiltonian read

$$H_{qp} = \sum_i \sum_{kk'\sigma} g_{i,kk'} \gamma_{2,k'\sigma} \gamma^\dagger_{1,k\sigma} \hat{S}_i \tag{2.28}$$

$$H_p = \sum_i \sum_{kk'\sigma} \tilde{g}_{i,kk'} \gamma_{1,k\sigma} \gamma_{2,k'-\sigma} \hat{S}_i \tag{2.29}$$

To achieve the given form of the coupling Hamiltonian we applied some assumptions. First we assume a spin independent coupling constant g between reservoirs and system and s-wave superconductivity. Latter implies that quasiparticle pairs as in the pair Hamiltonian always have opposite spin (s-wave) while for the single particle part we assume that no spin flips occur during tunneling since g is spin independent. We will see, that the Hamiltonian describing quasiparticle tunneling in a Josephson junction is exactly of the form 2.27.

In section 2.1.2 we found the diagrammatic rules for the system part of the diagrammatic expansion and postponed the rules for the reservoir parts into this section. As mentioned in previous section, we have to deal with averages of the form

$$\left\langle \gamma_{2,k'\sigma} \gamma^\dagger_{1,k\sigma} \cdots \gamma_{1,k_1\sigma} \gamma^\dagger_{2,k'_1\sigma} \right\rangle \tag{2.30}$$

which we can factorize in two operator expectation values using Wicks theorem. The Hamiltonian 2.27 is linear in reservoir operators for each reservoir inducing an uneven number of creation and annihilation operators for uneven orders in H_C. Since we have non zero expectation values only for combinations of one creation and one annihilation operator uneven orders in H_C vanish and the first non vanishing order is 2^{nd} order in H_C. With the same argument we can show that non vanishing diagrams have to have the same number of H_{qp} and $H^\dagger_{qp}$ as well as the same number of H_p and $H^\dagger_p$. For example the average

$$\left\langle H_{qp} H_p \right\rangle \sim \left\langle \gamma_{2,k'\sigma} \gamma^\dagger_{1,k\sigma} \gamma_{1,k\sigma} \gamma_{2,k'-\sigma} \right\rangle \tag{2.31}$$

vanishes. This statement only holds for diagonal reservoir Hamiltonians $H_{i,0}$, implying $H_{i,0} = \sum_{k\sigma} E_k \gamma^\dagger_{i,k\sigma} \gamma_{i,k\sigma}$. Now we analyze the example diagram in figure 2.3a. Using the system rules from previous section we evaluate the diagram to be

$$\begin{aligned} D_2 = \int_{t_0}^{t} \int_{t_0}^{t_j} dt_j dt_i e^{i\left\{E_{q'}(t_i - t_0) + E_{s'}(t - t_i) + E_s(t_j - t) + E_q(t_0 - t_j)\right\}} \langle q'|S_i|s'\rangle \langle s|S_j|q\rangle \\ \times \sum_{k_i k'_i \sigma_i} \sum_{k_j k'_j \sigma_j} g_{i,k_i k'_i} g^*_{j,k_j k'_j} \left\langle \gamma_{2,k'_i\sigma_i}(t_i) \gamma^\dagger_{1,k_i\sigma_i}(t_i) \gamma_{1,k_j\sigma_j}(t_j) \gamma^\dagger_{2,k'_j\sigma_j}(t_j) \right\rangle . \end{aligned} \tag{2.32}$$

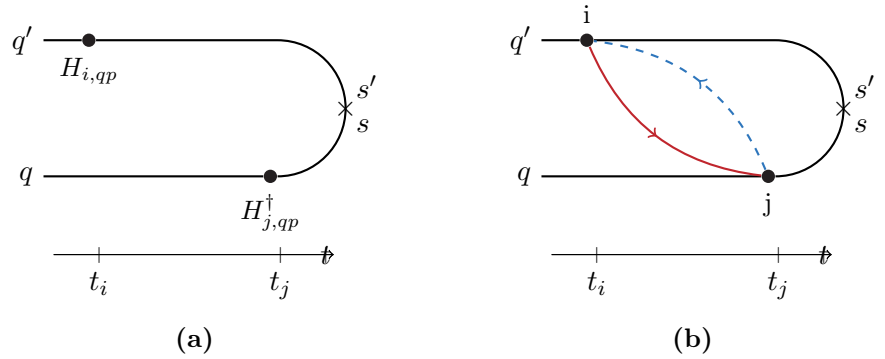

Figure 2.3: a: Example 2^{nd} order diagram with two single quasiparticle vertices. b: The same diagram with contractions between the vertices. Both vertices are quasiparticle vertices with one out and one in port each.

With Wick's theorem we find

$$\left\langle \gamma_{2,k_i'\sigma_i}(t_i)\gamma^\dagger_{1,k_i\sigma_i}(t_i)\gamma_{1,k_j\sigma_j}(t_j)\gamma^\dagger_{2,k_j'\sigma_j}(t_j)\right\rangle = \left\langle \gamma^\dagger_{1,k_i\sigma_i}(t_i)\gamma_{1,k_j\sigma_j}(t_j)\right\rangle \left\langle \gamma_{2,k_i'\sigma_i}(t_i)\gamma^\dagger_{2,k_j'\sigma_j}(t_j)\right\rangle . \quad (2.33)$$

Latter step leads us to the diagrammatic definition of a contraction. We represent a contraction between two vertices with a directed line pointing from annihilation to creation operator. A contraction for reservoir 1 is represented with a solid line while a dashed line represents a contraction for the second reservoir. Due to the form of the coupling Hamiltonian 2.27, every vertex has two ports, one for each reservoir. A 'port' can either be a annihilation (out port, contraction leaving the vertex) or a creation operator (in port, contraction joining the vertex). Therefore we can distinguish between $H_{i,qp}$, $H^\dagger_{i,qp}$, $H_{i,p}$ and $H^\dagger_{i,p}$ due to the connected contraction lines, see figure 2.3b as an illustration. In math, we define a contraction for reservoir i pointing from vertex m to vertex n as the correlation function

$$\gamma_i^>(t_n,t_m) = \left\langle \gamma_{i,k_n\sigma_n}(t_n)\gamma^\dagger_{i,k_m\sigma_m}(t_m)\right\rangle \quad (2.34)$$

$$\gamma_i^<(t_n,t_m) = \left\langle \gamma^\dagger_{i,k_n\sigma_n}(t_n)\gamma_{i,k_m\sigma_n}(t_m)\right\rangle , \quad (2.35)$$

where we have $(\gtrless)$ for $t_n \gtrless t_m$ with respect to the Keldysh contour. If $H_{i,0}$ is a free particle Hamiltonian we can calculate the contractions to be

$$\gamma_i^\gtrless = f_i^\pm(E_{k_n})e^{\pm iE_{k_n}(t_n-t_m)}\delta_{k_nk_m} . \quad (2.36)$$

Here we defined $f_i^+(E) := (1-f_i(E))$ and $f_i^- := f_i(E)$ where $f_i(E)$ is the quasiparticle distribution function for reservoir i, which in (quasi) equilibrium is a Fermi function

but might differ in more complex cases (e.g. non equilibrium quasiparticles). At this point we can put everything together and define a complete set of of rules for our diagrammatic expansion of the reduced density matrix. The diagrammatic rules in time space are

1. Each vertex represents either a pair or a single quasiparticle coupling Hamiltonian. Every quasiparticle vertex has one incoming and one outgoing port belonging to the different reservoirs. Every pair vertex has either two incoming or two outgoing ports. Every out port has to be connected to an in port with a contraction, where the in and out port have to belong to the same reservoir.

2. Every contraction for reservoir i running from vertex m (at time t_m) to vertex n (time t_n) contributes a factor $\gamma_i^{\gtrless}(t_n, t_m)$

3. Every vertex i gives rise to a factor $g^{\alpha}_{i,k_i k_i'}\langle q_{in}|\hat{S}_i|q_{out}\rangle$, where $g^{\alpha}_{i,k_i k_i'}$ is determined by the type of the vertex: $g_{i,k_k k_i'}$ for H_{qp}, $g^*_{i,k_k k_i'}$ for $H^{\dagger}_{qp}$, $\tilde{g}_{i,k_k k_i'}$ for H_p and finally $\tilde{g}^*_{i,k_k k_i'}$ for $H^{\dagger}_{qp}$

4. Every line segment of the Keldysh contour running from vertex m to vertex n contributes a factor $e^{-iE_{q_n}(t_n - t_m)}$ corresponding to free time evolution of the system.

5. Sum over all reservoir indices (momenta k_i, k_i' and spin σ_i), sum over all internal system states q_i and integrate over all internal times t_i with respect to the time ordering determined by the real time axis (choose appropriate integral boundaries $\int_{t_0}^{t}\int_{t_0}^{t_2} dt_2 dt_1 \cdots$).

6. The prefactor is determined by $i^m(-1)^{a+c}$ where m is the total number of vertices, a the number of vertices on the lower branch and c the number of fermionic reservoir line crossings.

2.1.4 Dyson Equation

In this section we use the diagrammatic rules derived in the previous section to find a Dyson like equation for the reduced density matrix $\rho_S(t)$. Therefore we go back to equation 2.13 governing the time evolution of the matrix element $\rho_{ss'}(t)$. We have already defined the time propagator (time evolution operator) $\Pi_{qq'\to ss'}(t, t_o)$ in section 2.1.1. The evolution operator describes the propagation from the matrix element $\rho_{qq'}$ at time t_0 to the matrix element $\rho_{ss'}$ at time t. We can write 2.13 as

$$\rho_{ss'}(t) = \sum_{qq'} \Pi_{qq'\to ss'}(t, t_0)\rho_{qq'}(t_0) \tag{2.37}$$

describing the scattering from all matrix elements into the element $\rho_{ss'}$ and vice versa. For convenience we recall the definition of $\Pi_{qq'\to ss'}(t,t_0)$

$$\Pi_{qq'\to ss'}(t,t_0) \equiv \langle q'|\mathrm{Tr}_R\{\rho_R(t_0)\sum_{n=0}^{\infty} i^n \int_{t_0}^{t} dt_1 \int_{t_0}^{t_1} dt_2 \cdots \\ \cdots \int_{t_0}^{t_{n-1}} dt_n T_\gamma[H_C(t_1)H_C(t_2)\cdots H_C(t_n)\hat{P}_{s's,I}(t)]\}|q\rangle\,. \quad (2.38)$$

In addition we define the superoperator $\Pi(t,t_0)$ which describes the time evolution of ρ_S from t_0 to t. Π is a tensor whose components are given by $\Pi_{qq'\to ss'}$. The final time dependence of ρ_S looks quite simple with this definition:

$$\rho_S(t) = \Pi(t,t_0)\rho(t_0)\,. \quad (2.39)$$

Graphically Π is the sum of all different diagrams, see figure 2.4.

We can distinguish two large classes of diagrams. One class consists of diagrams which have contractions that are connected with each other only with free time evolution segments. These diagrams can be separated into several parts without cutting a contraction line and we call them separable diagrams. In contrary, diagrams which cannot be cut into parts are called inseparable, see figure 2.5 for examples. From this point we proceed by defining the selfenergy Σ as the sum of all inseparable diagrams. Figure 2.6 shows some example diagrams belonging to the self energy. Since every diagram in the expansion for Π is either separable or inseparable we can expand Π in terms of the selfenergy connected by free time evolution lines. We define $\Pi_0(t_2,t_1)$ as the free time propagation superoperator from t_1 to t_2 (Π_0 is the 0^{th} order diagram in the expansion for Π). The expansion of Π in terms of the selfenergy is shown graphically in figure 2.7 and gives rise to a Dyson like equation for the time evolution operator Π. The graphical equation 2.7 has the form of a convolution between Π, Π_0 and Σ:

$$\Pi(t,t_0) = \Pi_0(t,t_0) + \int_{t_0}^{t} dt_1 \int_{t_0}^{t_1} dt_2\, \Pi_0(t,t_1)\Sigma(t_1,t_2)\Pi(t_2,t_0). \quad (2.40)$$

The time evolution superoperator acts on the entire reduced density matrix and hence is a tensor with its size depending on the system size, e.g. for a two state system (qubit) it has 16 components. To get rid of this huge dimensionality it's useful to go

back to the element wise definition. The Dyson equation for each component reads

$$\Pi_{qq'\to ss'}(t,t_0) = \Pi_{0,qq'\to ss'}(t,t_0) + \int_{t_0}^{t} dt_1 \int_{t_0}^{t_1} dt_2\, \Pi_{qq'\to q_2q_2'}(t_2,t_0)\Sigma_{q_2q_2'\to q_1q_1'}(t_1,t_2)\Pi_{0,q_1q_1'\to ss'}(t,t_1) \quad (2.41)$$

This expression can also be represented graphically, see figure 2.8.

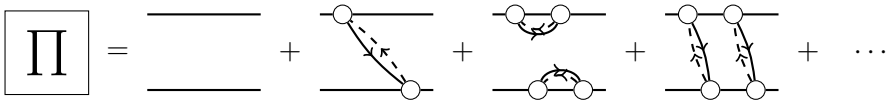

Figure 2.4: The time evolution of the reduced density matrix can be described with the superoperator $\Pi(t,t_0)$. This operator is the sum of all topological distinguishable diagrams.

(a) Inseparable diagram **(b)** Separable diagram

Figure 2.5: Examples for a separable (b) and an inseparable (a) diagram. In (a), no vertical line can be drawn between the leftmost and rightmost vertex without crossing a contraction while (b) consists of two parts connected only with free time evolution lines and can be cut into two parts.

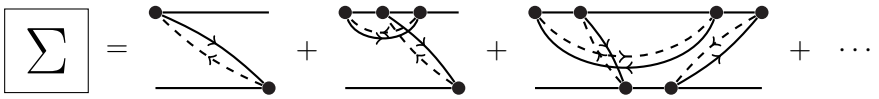

Figure 2.6: Part of the selfenergy Σ with a 2^{nd}, 4^{th} and 6^{th} order diagram.

2.1.5 Master Equation and Markov Approximation

In this section we derive the master equation for the propagator $\Pi(t,t_0)$ and apply the so called Markov approximation to this equation. The Master equation is the equation of motion (eof) for Π. To find the master equation we calculate the time derivate of

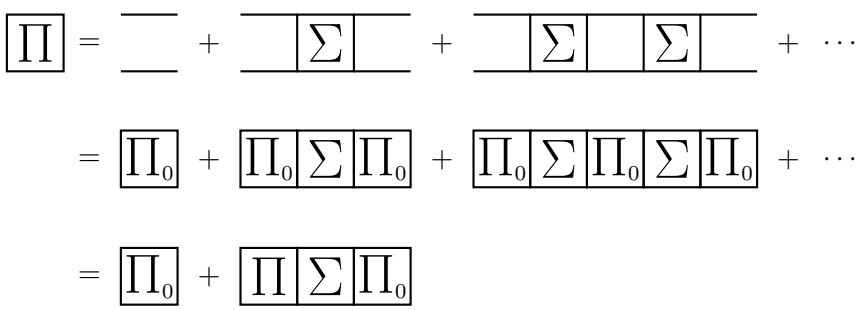

Figure 2.7: Expansion of time evolution operator in terms of the selfenergy and the resulting Dyson equation for the propagator $\Pi(t, t_0)$.

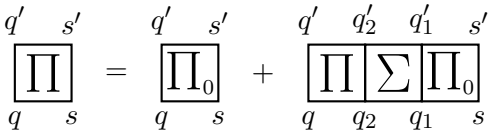

Figure 2.8: Component wise Dyson equation for the time propagator

equation 2.40. To find the time derivate of the entire expression, we investigate it term by term. First, we have to find the time derivate for the free propagator Π_0. The free propagator corresponds to the first diagram in figure 2.7 which, corresponding to the diagrammatic rules, reads

$$\Pi_{0,qq'\to ss'} = \delta_{q's'}\delta_{qs}e^{i(E_s-E_{s'})(t-t_0)}\,. \tag{2.42}$$

Hence, the time derivate of each element of the free propagator is rather simple, $\dot{\Pi}_{0,qq'\to ss'} = i(E_s - E_{s'})\Pi_{0,qq'\to ss'}$. In a compact notation we write

$$\dot{\Pi}_0(t, t_0) = i[H_S, \Pi_0(t, t_0)]\,, \tag{2.43}$$

where the commutator has to be calculated according to

$$\begin{aligned}[H_S, \Pi_{0,qq'\to ss'}] &= \langle q'|H_S U_S(t,t_0)|s'\rangle\langle s|U_S^\dagger(t,t_0)|q\rangle - \langle q'|H_S U_S(t,t_0)|s'\rangle\langle s|U_S^\dagger(t,t_0)H_S|q\rangle \\ &= (E_s - E'_s)\Pi_{0,qq'\to ss'}\,.\end{aligned}$$

In a second step we have to calculate the time derivate of the integral part of equation 2.40. This yields

$$\frac{\partial}{\partial t}\iint\cdots = i\int_{t_0}^{t} dt_1 \int_{t_0}^{t_1} dt_2\,[H_S, \Pi_0(t,t_1)]\Sigma(t_1,t_2)\Pi(t_2,t_0) + \int_{t_0}^{t} dt_1\,\Sigma(t,t_1)\Pi(t_1,t_0)\,, \tag{2.44}$$

where we can identify the first term with the commutator $[H_S, \Pi(t,t_0)]$. This yields the final master equation for the superoperator Π and for its components:

$$\frac{\partial}{\partial t}\Pi(t,t_0) = i[H_S, \Pi(t,t_0)] + \int_{t_0}^{t} dt'\, \Sigma(t,t')\Pi(t',t_0) \tag{2.45}$$

$$\frac{\partial}{\partial t}\Pi_{qq'\to ss'}(t,t_0) = i(E_s - E'_s)\Pi_{qq'\to ss'}(t,t_0) + \int_{t_0}^{t} dt'\, \Sigma_{q_1q'_1\to ss'}(t,t')\Pi_{qq'\to q_1q'_1}(t',t_0)\,. \tag{2.46}$$

To this point, the master equation is still exact since we didn't have to make any approximations to get to equation 2.45. In principle we can calculate the kernel Σ up to any arbitrary order in the coupling. Still, this is a very labor intense process and for many applications a first non-vanishing order (second order in the coupling) calculation is good enough. Yet we will encounter a problem later on, where a first order approximation does not give convergent results and we have to apply renormalization techniques based on the derived diagrammatic approach.

We want to close this section with a very common approximation, the Markov approximation. Assuming that the coherence time of reservoir correlations is short compared to the timescale provided by the propagator, we can approximate $\Pi(t',t_0)$ with $\Pi(t,t_0)\Pi_0^{-1}(t,t')$ in equation 2.45 and the master equation reduces to

$$\begin{aligned}\dot{\Pi}_{qq'\to ss'}(t,t_0) &= i(E_s - E_{s'})\Pi_{qq'\to ss'}(t,t_0) \\ &\quad + \sum_{q_1q'_1}\Pi_{qq'\to q_1q'_1}(t-t_0)\int_{-\infty}^{0}\Sigma_{q_1q'_1\to ss'}(t')\Pi_0^{-1}(t')_{qq'\to ss'}dt'\end{aligned} \tag{2.47}$$

We used time translational symmetry to replace $\Sigma(t,t')$ by $\Sigma(t-t')$. Further we let t_0 go to minus infinity which is possible because we expect the selfenergy to decay rapidly due to short coherence times of the bath such that we do not introduce significant errors with this extension of integral limits. We can write the master equation in the Markov approximation as a simple rate equation:

$$\dot{\Pi}_{qq'\to ss'}(t,t_0) = i(E_s - E_{s'})\Pi_{qq'\to ss'}(t,t_0) - \sum_{q_1q'_1}\Pi_{qq'\to q_1q'_1}(t-t_0)\Gamma_{q_1q'_1\to ss'} \tag{2.48}$$

where we defined the scattering rate from qq' to ss'

$$\Gamma_{qq'\to ss'} = -\int_{-\infty}^{0}\Sigma_{qq'\to ss'}(t')dt'. \tag{2.49}$$

In the upcoming chapter we will calculate the decay rates for a qubit caused by quasiparticles tunneling through a Josephson junction.

Chapter 3

3 Quasiparticle Tunneling & Qubit Decoherence

In this chapter we analyze qubit decoherence due to quasiparticle tunneling. We apply the technique developed in chapter 2 on a qubit coupled to quasiparticle degrees of freedom. The coupling arises due to single particle tunneling trough a Josephson junction and limits qubit coherence times to fundamental limits. First we calculate relaxation and pure dephasing rates in a lowest order approximation in the coupling 3.2. For relaxation this yields reasonable results which are in good agreement with experiment while lowest order dephasing rates are divergent. Hence we analyze qubit dephasing caused by quasiparticle tunneling in more detail in section 3.3. Within Markov approximation we find a self-consistent expression for the pure dephasing rate Γ_{2^*}. In the last section we renounce Markov approximation and find a 'time dependent rate' for qubit dephasing.

3.1 Relaxation and Dephasing - Basics

Finally we have all basics we need to deal with the actual subject of this thesis: Qubit relaxation and dephasing due to quasiparticle tunneling processes in the Josephson junction(s) building the qubit. The starting point for the discussion is the Hamiltonian

$$H = H_S + H_R + \tilde{H}_T \,, \tag{3.1}$$

where we have the qubit Hamiltonian $H_S = \frac{\delta E}{2}\sigma_z$, the BCS Hamiltonians for the two superconductors of the junction (H_R) and the modified tunnel Hamiltonian $\tilde{H}_T = H_T + E_J \cos\hat{\varphi}$, with H_T as in 1.56. We note that the thermal average of the tunneling Hamiltonian H_T gives rise to the Josephson term of the qubit Hamiltonian and we have to be careful about double counting of the corresponding terms. Therefore we introduced the modified tunneling Hamiltonian $\tilde{H}_T$. Nevertheless, we will use the

unmodified tunnel Hamiltonian for our calculations and analyze the influence of the modification later on. To make use of the diagrammatic technique developed in the previous chapter, we have to distinguish qubit operators from reservoir operators in the tunneling Hamiltonian. Therefore we recall the tunnel Hamiltonian once more:

$$H_T = g \sum_{kk'\sigma} e^{i\varphi/2} c_{k\sigma,l} c^\dagger_{k'\sigma,r} + h.c.\,, \tag{3.2}$$

where $c^{(\dagger)}_{k\sigma,\alpha}$ are electron annihilation (creation) operators in the superconducting leads. Since the qubit Hamiltonian is developed in the framework of QED, the phase drop φ across the junction is an operator in qubit space and we have the qubit part of the Hamiltonian, $\hat{S} = e^{i\varphi/2}$. The remains of the tunnel Hamiltonian make the reservoir part $\hat{R}$. Since we want to analyze relaxation and dephasing separately, we have to split the tunnel Hamiltonian into parts producing qubit state flips and parts that leave the qubit state unchanged. First contribute to both relaxation and dephasing while latter produce pure dephasing only. We project the qubit part of the tunnel Hamiltonian onto the spin space provided by the qubit and express the result in terms of the Pauli matrices σ_i. This yields

$$e^{i\varphi/2} = \alpha\sigma_z + (\beta_+\sigma_+ + \beta_-\sigma_-) + \gamma\sigma_0 \tag{3.3}$$

where we have the diagonal Pauli matrices σ_z and σ_0 leaving the qubit state unchanged and the ladder operators $\sigma_\pm$ producing qubit state flips. The remaining parameters are defined as

$$\alpha = \frac{1}{2}\left(\langle 1|e^{i\varphi/2}|1\rangle - \langle 0|e^{i\varphi/2}|0\rangle\right) \tag{3.4}$$

$$\gamma = \frac{1}{2}\left(\langle 1|e^{i\varphi/2}|1\rangle + \langle 0|e^{i\varphi/2}|0\rangle\right) \tag{3.5}$$

$$\beta_+ = \langle 1|e^{i\varphi/2}|0\rangle \tag{3.6}$$

$$\beta_- = \langle 0|e^{i\varphi/2}|1\rangle\,. \tag{3.7}$$

As we will see later it is favorable to express the exponential functions in these expressions with cosine and sine

$$\alpha = \frac{1}{2}\left(c_{11} - c_{00} + i[s_{11} - s_{00}]\right) \tag{3.8}$$

$$\gamma = \frac{1}{2}\left(c_{11} + c_{00} + i[s_{11} + s_{00}]\right) \tag{3.9}$$

$$\beta_+ = c_{10} + is_{10} \tag{3.10}$$

$$\beta_- = c_{01} + is_{01} \tag{3.11}$$

$$c_{ij} = \langle i|\cos(\varphi/2)|j\rangle \tag{3.12}$$

$$s_{ij} = \langle i|\sin(\varphi/2)|j\rangle\,. \tag{3.13}$$

With this projection the tunnel Hamiltonian reads

$$H_T = g\left\{\alpha\sigma_z + (\beta_+\sigma_+ + \beta_-\sigma_-) + \gamma\sigma_0\right\}\sum_{kk'} c_{k\sigma,l}c^\dagger_{k'\sigma,r} + h.c.\,. \tag{3.14}$$

Since we are dealing with BCS superconducting reservoirs electrons do not provide the best basis for calculations. In many situations it is favorable to use Bogolioubov quasiparticles instead. The transformed Hamiltonian in the BCS basis reads (see section 1.3):

$$H_T = H_{qp} + H_p \tag{3.15}$$

$$H_{qp} = g\sum_{kk'\alpha} A_{kk'}\gamma_{k\alpha,l}\gamma^\dagger_{k'\alpha,r} + h.c. \tag{3.16}$$

$$H_p = g\sum_{kk'\alpha} B_{kk'}\epsilon_\alpha\gamma_{k\beta,l}\gamma_{k'\alpha} + h.c.\,. \tag{3.17}$$

with coherence factors

$$A_{kk'} = e^{i\varphi/2}u_{k,l}u_{k',r} - e^{-i\varphi/2}v_{k,l}v_{k',r} \tag{3.18}$$

$$B_{kk'} = e^{i\varphi/2}u_{k,l}v_{k',r} + e^{-i\varphi/2}v_{k,l}u_{k',r}\,. \tag{3.19}$$

Replacing $e^{\pm i\varphi/2}$ with the projection 3.3 yields the corresponding operator for use in the diagrammatic framework.

For the sake of completeness and later use we give the expression for $\cos\varphi$ in terms of Pauli matrices, too:

$$\cos\varphi = \alpha\gamma\sigma_z + \beta_+\gamma\sigma_+ + \beta_-\gamma\sigma_- + \frac{1}{2}\left(\alpha^2+\gamma^2+\beta_+\beta_-\right)\sigma_+ + h.c. \tag{3.20}$$

In the next section we are going to calculate qubit relaxation and dephasing rates in the first non-vanishing order (e.g. 2^{nd} order in H_T). These rates correspond to rates emerging from golden rule calculations and yield reasonable results for qubit relaxation. On the other hand, the dephasing rate in second order suffers from a logarithmic divergence at the superconducting gap for two equal superconductors. To overcome this issue we will renormalize the dephasing rate using our diagrammatic technique in section 3.3. In addition we will calculate a non-Markovian dephasing 'rate' which demonstrates that for pure dephasing the assumption of an exponential decay of the off-diagonal density matrix arguments doesn't hold anymore and there a pure dephasing 'rate' is not defined for all cases.

3.2 Relaxation and Dephasing - Second Order

3.2.1 Golden Rule Rates

Relaxation and dephasing rates in first non vanishing order in H_T can be calculated with the diagrammatic technique presented in previous chapter but may also be derived

from golden rule calculations. In this section we will use Fermi's golden rule to derive the general form of decoherence rates due to quasiparticle tunneling. We will use these calculations to discuss the physical processes corresponding to dephasing and relaxation while we will use the diagrammatic technique to find the exact expressions for the rates in the section after. In figure 3.1 we show examples for different tunneling

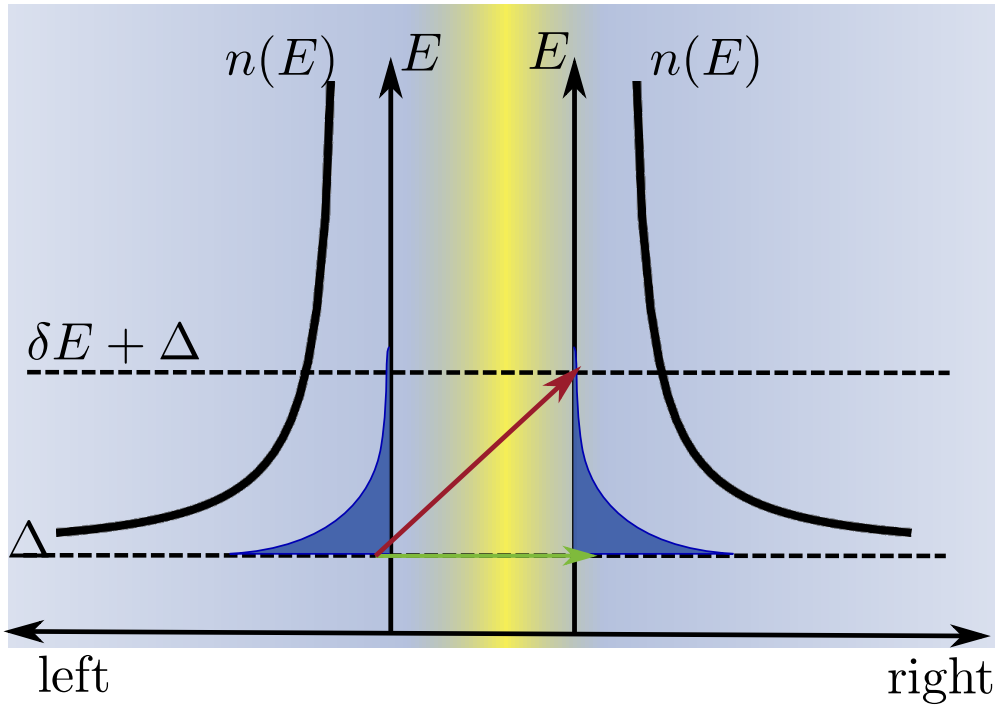

Figure 3.1: Sketch of a Josephson junction with all relevant information for quasiparticle tunneling: BCS density of states $n(E)$ for the superconductors (showing the characteristic divergence at the gap Δ) and the product $n(E)f(E)$ between density of states and quasiparticle distribution function (blue). The area beneath this product gives the number of quasiparticles present at a given energy (dark blue area). In realistic situations the distribution function $f(E)$ decreases rapidly for energies $E > 0$ and quasiparticles are present in a very narrow region above the gap only. The red and green arrow represent the two decoherence processes due to quasiparticle tunneling. The red arrow shows a tunneling process of a quasiparticle close to the gap to an empty state of the second superconductor at an energy $E \sim \Delta + \delta E$. During tunneling the quasiparticle gains an energy δE which it takes from the qubit.The green arrow represents a tunneling process with no energy transfer.

processes, red and green arrow. The red arrow represents a quasiparticle tunneling from an occupied state close to the gap ($E \sim \Delta$) to an empty state in the second

superconductor with energy $E \sim \Delta + \delta E$. During tunneling the quasiparticle gains an energy δE which it takes from the qubit. To preserve energy conservation the qubit has to relax from the excited state to the ground state to provide the energy δE. Therefore processes with energy gain/ loss of the quasiparticle contribute to qubit relaxation. To find the golden rule rate for relaxation we have to sum over all possible quasiparticle transitions from energy E to energy $E+\delta E$ weighted with the corresponding transition matrix for the qubit and the probability $f(E_k)$ for the first state to be occupied and the probability $1 - f(E_{k'})$ for the second state to be empty:

$$\Gamma_1 = \sum_{kk'} |M_{1,kk'}|^2 f(E_k)(1 - f(E_{k'}))\delta(E_{k'} - E_k - \delta E) \tag{3.21}$$

The δ-function ensures energy conservation during the process. We change from summation to integration over energy and find

$$\Gamma_1 = \iint dE_1 dE_2 |M_1(E_1, E_2)|^2 n(E_1) f(E_1) n(E_2)(1 - f(E_2))\delta(E_2 - E_1 - \delta E) \tag{3.22}$$

In latter expression the product of the density of states $n(E)$ and the distribution function $f(E)$ appears. The area beneath this product is a measure for the number of quasiparticles present at a given temperature, see dark blue areas in figure 3.1. As illustrated in the figure, the number of quasiparticles at energies larger than the gap is negligible compared to the number of quasiparticles present close to the gap (both due to the divergence of the density of states as well as the strong decrease of $f(E)$ with increasing energy). Hence most processes relevant for relaxation rates will occur at energies close to the gap. The rates for dephasing are similar but the quasiparticle energies on the left and right side have to be identical (green arrow in figure 3.1) such that we have

$$\Gamma_{2^*} = \sum_{kk'} |M_{2,kk'}|^2 f(E_k)(1 - f(E_{k'}))\delta(E_k - E_{k'}) \tag{3.23}$$

We will calculate the exact rates in the next section so that we do not bother with the exact form of M_i. We want to emphasize that the only relevant quasiparticle parameter (besides the tunneling matrix element g) in the golden rule rates is the distribution function $f(E)$. In thermal equilibrium the distribution function is a Fermi distribution which is close to zero for energies above the gap and small temperatures. Therefore decoherence rates due to equilibrium quasiparticles are negligible at usual qubit operation temperatures. Nonetheless recent experiments clearly show the influence of quasiparticles on qubit relaxation [28][29] also at low temperatures. This can be explained with the presence of non equilibrium quasiparticles in the junction region. Possible sources of quasiparticles are for example leakage from electronic surroundings or quasiparticles generated by infrared radiation. Corresponding distribution functions can be calculated numerically with a Boltzmann equation taking account of quasiparticle generation and relaxation. These calculations are not part of this thesis and we will

simply assume quasi equilibrium distributions for our calculations. In the next section we will use our diagrammatic technique to calculate the exact second order results for qubit relaxation/ dephasing.

3.2.2 Qubit Decoherence - Diagrammatic Notation & General Remarks

Compared to chapter 2 we will change the notation slightly in the following sections. We had introduced the components of the propagator Π as $\Pi_{qq'\to ss'}(t,t_0)$ in previous chapter. This notation is going to be lengthy and confusing. Thus we introduce an alternative notation:

$$\Pi_{qq'\to ss'} \to \Pi_{qs}^{q's'} \,. \tag{3.24}$$

Within this notation the position of the indices in mathematical notation equal their position in the corresponding diagrams such that comparison between mathematical and graphical language is going to be straightforward. In this notation the matrix elements of the reduced density matrix read

$$\rho_{ss'}(t) \to \rho_s^{s'}(t)\,, \tag{3.25}$$

and the governing equation for the reduced density matrix changes to

$$\rho_s^{s'}(t) = \sum_{qq'} \rho_q^{q'}(t_0)\Pi_{qs}^{q's'}(t,t_0) \tag{3.26}$$

Since we deal with a two level system the states $|s\rangle$ represent either the excited state ($s=1$) or the ground state ($s=0$) which simplifies the calculations significantly since all summations over internal indices run over two different states only.

In this section we will calculate decoherence rates using the second order Markov approximation, see equation 2.47. Hence we need the self energy Σ in second order. There are four topological different diagrams in second order for the quasiparticle Hamiltonian

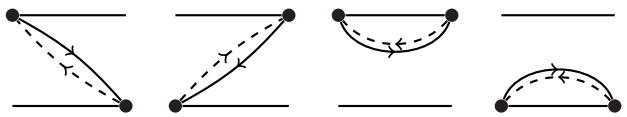

as well as for the pair Hamiltonian

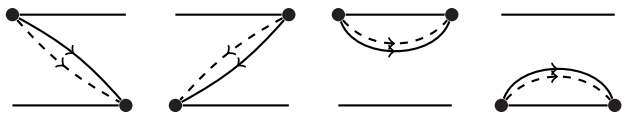

To every diagram there exits another diagram with flipped arrow directions such that their is a total of eight quasiparticle and eight pair diagrams in second order which we have to sum up to find the selfenergy in second order approximation. The diagrams with flipped arrow directions yield the same contributions as the plotted diagrams but with the two superconductors exchanged. For identical superconductors their is no difference between diagramms with flipped arrows. When talking about relaxation every vertex represents a ladder operator $\sigma_\pm$ while for pure dephasing every vertex represents the σ_z Pauli matrix.

3.2.3 Relaxation Rate

In this section we will use our diagrammatic technique to find expressions for relaxation rates in second order which is the lowest non vanishing order in H_T. For pure relaxation we truncate the tunnel Hamiltonian to the dissipative part proportional to the ladder operators $\sigma_\pm$ and split it into quasiparticle and pair Hamiltonian:

$$H_{qp} \equiv g \sum_{kk'\alpha} \left\{ \sigma_+ \underbrace{\left[\beta_+ u_{k,l} u_{k',r} - \beta_-^* v_{k,l} v_{k',r}\right]}_{A^+_{kk'}} + \sigma_- \underbrace{\left[\beta_- u_{k,l} u_{k',r} - \beta_+^* v_{k,l} v_{k',r}\right]}_{A^-_{kk'}} \right\} \gamma_{k\alpha,l} \gamma^\dagger_{k'\alpha,r} + h.c. \tag{3.27}$$

$$H_{p} \equiv g \sum_{kk'\alpha} \epsilon_\alpha \left\{ \sigma_+ \underbrace{\left[\beta_+ u_{k,l} v_{k',r} - \beta_-^* v_{k,l} u_{k',r}\right]}_{B^+_{kk'}} + \sigma_- \underbrace{\left[\beta_- u_{k,l} v_{k',r} - \beta_+^* v_{k,l} u_{k',r}\right]}_{B^-_{kk'}} \right\} \gamma_{k\beta,l} \gamma_{k'\alpha,r} + h.c. \tag{3.28}$$

Since relaxation describes the decay of the qubits excited state, we analyze the density matrix element $\rho_1^1(t)$. Its time evolution is determined by four propagators and the corresponding matrix elements at time t_0:

$$\rho_1^1(t) = \rho_1^1(t_0)\Pi_{11}^{11}(t,t_0) + \rho_0^0(t_0)\Pi_{01}^{01}(t,t_0) + \rho_1^0(t_0)\Pi_{11}^{01}(t,t_0) + \rho_0^1(t_0)\Pi_{01}^{11}(t,t_0)\,. \tag{3.29}$$

Here the first term on the ride hand side (rhs) describes decay of the matrix element ρ_1^1 while the second term describes qubit excitation from the ground to the excited state due to the reservoirs. The last two terms describe scattering from off diagonal elements into diagonal elements and belong to dephasing. They only occur if we have σ_z as well as $\sigma_\pm$ coupling at the same time. In our calculations we will restrict the tunneling Hamiltonian to either its dissipative part ($\sim \sigma_\pm$) contributing to relaxation or to its non dissipative part $\sim \sigma_z$ contributing to pure dephasing. Therefore the last

two terms of the rhs will always vanish in our calculations and we will neglect them from this point on. In Markov approximation (equation 2.47) the Master equations for the remaining two propagators read

$$\dot{\Pi}_{11}^{11}(t) = \Pi_{11}^{11}(t) \int_{-\infty}^{0} dt' \Sigma_{11}^{11}(t') + \Pi_{01}^{01}(t) \int_{-\infty}^{0} dt' \Sigma_{10}^{10}(t') \tag{3.30}$$

$$\dot{\Pi}_{01}^{01}(t) = \Pi_{01}^{01}(t) \int_{-\infty}^{0} dt' \Sigma_{00}^{00}(t') + \Pi_{11}^{11}(t) \int_{-\infty}^{0} dt' \Sigma_{01}^{01}(t') \,. \tag{3.31}$$

Hence one has to calculate the second order diagrams for the four surviving selfenergy components which than can be used to find the rates defined by the time integrals over those selfenergies. These four rates govern the entire time evolution of matrix element $\rho_1^1(t)$. Qubit decay or relaxation is described by the rate $\int_{-\infty}^{0} dt' \Sigma_{10}^{10}(t')$ which describes relaxation from the excited to the ground state.

We show now how to calculate the diagrams, selfenergy and finally the relaxation rate for the component $\Sigma_{10}^{10}(t)$. The four quasiparticle diagrams contributing to this specific component of Σ are

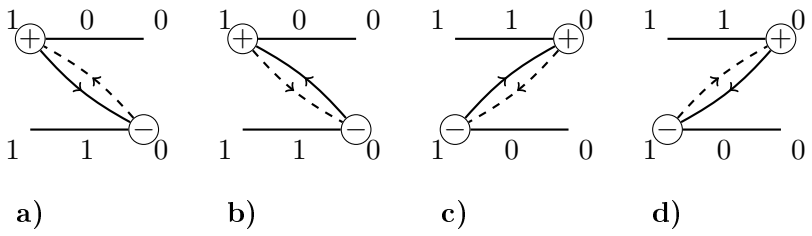

Here numbers (0 and 1) represent the qubit states while the nodes are labeled with the ladder operator (+ or −) corresponding to the vertex (their exists only one possibility at each vertex since e.g. $\sigma_+|1\rangle = 0$). First we evaluate diagrams **a)** and **b)** and find

$$\begin{aligned} a) + b) = -g^2 \langle 1|\sigma_+|0\rangle\langle 0|\sigma_-|1\rangle \sum_{kq\alpha} \Big\{ & |A_{kq}^{+}|^2 \gamma_k^{>}(t-t')\gamma_q^{<}(t'-t) e^{-i\delta E(t-t')} \\ & + |A_{kq}^{-}|^2 \gamma_k^{<}(t'-t)\gamma_q^{>}(t-t') e^{-i\delta E(t-t')} \Big\} \end{aligned} \tag{3.32}$$

The remaining diagrams **c)** and **d)** yield the same contribution but with t and t' exchanged. With the explicit form of $\gamma_k^{\gtrless}(t-t') = f^{\pm} e^{iE_k(t-t')}$ we note that **c)** and **d)** are the complex conjugate of **a)** and **b)**. Using this and interchanging k and q in

the second term (which is possible since we assume identical superconductors on both sides) we obtain the final form for Σ_{01}^{01}:

$$\Sigma_{10}^{10}(t-t') = -2g^2 \sum_{kq\sigma} (|A_{kq}^{+}|^2 + |A_{kq}^{-}|^2) f_q(1-f_k) \mathrm{Re}\left\{ e^{i(E_k - E_q - \delta E)(t-t')} \right\} . \quad (3.33)$$

The corresponding decay rate is defined in equation 2.49 and yields a time integral which we can solve using the Sokhotski–Plemelj theorem

$$\int_0^\infty g(E) e^{i(E-\omega)} dt' = \pi g(E)\delta(E-\omega) - iP\frac{g(E)}{E-\omega}. \quad (3.34)$$

Here $P\frac{1}{x}$ denotes the Cauchy principal value. From equation 3.33 we know that the decay rate is purely real such that the principal values of former expression vanish. Changing summation over k-vectors into integration over energies yields

$$\sum_{kq\sigma} \to 2 \int_{-\infty}^{\infty} \int_{-\infty}^{\infty} d\xi_1 d\xi_2 N(\xi_1) N(\xi_2) \to 8N_0^2 \int_0^\infty \int_0^\infty d\xi_1 d\xi_2.$$

Here $N(\xi_k)$ is the electron density of states in the superconductor and ξ_k are electron energies. In the second step we used that electrons participating in the tunneling processes are close to the Fermi surface and replaced $N(\xi)$ with it's value at the Fermi surface $N(0) = N_0$. In the second step we used that the functions we integrate depend either linear ($A_{kq} \sim \xi_k/E_k$) or quadratic on electron energies ξ_k. Integrating from $infty$ to ∞ kills summands linear in ξ while for the quadratic part we can change the region of integration to $[0,\infty]$ and multiply a factor 2. In a final step we change the integration variables from electron energies ξ_k to quasi particles energies $E_k = \sqrt{\xi_k^2 + \Delta^2}$ yielding

$$8N_0^2 \int_0^\infty \int_0^\infty d\xi_1 d\xi_2 \to 8N_0^2 \int_\Delta^\infty \int_\Delta^\infty dE_1 dE_2 \, n(E_1) n(E_2) \quad (3.35)$$

with the normalized quasi particle density of states $n(E) = E/\sqrt{E^2 - \Delta^2}$. We assume that there occur no transitions with energy transfer $\delta E > 2\Delta$ so that we can ignore 'band-to-band' transitions from the Cooper pair condensate into the quasi particle band. This process would describe breaking of a Cooper pair leaving a hole in the condensate and free quasiparticles above the gap. A process requiring an energy of 2Δ. Such processes would require qubit transition frequencies $\delta E \geq 2\Delta$ which is not reasonable for any real qubit. To obtain our final result for the relaxation rate we need the coherence factors $|A_{kk'}^{\pm}|^2$. Using equation 3.27 we find

$$|A_{kq}^{\pm}|^2 = |\beta_+|^2 u_{k,l}^2 u_{q,r}^2 + |\beta_-|^2 v_{k,l} v_{q,r} - 2\mathrm{Re}(\beta_+\beta_-) u_{k,l} u_{q,r} v_{k,l} v_{q,r} \, . \quad (3.36)$$

With the definitions 3.8 and using $|c_{10}|^2 = |c_{01}|^2$ (which holds for the sine terms as well) the coherence factors read

$$|A_{kq}^{\pm}|^2 = |c_{10}|^2(u_{k,l}u_{q,r} - v_{k,l}v_{q,r})^2 + |s_{10}|^2(u_{k,l}u_{q,r} + v_{k,l}v_{q,r})^2 \,. \tag{3.37}$$

With the identity

$$(u_k u_q \pm v_k v_q)^2 = \frac{1}{2}(1 \pm \frac{\Delta^2}{E_k E_q})$$

we can further simplify the coherence factors to their final form:

$$|A_{kq}^{\pm}|^2 = |c_{10}|^2 \frac{1}{2}\left(1 - \frac{\Delta^2}{E_k E_q}\right) + |s_{10}|^2 \frac{1}{2}\left(1 + \frac{\Delta^2}{E_k E_q}\right) . \tag{3.38}$$

Now we can plug all the ingredients together to find our final result for the qubit relaxation rate due to quasiparticle tunneling:

$$\Gamma_1 = \Gamma_{10}^{10} = 16\pi N_0^2 g^2 \int_{\Delta}^{\infty}\int_{\Delta}^{\infty} \frac{(EE' - \Delta^2)|c_{10}|^2 + (EE' + \Delta^2)|s_{10}|^2}{EE'} \times n(E)n(E')f(E)(1 - f(E'))\delta(E' - E - \delta E) \tag{3.39}$$

This rate is exactly of the form we have already derived with Fermi's golden rule, see 3.22: We have the probability $f(E)$ to find a quasiparticle at energy E, the probability of an empty state at an energy $E + \delta E$ (forced by the delta function) and the density of states at both energies yielding the number of available quasiparticles for these tunneling processes. The qubit itself influences the relaxation rate solely due to the matrix elements $|c/s_{01}|^2$ which depend on the qubit Hamiltonian and the corresponding parameters and eigenfunctions. We will calculate the matrix elements later for a Transmon as an example.

Here we want to proceed by taking a look on the low energy limit of the relaxation rate. We assume that the qubit transition energy δE is way smaller than the superconducting gap and the distribution function has finite values only in a narrow region above gap such that $1 - f(E) \approx 1$ and $f(E) \approx 0$ for $E > \Delta$. In this case the main contribution to the integral arises from energies which fulfill $E - \Delta \ll \delta E$ and we can approximate one energy integration according to

$$2N_0 \int_{\Delta}^{\infty} dE n(E)f(E)\cdots \to n_{qp}\int_{\Delta}^{\infty} dE\delta(E - \Delta)\cdots \tag{3.40}$$

with the quasiparticle density

$$n_{qp} = 2N_0 \int_{\Delta}^{\infty} dE n(E)f(E)\,. \tag{3.41}$$

In the low energy limit we find a simple form for the relaxation rate, which very well fits experimental data:

$$\Gamma_1 = 8N_0\pi g^2 n_{qp} n(\Delta+\delta E)\frac{\delta E|c_{01}|^2 + (2\Delta+\delta E)|s_{01}|^2}{\Delta+\delta E} \tag{3.42}$$

Equation 3.42 is our final result for the qubit relaxation rate due to quasiparticle tunneling. The remarkable feature is the linear dependence on the quasiparticle density n_{qp} which can be verified experimentally and has proven to be consistent with experimental data [10][11][12].

At this point one question remains: what about the pair Hamiltonian? Of course this Hamiltonian already had its part generating the Josephson term but on the other hand one may argue that either one takes into account only the Josephson effect at zero temperature or one had to pay attention to the quasiparticle Hamiltonian as well when it comes to the Josephson effect at elevated temperatures. Hence we will calculate the relaxation rates due to the pair Hamiltonian and will analyze that rate with respect to the fact that the pair Hamiltonian already has been used to a certain degree. Similar to the quasiparticle induced rate there is a total of four diagrams contributing to the relaxation rate due to pair tunneling. The selfenergy is similar to the one for the quasiparticle Hamiltonian:

$$\begin{aligned}\Sigma_{10}^{10}(t-t') = -2g^2\sum_{kq\alpha}|B_{kq}|^2\Big\{&\big(1-f(E_k)\big)\Big(1-f(E_q)\Big)\,\mathrm{Re}(e^{i(E_k+E_q+\delta E)(t-t')})\\ &+f(E_k)f(E_q)\mathrm{Re}(e^{i(E_k+E_q-\delta E)(t-t')})\Big\}\end{aligned} \tag{3.43}$$

The coherence factor $|B_{kq}^{\pm}|^2$ equals the quasiparticle coherence factor $|A_{kq}^{\pm}|^2$ and the time integration arising from the Markov approximation yields the relaxation rate due to the pair tunneling Hamiltonian:

$$\begin{aligned}\Gamma_1 = 16\pi N_0^2 g^2 \int_{\Delta}^{\infty}\int_{\Delta}^{\infty}&\frac{(EE'-\Delta^2)|c_{10}|^2 + (EE'+\Delta^2)|s_{10}|^2}{EE'}n(E)n(E')\\ \times&\Big\{(1-f(E))(1-f(E'))\delta(E'+E+\delta E) + f(E)f(E')\delta(E'+E-\delta E)\Big\}\end{aligned} \tag{3.44}$$

One can easily see that this rate vanishes since the arguments of both δ-functions can never be zero. With $E \geq \Delta$ the argument of the first function is always greater than zero while for the second δ-function we have $E+E' \geq 2\Delta \gg \delta E$. Thus both δ-functions give no contribution and the relaxation rate due to the pair Hamiltonian vanishes as one would expect since pair tunneling is a coherent non dissipative process.

3.2.4 Dephasing Rate

In previous section we successfully applied a second order (golden rule) approximation to qubit relaxation due to single quasiparticle tunneling through the junction. Hence we apply the same approximation to pure qubit dephasing which describes off diagonal element decay of the density matrix. For pure dephasing we truncate the tunnel Hamiltonian to the part proportional to σ_z,

$$H_{qp} = \sigma_z g \sum_{kq\alpha} \frac{1}{2} \underbrace{\Big\{ \left[c_{11} - c_{00} + i(s_{11} - s_{00})\right] u_{k,l} u_{q,r} - \left[c_{11} - c_{00} - i(s_{11} - s_{00})\right] v_{k,l} v_{q,r} \Big\}}_{A^z_{kq}} \gamma_{k\alpha,l} \gamma^\dagger_{q\alpha,r} + h.c. \tag{3.45}$$

and analyze the off diagonal density matrix elements. We will focus on one off diagonal element, namely $\rho^1_0(t)$:

$$\rho^1_0(t) = \rho^1_0(t_0)\Pi^{11}_{00}(t,t_0) + \rho^0_1(t_0)\Pi^{01}_{10}(t,t_0) + \rho^1_1(t_0)\Pi^{11}_{10}(t,t_0) + \rho^0_0(t_0)\Pi^{01}_{00}(t,t_0) \tag{3.46}$$

Since we consider σ_z coupling solely no spin-flips occur and only one propagator survives, namely $\Pi^{11}_{00}(t,t_0)$. Therefor, as for the propagators, only selfenergy components without any spin flips survive and the equation of motion for the only surviving propagator in Markov approximation is

$$\dot{\Pi}^{11}_{00}(t,t_0) = \Pi^{11}_{00} \left\{ i\,\delta E + \int_{-\infty}^{0} dt' \Sigma^{11}_{00}(t') e^{-i\,\delta E\, t'} \right\} \tag{3.47}$$

Altogether there are eight diagrams contributing to the selfenergy from which we plot four here since the remaining four can be obtained by simply changing all arrow directions. The four diagrams we want do discuss in more detail are

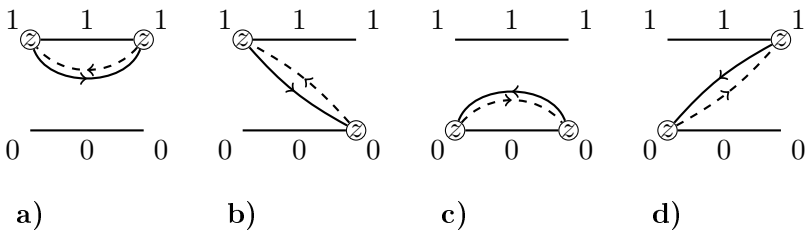

where we begin with diagrams **a)** and **b)**. With our diagrammatic rules we obtain their contributions

$$\mathbf{a)} \quad = -2g^2\langle 1|\sigma_z|1\rangle\langle 1|\sigma_z|1\rangle \sum_{kq} |A^z_{kq}|^2 \gamma^>_k(t-t')\gamma^<_q(t'-t)e^{i\,\delta E(t-t')} \tag{3.48}$$

$$\mathbf{b)} \quad = \; 2g^2\langle 1|\sigma_z|1\rangle\langle 0|\sigma_z|0\rangle \sum_{kq} |A^z_{kq}|^2 \gamma^>_k(t-t')\gamma^<_q(t'-t)e^{i\,\delta E(t-t')}\,. \tag{3.49}$$

Due to the σ_z matrix elements the second diagram obtains an additional minus sign such that both end up with the same sign. Diagrams **c)** and **d)** yield the same contribution with t and t' exchanged while the four diagrams we didn't show yield the same contribution as diagrams **a) - d)** but with left and right superconductor exchanged. Since we assume identical superconductors we obtain the self energy Σ^{11}_{00}

$$\Sigma^{11}_{00} = -16g^2 \sum_{kq} |A^z_{kq}|^2 (1-f(E_k))f(E_q)\mathrm{Re}\left(e^{i(E_k-E_q)(t-t')}\right) e^{i\,\delta E(t-t')} \tag{3.50}$$

The coherence factor $|A^z_{kq}|^2$ differs from the factors occurring for relaxation rates only due to the matrix elements of sine and cosine of the phase across the junctions. We find it to be

$$\begin{aligned} |A^z_{kq}|^2 &= \frac{1}{4}(c_{11}-c_{00})^2(u_{k,l}u_{q,r}-v_{k,l}v_{q,r})^2 + \frac{1}{4}(s_{11}-s_{00})^2(u_{k,l}u_{q,r}+v_{k,l}v_{q,r})^2 \\ &= \frac{1}{4}c^2\frac{1}{2}\left(1-\frac{\Delta^2}{E_kE_q}\right) + \frac{1}{4}s^2\frac{1}{2}\left(1+\frac{\Delta^2}{E_kE_q}\right) \end{aligned} \tag{3.51}$$

with the definition $c^2 = \frac{1}{4}(c_{11}-c_{00})^2$ and likewise for the sine elements. We calculate the dephasing rate according to $\Gamma_{2^*} = \int_{-\infty}^{0} dt'\Sigma(t')e^{-i\,\delta E\,t'}$ and find

$$\Gamma_{2^*} = 16g^2\pi \sum_{kq} |A^z_{kq}|^2 (1-f(E_k))f(E_q)\delta(E_k-E_q)\,. \tag{3.52}$$

As usual we convert the summation into integration over energies and find our final result for the dephasing rate

$$\begin{aligned} \Gamma_{2^*} = 32N_0^2g^2\pi \int_\Delta^\infty \int_\Delta^\infty dEdE' &\frac{(EE'-\Delta^2)c^2 + (EE'+\Delta^2)s^2}{EE'} \\ &\times n(E)n(E')f(E')(1-f(E))\delta(E-E')\,. \end{aligned} \tag{3.53}$$

We analyze the dephasing rate separate for the part proportional to c^2 and the one proportional to s^2 since they show entirely different behavior. We begin with the cosine part since it is of good nature and can be treated without special care. The remaining

part of the dephasing rate will induce difficulties since it is divergent at the gap Δ and we will find ourselves in need for more subtle methods to get rid of that divergence. But let's first investigate the fair part proportional to c^2. First we evaluate one integral using the δ-function. This yields

$$\begin{aligned}\Gamma_{2^*,c} &= 32N_0^2g^2\pi c^2\int_\Delta^\infty dE\frac{E^2-\Delta^2}{E^2}\frac{E}{\sqrt{E^2-\Delta^2}}(1-f(E))n(E)f(E)\\ &= 32N_0^2g^2\pi c^2\int_\Delta^\infty dE(1-f(E))f(E)\approx 32N_0^2g^2\pi c^2 f(\Delta)\delta f\,,\end{aligned} \tag{3.54}$$

with the width δf of the distribution function. The remaining integral in the last expression (before the approximation $\int\sim f(\Delta)\delta f$) for the dephasing rate is convergent in any case and the dephasing rate is well defined. In the last step we approximated the integral with its value at the gap since the distribution function vanishes rapidly at higher energies. Since the distribution function is very small even at the gap it is obvious that the dephasing rate arising from quasiparticles and the cosine matrix elements c_{11} and c_{00} only is very small compared to the relaxation rate if not the matrix elements are huge compared to the corresponding matrix elements c_{01} and s_{01} appearing in the relaxation rate. We will compare matrix elements later in the section on the transmon qubit where we will see that indeed matrix elements for dephasing are way smaller than elements appearing in relaxation. Though we want to make a short remark on the matrix elements at this point. If the qubit Hamiltonian is symmetric in the phase difference φ across the junction the resulting wave functions will all have a certain parity in φ. Therefore all matrix elements of the form $\langle i|\sin(\varphi/2)|i\rangle$ and $\langle 0|\cos(\varphi/2)|1\rangle$ will vanish for such a qubit. A qubit which falls into this class is e.g. the transmon. More details, as mentioned before, in section 4. So finally we have to deal with the part of the dephasing rate proportional to s^2 (although this matrix elements vanish in many cases). Again we use the δ-function to eliminate on energy integral leaving us with following expression for the sine part of the dephasing rate:

$$\Gamma_{2^*,s} = 32N_0^2g^2\pi s^2\int_\Delta^\infty dE\frac{E^2+\Delta^2}{E^2-\Delta^2}f(E)(1-f(E)) \tag{3.55}$$

Unfortunately the integral appearing in last expression has a logarithmic divergence at the gap and cannot be calculated. To overcome this issue we will improve our second order approximation in the next section and will find a self-consistent dephasing rate which is well defined.

3.3 Dephasing

Up to now we have calculated relaxation and dephasing rates in second order Markov approximation. While everything is fine for relaxation we had to realize that the

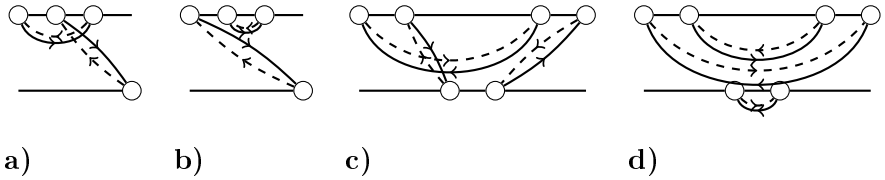

Figure 3.2: a) and c) are examples for diagrams not belonging to the nested class while b) and d) are nested.

dephasing rate obtained within this approximation is not well defined in any case but lacks of a logarithmic divergence. The goal of this section is to find dephasing rates which are defined in any case. In a first step we will re-normalize the second order results to obtain a self-consistent rate. We find a rate that coincides with a self-consistent rate obtained in [13]. We then will take one more step and calculate a non Markovian dephasing rate which will yield clearly different results compared to the Markovian rates: Instead of an ordinary exponential decay with an exponent linear in time t we will find exponents with more complex time dependence.

3.3.1 Self Consistent Rate

In this section we re-normalize the second order diagrams in a straightforward way to obtain a self-consistent equation for the propagator Π which reflects itself into a self consistent equation for the dephasing rate Γ_{2^*}. We re-normalize the second order dephasing rate by replacing the free propagator which appears in every second order diagram with the full propagator, e.g.:

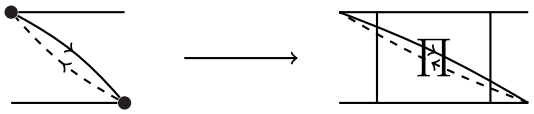

similar to a self-consistent Born approximation in equilibrium solid state theory. Taking a closer look on the diagrams arising from this step we see, that within this re-normalization we sum up all diagrams belonging to a class we call "nested" diagrams. A nested diagram is characterized by a contraction which connects the most left vertex with the one most right, see figure 3.2 for examples. We can apply the diagrammatic rules to the last diagram above which yields a contribution (without qubit matrix elements) proportional to

$$\sim \sum_{kq\alpha} |A_{kq}|^2 \gamma_k^{>}(t-t')\gamma_q^{<}(t'-t)\Pi(t-t')\,. \tag{3.56}$$

Since we replaced the free propagator in the diagram with the full propagator the only difference to the second order diagram is the change from the free time evolution $e^{i\,\delta E\,(t-t')}$ to the full time dependence $\Pi(t,t')$. Therefore we obtain the self energy $\Sigma_{00}^{11}(t,t')$ by replacing the exponential factor in equation 3.50 with the propagator $\Pi_{00}^{11}(t,t')$ which yields

$$\Sigma_{00}^{11} = -32g^2 \sum_{kq} |A_{kq}^z|^2 (1-f(E_k)) f(E_q) \mathrm{Re}\left(e^{i(E_k-E_q)(t-t')}\right) \Pi_{00}^{11}(t,t')\,. \tag{3.57}$$

We insert the self energy into the master equation for the propagator Π which leaves us with a self consistent integral-differential equation for Π, namely

$$\begin{aligned}\left(\partial_t - i\,\delta E\right)\Pi_{00}^{11}(t-t') = -32g^2 \sum_{kq} |A_{kq}^z|^2 (1-f(E_k)) f(E_q) \\ \times \int_{t_0}^{t} dt' \mathrm{Re}\left(e^{i(E_k-E_q)(t-t')}\right) \Pi_{00}^{11}(t-t_0)\Pi_{00}^{11}(t'-t_0)\,.\end{aligned} \tag{3.58}$$

In principle one could solve this equation for Π (at least numerically) and obtain a result without Markov approximation. Instead we apply the Markov approximation again. Since the Markov equation always hast the form of a rate equation for the propagator, we already know from this approximation that the propagator is of exponential form, $\Pi(t) \sim e^{(i\delta E - \Gamma_{2^*})t}$. We plug that explicit form in the defining equation for the dephasing rate 2.49 and obtain the self consistent equation for the dephasing rate:

$$\Gamma_{2^*} = 32g^2 \sum_{kq} |A_{kq}^z|^2 (1-f(E_k)) f(E_q) \int_0^\infty dt' \mathrm{Re}\left(e^{i(E_k-E_q)(t')}\right) e^{-\Gamma_{2^*}t'}\,. \tag{3.59}$$

Calculating the time integral is straightforward and yields a Lorentzian with width Γ which can be understood due to the fact that the coupling to quasiparticle tunneling induces a finite lifetime for the qubit states/ quasiparticle states which reflects in a broadening of the δ-function spectral density for the superconductors into a Lorentz peak $\delta(E_q - E_k) \to \frac{\Gamma}{(E_k-E_q)^2+\Gamma^2}$, similar to particle physics where finite particle lifetimes can be calculated with the width of the Lorentzian peaks. Replacing sums with integrals yields the final form for the self-consistent rate:

$$\begin{aligned}\Gamma_{2^*} = 32N_0^2 g^2 \int_\Delta^\infty \int_\Delta^\infty dE dE' \frac{(EE'-\Delta^2)c^2 + (EE'+\Delta^2)s^2}{EE'} \\ \times n(E)n(E')f(E')(1-f(E)) \frac{\Gamma_{2^*}}{(E-E')^2+\Gamma_{2^*}^2}\,.\end{aligned} \tag{3.60}$$

This expression for the self-consistent dephasing rate equals equation (28) from [13]. We can simplify the expression with the low energy approximation we have used before

to get rid of distribution functions $f(E)$. We note that this approximation is not necessarily valid for dephasing. We will discuss this at the end of this chapter in more detail. Yet, in the low energy limit the self-consistent equation reduces to

$$\Gamma_{2^*} = 16N_0 g^2 n_{qp} \int_\Delta^\infty dE \frac{(E-\Delta)c^2 + (E+\Delta)s^2}{\sqrt{E^2-\Delta^2}} \frac{\Gamma_{2^*}}{(E-\Delta)^2 + \Gamma_{2^*}^2} \tag{3.61}$$

which we want to solve for the special case $s = 0$ which for instance happens to be true for a transmon qubit. In this case the golden rule approximation too is valid as we have mentioned before but the golden rule rate 3.54 is determined by the integral over the distribution function and is not directly connected to the quasiparticle density n_{qp} which is accessible in experiments. For $s = 0$ we write the self consistent dephasing rate as

$$\Gamma_{2^*} = 16N_0 g^2 c^2 n_{qp} \frac{1}{\Delta} \int_0^\infty dx \sqrt{\frac{x}{x+2}} \frac{\Gamma_{2^*}}{x^2 + (\Gamma_{2^*}/\Delta)^2} \tag{3.62}$$

which can be solved exactly if we apply one more approximation. Since the main contribution to the integral comes from $x \approx 0$ we additionally assume $\sqrt{x+2} \approx \sqrt{2}$. With these assumptions the final low energy dephasing rate in the 'transmon-case' reads

$$\Gamma_{2^*} = \left[16N_0^2 g^2 c^2 \pi x_{qp}\right]^2 \frac{\Delta}{2}. \tag{3.63}$$

For the transmon we will find not only that $s^2 = 0$ but also $c_{01} = 0$ so that for the transmon the ratio between self consistent dephasing rate and relaxation rate in the low energy approximation becomes

$$\frac{\Gamma_1}{\Gamma_{s^*}} = \frac{|s_{01}|^2}{c^4} \frac{1}{8N_0^2 g^2 x_q p \Delta} \sqrt{\frac{2+\delta E/\Delta}{\delta E/\Delta}} \tag{3.64}$$

Since $\delta E \ll \Delta$ and $c^2 \ll |s_{01}|^2$ (see figure 4.3) the dephasing rate due to quasiparticle tunneling for the transmon is very small compared to the pure relaxation rate Γ_1 and the decoherence time is determined by relaxation solely.

We finish this section with a short note on renormalization with the qubit relaxation rate Γ_1 instead of the dephasing rate itself. The corresponding diagrams are achieved by plugging in in the propagator $\Pi^{00}_{11,\pm}$ instead of the dephasing propagator plugged in above. The propagator $\Pi^{00}_{11,\pm}$ is achieved in second order approximation from pure $\sigma_\pm$ coupling and has the form $e^{(i\delta E - \Gamma_1)t}$ and the corresponding rate is (of course not self consistent) given by

$$\Gamma_{2^*} = 32N_0^2 g^2 \int_\Delta^\infty \int_\Delta^\infty dE dE' \frac{(EE'-\Delta^2)c^2 + (EE'+\Delta^2)s^2}{EE'} \times n(E)n(E')f(E')(1-f(E)) \frac{\Gamma_1}{(E-E')^2 + \Gamma_1^2} \tag{3.65}$$

3.3.2 Non- Markovian Ansatz

In this section we will approach the problem of a qubit coupled to quasiparticle tunneling from an entirely new side, similar to an approach in [30]. Therefore we will go back from the diagrammatic technique to the exact time evolution of the reduced density matrix, equation 2.10

$$\rho_{ss'}(t) = \sum_{qq'} \rho_{qq'}(t_0)\langle q'|\mathrm{Tr}_R\left\{\rho_R(t_0)U_I^\dagger(t,t_0)\hat{P}_{s's,I}(t)U_I(t,t_0)\right\}|q\rangle \tag{3.66}$$

which can be simplified making use of the fact that the coupling Hamiltonian $H_T \sim \sigma_z$ is diagonal in spin space for pure dephasing. In this case we can write $H_T(t) = \sigma_z\hat{R}(t)$ where $\hat{R}$ is the reservoir part of the tunneling Hamiltonian. For quasi particle tunneling we have

$$\hat{R} = g\sum_{kq\sigma} \alpha c_{k\sigma,l}c^\dagger_{q\sigma,r} + h.c.\,, \tag{3.67}$$

where we use electron operators throughout this section. With latter notation and defining numbers $s = \pm 1$ for the excited and ground state respectively we find

$$\rho_{ss'}(t) = e^{-i\frac{\omega_0(s-s')}{2}(t-t_0)}\rho_{ss'}(t_0)\left\langle \bar{T}\exp\left\{is'\int_{t_0}^{t} R(t')dt'\right\} T\exp\left\{-is\int_{t_0}^{t} R(t')dt'\right\}\right\rangle_R . \tag{3.68}$$

On one hand latter equation yields constant diagonal elements ($\rho_{ss}(t) = \rho_{ss}(t_0)$) while on the other hand off diagonal elements are governed by

$$\rho_{10}(t) = e^{-i\delta E(t-t_0)}\rho_{10}(t_0)\left\langle \bar{T}\exp\left\{-i\int_{t_0}^{t} R(t')dt'\right\} T\exp\left\{-i\int_{t_0}^{t} R(t')dt'\right\}\right\rangle_R \tag{3.69}$$

$$\rho_{01}(t) = e^{i\delta E_0(t-t_0)}\rho_{01}(t_0)\left\langle \bar{T}\exp\left\{i\int_{t_0}^{t} R(t')dt'\right\} T\exp\left\{i\int_{t_0}^{t} R(t')dt'\right\}\right\rangle_R \tag{3.70}$$

Since $R(t)$ and $R(t')$ do not commute it's difficult to calculate above averages. Hence we will try to simplify the averages. Therefore we have a look on the Hamiltonian of the full system again

$$H = H_R + H_S + \sigma_z\hat{R}\,. \tag{3.71}$$

Comparing this expression with 3.68 we see that the σ_z operator yields factors $s = \pm 1$ in the exponent of the reduced density matrix elements. Replacing σ_z with $\sigma_z - \sigma_0$ will

lead to a factor of 0 or 2 for $s = \pm 1$ and hence either the time ordered oder anti time ordered exponent would simply yield a one. Hence we write the Hamiltonian 3.71 as

$$H = H_R + \sigma_0 \hat{R} + (\sigma_z - \sigma_0)\hat{R} \tag{3.72}$$

with the unit matrix in Pauli space σ_0. Now we redefine the reservoir Hamiltonian to $\widetilde{H}_R := H_R + \hat{R}$ leaving us with the new coupling/ tunnel Hamiltonian $\widetilde{H}_T := (\sigma_z - \sigma_0)\hat{R}$. Using the re-defined Hamiltonians in eq (3.66) we find

$$\begin{aligned}\rho_{ss'}(t) = e^{-i\frac{\delta E(s-s')}{2}(t-t_0)}\rho_{ss'}(t_0)\times \\ \times \left\langle \bar{T}\exp\left\{ i(s'-1)\int_{t_0}^{t} R(t')dt' \right\} T\exp\left\{ -i(s-1)\int_{t_0}^{t} R(t')dt' \right\} \right\rangle_{\widetilde{R}}\end{aligned} \tag{3.73}$$

where the thermal average has to be taken with respect to the new bath Hamiltonian $\widetilde{H}_R$. To obtain this expression for the reduced density matrix elements we have to assume that the initial density matrix still factorizes into the density matrix for the new reservoir and the system density matrix. Hence we want to emphasize that the initial condition should influence the short time dynamics but play no role at longer times. For both off-diagonal elements one of the (anti) time ordered exponentials has a zero argument and evaluates to one so that

$$\rho_{10}(t) = e^{-i\delta E(t-t_0)}\rho_{10}(t_0)\left\langle \bar{T}\exp\left\{ -2i\int_{t_0}^{t} R(t')dt' \right\} \right\rangle_{\widetilde{R}} \tag{3.74}$$

$$\rho_{01}(t) = e^{i\delta E(t-t_0)}\rho_{01}(t_0)\left\langle T\exp\left\{ -2i\int_{t_0}^{t} R(t')dt' \right\} \right\rangle_{\widetilde{R}} . \tag{3.75}$$

With that method we were able to simplify the operators in the thermal average brackets at the cost of a more complicated bath Hamiltonian which is no longer diagonal in quasiparticle space. Therefore we have to treat thermal averages with more care but we can tackle them with the Greens function methods we have already applied to the BCS Hamiltonian and it will turnout that the change due to the "new" reservoir which is made of the two coupled superconductors doesn't change the Greens functions to much. To relate the Green's function with the time evolution, we take the average in 3.74 and expand the exponential yielding

$$\left\langle \bar{T}\exp\left\{ -2i\int_{t_0}^{t} R(t')dt' \right\} \right\rangle_{\widetilde{R}} = \sum_n \frac{(-2i)^n}{n!}\int_{t_0}^{t} dt_1 \cdots \int_{t_0}^{t} dt_n \left\langle T\left\{ R(t_1)R(t_2)\cdots R(t_n) \right\} \right\rangle . \tag{3.76}$$

First we note that only even orders survive since for every uneven order we have unbalanced creation/ annihilation numbers such that the averages vanish. Second we apply Wicks theorem to the thermal average which factorizes the average into products of two operator Greens functions

$$\begin{aligned}\sum_n \frac{(-2i)^n}{n!}\int_{t_0}^{t} dt_1 \cdots \int_{t_0}^{t} dt_n \left\langle T\left\{R(t_1)R(t_2)\cdots R(t_n)\right\}\right\rangle \\ = \sum_n \frac{-2^n}{n!}\left(\int_{t_0}^{t} dt_1 \int_{t_0}^{t} dt_2 \left\langle T\left\{R(t_1)R(t_2)\right\}\right\rangle\right)^n \\ = \exp\left(-2\int_{t_0}^{t} dt_1 \int_{t_0}^{t} dt_2 \left\langle T\left\{R(t_1)R(t_2)\right\}\right\rangle\right) \end{aligned} \tag{3.77}$$

Hence the entire problem to find an expression for the time evolution of the density matrix has reduced to the problem of evaluating the reservoir-reservoir correlation function $\left\langle T\left\{R(t_1)R(t_2)\right\}\right\rangle$ where we have to take the average with respect to the "new" reservoir $\widetilde{H}_R = H_R + R$. To evaluate it we express the average in terms of electron correlation functions which yields

$$\begin{aligned}\left\langle T\left\{R(t_1)R(t_2)\right\}\right\rangle = \sum_{kk'}\sum_{qq'} g^2\alpha^2 \Big(\left\langle Tc_{k,l}(t_1)c_{q,r}(t_1)^\dagger\right\rangle \left\langle Tc_{k',l}(t_2)c_{q',r}(t_2)^\dagger\right\rangle \\ + \left\langle Tc_{k,l}(t_1)c_{q',r}(t_2)^\dagger\right\rangle \left\langle Tc^\dagger_{q,r}(t_1)c_{k',l}(t_2)^\dagger\right\rangle - \left\langle Tc_{k,l}(t_1)c_{k',l}(t_2)\right\rangle \left\langle Tc^\dagger_{q,r}(t_1)c_{q',r}(t_2)^\dagger\right\rangle\Big) \\ + g^2\alpha^{*2}\Big(\left\langle Tc_{q,r}(t_1)c_{k,l}(t_1)^\dagger\right\rangle \left\langle Tc_{q',r}(t_2)c_{k',l}(t_2)^\dagger\right\rangle + \left\langle Tc_{q,r}(t_1)c_{k',l}(t_2)^\dagger\right\rangle \left\langle Tc^\dagger_{k,l}(t_1)c_{q',r}(t_2)^\dagger\right\rangle \\ - \left\langle Tc_{q,r}(t_1)c_{q',r}(t_2)\right\rangle \left\langle Tc^\dagger_{k,l}(t_1)c_{k',l}(t_2)^\dagger\right\rangle\Big) + g^2|\alpha|^2\Big(\left\langle Tc_{k,l}(t_1)c_{q,r}(t_1)^\dagger\right\rangle \left\langle Tc_{q',r}(t_2)c_{k',l}(t_2)^\dagger\right\rangle \\ + \left\langle Tc_{k,l}(t_1)c_{k',l}(t_2)^\dagger\right\rangle \left\langle Tc^\dagger_{q,r}(t_1)c_{q',r}(t_2)\right\rangle - \left\langle Tc_{k,l}(t_1)c_{q',r}(t_2)\right\rangle \left\langle Tc^\dagger_{q,r}(t_1)c_{k',r}(t_2)^\dagger\right\rangle \\ + \left\langle Tc_{q,r}(t_1)c_{k,l}(t_1)^\dagger\right\rangle \left\langle Tc_{k',l}(t_2)c_{q',r}(t_2)^\dagger\right\rangle + \left\langle Tc_{q,r}(t_1)c_{q',r}(t_2)^\dagger\right\rangle \left\langle Tc^\dagger_{k,l}(t_1)c_{k',l}(t_2)^\dagger\right\rangle \\ - \left\langle Tc_{q,r}(t_1)c_{k',l}(t_2)\right\rangle \left\langle Tc^\dagger_{k,l}(t_1)c_{q',r}(t_2)^\dagger\right\rangle\Big)\,. \end{aligned} \tag{3.78}$$

In that expression every thermal average represents a electron Greens function where we have 'normal' Greens functions which are correlation functions between creation and annihilation operators and anomalous Greens functions (correlations between two creation/ annihilation operators) for both superconductors separately as well as Greens

functions measuring the correlation between both superconductors. The mixed Greens functions give rise to the Josephson effect and to avoid double counting we will neglect these correlation functions if it comes to dephasing. Using Nambu spinors 1.39 we can cover all twelve different kinds of Greens functions that appear in the bath-bath correlation function with three averages, namely the one-side Greens function

$$G_i(kk'\sigma,\tau) = -\langle T_\tau \Psi_{k,i}(\tau)\Psi^\dagger_{k',i}\rangle = -\begin{pmatrix} \langle T_\tau c_{k\sigma,i}(\tau)c^\dagger_{k'\sigma',i}\rangle & \langle T_\tau c_{k\sigma,i}(\tau)c_{-k'-\sigma',i}\rangle \\ \langle T_\tau c^\dagger_{-k-\sigma,i}(\tau)c^\dagger_{k'\sigma',i}\rangle & \langle T_\tau c^\dagger_{-k-\sigma,i}(\tau)c_{-k'-\sigma',i}\rangle \end{pmatrix} \tag{3.79}$$

and the left-right (right-left respectively) functions

$$G_{ji}(kk'\sigma,\tau) = -\langle T_\tau \Psi_{k,j}(\tau)\Psi^\dagger_{k',i}\rangle = -\begin{pmatrix} \langle T_\tau c_{k\sigma,j}(\tau)c^\dagger_{k'\sigma,i}\rangle & \langle T_\tau c_{k\sigma,j}(\tau)c_{-k'-\sigma,i}\rangle \\ \langle T_\tau c^\dagger_{-k-\sigma,j}(\tau)c^\dagger_{k'\sigma,i}\rangle & \langle T_\tau c^\dagger_{-k-\sigma,j}(\tau)c_{-k'-\sigma,i}\rangle \end{pmatrix}, \tag{3.80}$$

where i,j represent either the l(eft) or r(ight) superconductor and $\tau = it$ is the imaginary time. Now we carry out the same steps as we have in section 1.2.2 where we used the Greens function formalism to derive the BCS superconductivity. Due to the tunnel Hamiltonian which now appears in the Hamiltonian, the Greens functions will experience a derivation from their unperturbed BCS form $G^0_i(k\sigma, i\omega_n) = (i\omega_n - \xi_k\tau_3 + \sigma\Delta\tau_1)^{-1}$. The Heisenberg equations of motion ($\frac{\partial}{\partial\tau}c_{k\sigma,i}(\tau) = [H, c_{k\sigma,i}(\tau)]$) have to be taken with respect to the Hamiltonian $H = H_0 + H_T$ where we have

$$H_0 = \sum_{i=l,r}\sum_{k,\sigma}\xi_k c^\dagger_{k\sigma,i}c_{k\sigma,i} - \sum_k\left(\Delta^* c_{-k\downarrow,i}c_{k\uparrow,i} + \Delta c^\dagger_{k\uparrow,i}c^\dagger_{-k\downarrow,i}\right) \tag{3.81}$$

$$H_T = g\sum_{kq}\alpha c^\dagger_{k\sigma,l}c_{q\sigma,r} + \alpha^* c^\dagger_{q\sigma,r}c_{k\sigma,l}\,. \tag{3.82}$$

This yields the eof for the Nambu Gorkov Greens functions

$$\begin{aligned}(-\partial\tau - \xi_k\tau_3 + \sigma\Delta\tau_1)G_l(kk'\sigma,\tau) =& \delta(\tau)\delta_{kk'} \\ &+ (g_1\tau_3 + ig_2\tau_0)\sum_q G_{rl}(qk'\sigma,\tau)\end{aligned} \tag{3.83}$$

$$(-\partial\tau - \xi_q\tau_3 + \sigma\Delta\tau_1)G_{rl}(qk'\sigma,\tau) = (g_1\tau_3 - ig_2\tau_0)\sum_K G_l(kk'\sigma,\tau)\,. \tag{3.84}$$

and the same equations with right and left exchanged. We defined $g_1 = \mathrm{Re}\left[g\alpha\right]$ and $g_2 = \mathrm{Im}\left[g\alpha\right]$. Applying a discrete Fourier transformation to these equations yields the

following algebraic equations for the Greens functions:

$$G_l(kk'\sigma, i\omega_n) = G_l^0(k\sigma, i\omega_n)\delta_{kk'} + G_l^0(k\sigma, i\omega_n)(g_1\tau_3 + ig_2\tau_0) \times \sum_q G_{rl}(qk'\sigma, i\omega_n) \tag{3.85}$$

$$G_{rl}(qk'\sigma) = G_r^0(q\sigma, i\omega_n)(g_1\tau_3 - ig_2\tau_0)\sum_k G_l(kk'\sigma, i\omega_n)\,. \tag{3.86}$$

As it becomes clear from 3.78 we do not need the entire Greens function of the system but only the density of states $\sim \sum_{kk'} G(k, k', i\omega_n)$. Therefore we define the density of states in imaginary frequency space

$$F_i(i\omega_n) = \sum_{kk'} G_i(k, k', i\omega_n) \tag{3.87}$$

$$F_{ij}(i\omega_n) = \sum_{kk'} G_{ij}(k, k', i\omega_n) \tag{3.88}$$

$$F_i^0(i\omega_n) = \sum_k G_i^0(k, i\omega_n)\,, \tag{3.89}$$

yielding two very simple algebraic equations for the one- and two sided densities:

$$F_i(i\omega_n) = F_i^0(i\omega_n) + F_i^0(i\omega_n)(g_1\tau_3 + ig_2\tau_0)F_{ji}(i\omega_n) \tag{3.90}$$

$$F_{ji}(i\omega_n) = F_j^0(i\omega_n)(g_1\tau_3 - ig_2\tau_0)F_i^0(i\omega_n)\,. \tag{3.91}$$

As mentioned before the two-sided functions give rise to the Josephson effect so that we will neglect the corresponding terms in the bath-bath correlation function. For the one sided functions we find

$$F_i^{-1}(i\omega_n) = (F_i^0)^{-1}(i\omega_n) - (g_1\tau_3 + ig_2\tau_0)F_j^0(i\omega_n)(g_1\tau_3 - ig_2\tau_0)\,, \tag{3.92}$$

which can be solved by use of the relation

$$\sum_k G_i^0(k, i\omega_n) = -\sum_k \frac{i\omega_n + \xi_k\tau_3 - \Delta\tau_1}{\omega_n^2 + \xi_k^2 + \Delta^2} = -N_0 \int_{-\infty}^{\infty} d\xi \frac{i\omega_n - \Delta\tau_1}{\omega_n^2 + \xi^2 + \Delta^2} = N_0\pi\frac{i\omega_n - \Delta\tau_1}{\sqrt{\omega_n^2 + \Delta^2}}\,. \tag{3.93}$$

After short computation we obtain the on-side density of states in imaginary frequency space

$$F_i(i\omega_n) = \frac{N_0\pi}{1 + \gamma|\alpha|^2}\frac{\sqrt{\omega_n^2 + \Delta^2}}{\omega_n^2 + \Delta^2(1+\delta)}\begin{pmatrix} i\omega_n & -\tilde{\Delta} \\ -\tilde{\Delta}^* & i\omega_n \end{pmatrix} \tag{3.94}$$

with the parameter δ and the gap

$$\delta = \frac{2\gamma|\alpha|^2\left(\cos(2\varphi_\alpha)-1\right)}{(1+\gamma|\alpha|^2)^2} \tag{3.95}$$

$$\tilde{\Delta} = \frac{1+\gamma\alpha^2}{1+\gamma|\alpha|^2}\Delta \tag{3.96}$$

where we defined $\gamma = g^2N_0^2\pi^2$ which is of course nothing else than the Josephson energy normalized to the gap, $\gamma = E_J/\Delta$ and $\varphi_\alpha = \arg(\alpha)$. We see that the gap obtains an additional phase and is no longer pure real. The derivation up to this point was not much different to the derivation of the Josephson effect using Nambu-Gorkov Greens functions in chapter 1 1.3.2. Still their are important differences since we have already included the Josephson term in the qubit Hamiltonian and found the new parameter α playing the role of the phase factor $e^{i\varphi/2}$. Now we obtain the density of states using $n(\omega) = \frac{-1}{\pi}\mathrm{Im}\left[F_i(i\omega_n \to \omega + i0)\right]$, yielding

$$\mathcal{N}(\omega) = \frac{N_0}{1+\gamma|\alpha|^2}\frac{\sqrt{\omega^2-\Delta^2}}{\omega^2-\Delta^2(1+\delta)}\begin{pmatrix}\omega & -\Delta\frac{1+\gamma|\alpha|^2\cos(2\varphi_\alpha)}{1+\gamma|\alpha|^2}\\ -\Delta\frac{1+\gamma|\alpha|^2\cos(2\varphi_\alpha)}{1+\gamma|\alpha|^2} & \omega\end{pmatrix}\Theta(\omega^2-\Delta^2)$$
$$+\frac{N_0}{1+\gamma|\alpha|^2}\frac{\sqrt{\Delta^2-\omega^2}}{\omega^2-\Delta^2(1+\delta)}\begin{pmatrix}0 & -\Delta\frac{\gamma|\alpha|^2\sin(2\varphi_\alpha)}{1+\gamma|\alpha|^2}\\ \Delta\frac{\gamma|\alpha|^2\sin(2\varphi_\alpha)}{1+\gamma|\alpha|^2} & 0\end{pmatrix}\Theta(\Delta^2-\omega^2)\,. \tag{3.97}$$

The first part is similar to the usual BCS density of states with the important difference that the singularity is shifted away from the gap Δ. Since $\delta \leq 0$ and $|\delta| \leq 1$ we have $(1+\delta)\Delta \leq \Delta$ and for $|\omega| \geq \Delta$ no singularity appears at all. The second part arises due to the imaginary part of the phase obtained by the gap. This part of the dos has a singularity at $\omega^2 = \Delta^2(1+\delta)$. For the special of α being real we have $\cos(2\varphi_\alpha) = 1$ and the parameter δ as well as $\sin(2\varphi_\alpha)$ equal zero so that we recover the usual BCS dos scaled with the factor $(1+\gamma|\alpha|^2)^{-1}$. From this point on our calculation of the reservoir correlation is similar to the work of Leppäkangas and Marthaler on flux qubit relaxation[6]. Before we calculate the reservoir correlation functions we introduce the greater and lesser Greens functions as

$$G^{>}(k,k',\sigma,t) = \left\langle c_{k\sigma}(t)c^\dagger_{k'\sigma}\right\rangle\,, \qquad G^{<}(k,k',\sigma,t) = \left\langle c^\dagger_{k\sigma}c_{k'\sigma}(t)\right\rangle \tag{3.98}$$

$$F^{>}(k,k',\sigma,t) = \left\langle c_{k\sigma}c_{k'-\sigma}(t)\right\rangle\,, \qquad F^{>}(k,k',\sigma,t) = \left\langle c^\dagger_{k\sigma}(t)c^\dagger_{k'-\sigma}\right\rangle\,. \tag{3.99}$$

Their Fourier transforms $G(\omega) = \int dt e^{i\omega t}G(t)$ are related to the single electron spectral function $A(k,k',\omega)$ and the pair spectral function $B^{\gtrless}(k,k',\omega)$ as[31]

$$G^{\gtrless}(k,k',\omega) = A(k,k',\omega)f^{\pm}(\omega) \tag{3.100}$$

$$F^{\gtrless}(k,k',\uparrow) = -F^{\gtrless}(k,k',\downarrow) = B^{\gtrless}(k,k',\omega)f^{\pm}(\omega)\,. \tag{3.101}$$

The spectral functions introduced above themselves are related to the density of states in the usual way:

$$\sum_{k,k'} A(k,k',\omega) = \pi n_{11}(\omega) = \pi n_{22}(\omega) = \pi n(\omega) \tag{3.102}$$

$$\sum_{k,k'} B^{>}(k,k',\omega) = -\pi n_{21}(\omega) = \pi \bar{p}(\omega)\,, \quad \sum_{k,k'} B^{<}(k,k',\omega) = -\pi n_{12}(\omega) = \pi p(\omega)\,, \tag{3.103}$$

where $p(\omega)$ can be interpreted as 'pair density of states' while $n(\omega)$ is the usual density of states for quasiparticles. With this tools we are finally in the position to calculate the reservoir correlation functions. We do this for one function exemplary since the procedure is all the same for the remaining functions. We begin with

$$\begin{aligned}\sum_{\sigma}\sum_{kk'}\sum_{qq'} \left\langle T c_{k\sigma,l}(t_1) c^{\dagger}_{k'\sigma,l}(t_2)\right\rangle \left\langle T c^{\dagger}_{q\sigma,r}(t_1) c_{q'\sigma,r}(t_2)\right\rangle = \\ 2\sum_{kk'}\sum_{qq'} \Theta(t_1-t_2) G^{>}(k,k',\sigma,t_1-t_2) G^{<}(q,q',\sigma,t_2-t_1) \\ +\Theta(t_2-t_2) G^{<}(k,k',\sigma,t_1-t_2) G^{>}(q,q',\sigma,t_2-t_1)\,,\end{aligned} \tag{3.104}$$

express the Green's functions with their Fourier transforms 3.100 and finally use relation 3.102 to introduce the density of states into above expression and find

$$\begin{aligned}2\sum_{kk'}\sum_{qq'} \left\langle T c_{k\sigma,l}(t_1) c^{\dagger}_{k'\sigma,l}(t_2)\right\rangle \left\langle T c^{\dagger}_{q\sigma,r}(t_1) c_{q'\sigma,r}(t_2)\right\rangle = \\ 2\pi^2 N_0^2 \int_{-\infty}^{\infty}\int_{-\infty}^{\infty} \frac{d\omega_1 d\omega_2}{(2\pi)^2} n(\omega_1) n(\omega_2) \Big[\Theta(t_1-t_2) f(\omega_2)(1-f(\omega_1)) e^{-i(\omega_1-\omega_2)(t_1-t_2)} \\ +\Theta(t_2-t_1) f(\omega_2)(1-f(\omega_1)) e^{-i(\omega_1-\omega_2)(t_2-t_1)}\Big]\,.\end{aligned} \tag{3.105}$$

The remaining averages contribute similar expressions to the reservoir correlation $\langle T R(t_1) R(t_2)\rangle$. We carry out the time integral in the time evolution of $\rho_{01}(t)$, eq. 3.74, and find the final form of the exponent, the time dependent dephasing 'rate'

$$\begin{aligned}J_{2^*}(t-t_0) = 32\pi^2 g^2 N_0^2 |\alpha|^2 \iint \frac{d\omega_1 d\omega_2}{(2\pi)^2} \left[n(\omega_1) n(\omega_2) - \frac{\alpha^2+\alpha^{*2}}{2|\alpha|^2} p(\omega_1)\bar{p}(\omega_2)\right] \\ \times f(\omega_2)(1-f(\omega_1)) \frac{2\sin^2(\frac{\omega_1-\omega_2}{2}(t-t_0))}{(\omega_1-\omega_2)^2}\,.\end{aligned} \tag{3.106}$$

This integral is convergent even for the BCS density of states with singularity at the gap. In addition to the decay governed by the rate Γ_{2^*} the qubit experiences a frequency shift due to quasiparticle tunneling induced dephasing. The frequency shift is given by the imaginary part of the exponent

$$\nu(t-t_0) = -32\pi^2 g^2 N_0^2 |\alpha|^2 \iint \frac{d\omega_1 d\omega_2}{(2\pi)^2} \left[n(\omega_1)n(\omega_2) - \frac{\alpha^2+\alpha^{*2}}{2|\alpha|^2} p(\omega_1)\bar{p}(\omega_2) \right] f(\omega_2)(1-f(\omega_1)) \times \frac{(\omega_1-\omega_2)(t-t_0) - \sin((\omega_1-\omega_2)(t-t_0))}{(\omega_1-\omega_2)^2} . \quad (3.107)$$

The main contribution to the integral will arise from $\omega_1 \approx \omega_2$ such that we can truncate both frequency integrals to positive ω-values. With latter approximation and if we take the standard BCS quasiparticle and pair density ($n_0(\omega) = \omega/\sqrt{\omega^2-\Delta^2}$ and $p_0(\omega) = \Delta/\sqrt{\omega^2-\Delta^2}$) and replace the last time dependent fraction with a δ function in expression 3.106 we recover the golden rule dephasing rate obtained earlier in this work. We can express the matrix element ρ_{01} with these rates and find

$$\rho_{01}(t-t_0) = e^{i(\delta E\cdot(t-t_0) - \nu(t-t_0)) - J_{2^*}(t-t_0)} \quad (3.108)$$

At the end of this section we analyze the non Markovian dephasing rate for the special case of real α as it is the case for the transmon qubit. In this case the densities of states reduce to there BCS form and, after applying the low energy approximation, we obtain

$$J_{2^*}(t) \approx \frac{16g^2|\alpha|^2 N_0 n_{qp}}{1+\gamma|\alpha|^2} \frac{t}{2} \int_0^\infty dx \sqrt{\frac{x}{x+\Delta t}} \frac{2\sin^2 x}{x^2} \quad (3.109)$$

Usually the superconducting gap is of order $10^9 - 10^{11} Hz$ while we expect the time to be at least of the order of relaxation yielding $t \sim 10^-6 s$. Hence the parameter Δt is of order $10^3 - 10^5$ while the main contribution to the integral comes from $x \approx 0$ and we can approximate the expression for the dephasing rate with

$$\begin{aligned} J_{2^*}(t) &\approx \left[\frac{16g^2|\alpha|^2 N_0 n_{qp}}{1+\gamma|\alpha|^2} \int_0^\infty dx \sqrt{x} \frac{2\sin^2 x}{x^2} \right] \frac{t^{1/2}}{2\sqrt{\Delta}} \\ &= \frac{16g^2|\alpha|^2 N_0 n_{qp}}{1+\gamma|\alpha|^2} \sqrt{\frac{2\pi}{\Delta}} t^{1/2} . \end{aligned} \quad (3.110)$$

This time dependent rate looks quite familiar since (despite to the small factor $\gamma|\alpha|^2$ in the denominator) the prefactor is the same as the one we have already seen for the relaxation as well as the self consistent dephasing rate. Nevertheless we see that,

although we can define a golden rule rate without running into the square root singularity, an exact non Markovian treatment yields a different time dependence compared to the Markovian self-consistent or golden rule calculation: $\sim \Gamma_{2^*} t^{1/2}$ instead of $\Gamma_{2^*} t$. We will later see that $J(t) = at^b$ very well fits numerical results but with b different to 1/2 (we will even encounter a case with $b \approx 1$). The exponent b depends on the exact shape of the distribution function since for the low energy approximation to be valid we need a very narrow distribution function while a smeared out distribution as the equilibrium Fermi distribution will lead to linear time dependence instead of the square root dependence, see section 4.1.2.

For a theoretical qubit with a pure imaginary matrix element $\alpha = is$, we can apply a similar approximation and find a rate proportional to $t^{3/2}$:

$$\begin{aligned} J_{2^*}(t) &\approx \left[\frac{16g^2|\alpha|^2 N_0 n_{qp}}{1+\gamma|\alpha|^2} \int_0^\infty dx \sqrt{x} \frac{2\sin^2 x}{x^2} \right] \frac{t^{1/2}}{2\sqrt{\Delta}} \\ &= \frac{16g^2|\alpha|^2 N_0 n_{qp}}{1+\gamma|\alpha|^2} \frac{4\sqrt{\pi}}{3\sqrt{\Delta}} t^{3/2} \end{aligned} \tag{3.111}$$

We want to emphasize that, in contrary to relaxation, the low energy approximation has to be used with care for pure dephasing. To clarify this, we first have a look on relaxation again. There a tunneling process is related to an energy transfer of size δE from the qubit to the quasiparticle. This results in the energy conserving delta function forcing $E - E' = \delta E$ in the integrand for the golden rule relaxation rate 3.39. Therefore the relevant energy scale besides the superconducting gap is the qubit energy splitting δE. The low energy approximation is valid as long as the distribution function in the integrand decreases so fast that the main contribution to the integral arises from energies $E - \Delta \ll \delta E$ which is valid for almost every realistic distribution function. The situation for pure dephasing is entirely different. Here, no energy is transfered between qubit and quasiparticle. Hence the main contribution to the dephasing rates arises from $E \approx E'$ in the integrals defining the rates. This holds for the golden rule rate where a delta function enforces $E = E'$ as well as for the self-consistent 3.60 and non-Markovian rate 3.106 where the integrands have pronounced maxima at $E = E'$. Hence the low energy approximation is valid only when the distribution function is very close to a delta function, $f(E) \approx \delta(E - \Delta)$. In chapter 4 we calculate dephasing rates for a transmon using a Fermi distribution. In this case the distribution function doesn't fulfill this requirement and the low energy approximation fails for dephasing while yielding very good results for relaxation. In this case the non-Markovian 'rate' J_{2^*} becomes even linear in t and we are able to define a true non-Markovian dephasing rate which is in good agreement with the self-consistent rate.

Chapter 4

4 Relaxation and Dephasing for a Transmon Qubit

In this chapter we calculate relaxation and dephasing times ($T_i = \Gamma_i^{-1}$) for transmon qubits. Relaxation rates obtained in the low energy approximation show good agreement with experimental results. In contrary to our approximate low energy approximation the non Markovian dephasing rate shows a linear behavior in time and we compare it to the self-consistent and golden rule rate (which converges for the transmon). In the second part of this chapter we analyze a transmission line embedded Josephson junction and find that the design provides no advantage compared to a lumped element transmon in matters of quasiparticle induced decoherence.

4.1 Lumped Element Transmon

In this chapter we will use the rate equations we found in previous sections to calculate the decoherence of a transmon [22] qubit. As mentioned in section 1.1.3 a transmon in the lumped element representation obeys the Hamiltonian

$$H = 4E_C\hat{n}^2 - E_J\cos(\phi) \tag{4.1}$$

with charging energy $E_C = e^2/2(C_J + C_S)$ for a Josephson junction in parallel with a shunting capacity C_S, Cooper pair number operator $\hat{n}$ and phase drop ϕ across the junction. As we have mentioned already for a transmon with $E_J \gg E_c$ the particle will be trapped in the first minimum of the cosine potential with a narrow peaked wave function such that we can approximate the potential for the lowest lying energy levels as a harmonic potential

$$H \approx 4E_C(\hat{n} - n_g)^2 + \frac{E_J}{2}\hat{\varphi}^2\,. \tag{4.2}$$

To analyze the qubit anharmonicity we treat the next order of the cosine $\sim \phi^4$ as a perturbation and calculate the energy shift in first order perturbation theory we find

$$\delta E_n = -\frac{E_C}{4}(2n^2 + 2n + 1)\,. \tag{4.3}$$

We define the absolute and relative anharmonicity by

$$\alpha = E_{32} - E_{21} \qquad \alpha_r = \frac{\alpha}{E_{21}} \tag{4.4}$$

where $E_{21} = E_2 - E_1$. Using the energy levels calculated with perturbation theory we find

$$\alpha = -E_C \qquad \alpha_r = \frac{-1}{\sqrt{8E_J/E_C} - 2} \tag{4.5}$$

The absolute anharmonicity depends on the charging energy only while the relative anharmonicity decreases with the ratio E_J/E_C suggesting that we need this ratio as small as possible which is the case for e.g. the charge qubit. On the other hand the transmon is defined in a region with $E_J \gg E_C$ which is necessary to provide the transmon with its outstanding protection against charge noise [22]. The price to pay is the weak anharmonicity which, on the other hand, allows for the harmonic oscillator approximation we will use to calculate the matrix elements for decoherence rates. We will later on compare the dependence of decoherence rates on the ratio E_J/E_C with the anharmonicity. The only qubit dependent parameters in the expression 3.42 for the relaxation rate in low energy approximation (and the corresponding dephasing rates) are the matrix elements s_{ij} and c_{ij} which can easily be calculated using the harmonic oscillator wave functions for the ground state $n = 1$ and the first excited state $n = 2$. We find

$$s_{00} = s_{11} = c_{10} = c_{01} = 0 \tag{4.6}$$

$$c_{00} = e^{-\frac{1}{2}\sqrt{\frac{E_C}{8E_J}}} \tag{4.7}$$

$$c_{11} = \left(1 - \sqrt{E_C/8E_J}\right) e^{-\frac{1}{2}\sqrt{\frac{E_C}{8E_J}}} \tag{4.8}$$

$$s_{01} = s_{10} = \left(E_C/8E_J\right)^{1/4} e^{-\frac{1}{2}\sqrt{\frac{E_C}{8E_J}}} \tag{4.9}$$

The qubit energy splitting in this approximation equals the junctions plasma frequency $\delta E = \sqrt{8E_J E_C}$.

4.1.1 Relaxation

With expression 3.42 for the relaxation rate in low energy approximation we find the transmons relaxation rate due to quasiparticle tunneling

$$\Gamma_1 = 8N_0\pi g^2 n_{qp}\sqrt{\frac{2+\delta}{\delta}}\sqrt{\frac{E_C}{8E_J}}e^{-\sqrt{\frac{E_C}{8E_J}}}\,, \tag{4.10}$$

with the small parameter $\delta = \frac{\delta E}{\Delta} = \sqrt{\frac{8E_C E_J}{\Delta^2}} \ll 1$. We use equation 1.70 to express the tunneling matrix element g^2 in terms of the gap Δ and the Josephson energy E_J yielding $\pi^2 N_0^2 g^2 \Delta = E_J$. In addition we define $x_{qp} = \frac{n_{qp}}{2N_0\Delta}$, the quasiparticle density normalized to the Cooper pair density. Substituting those expressions into the relaxation rate yields our final result for the relaxation rate of a transmon due to single quasiparticle tunneling

$$\Gamma_1 = \frac{2x_{qp}}{\pi}\sqrt{\frac{2+\delta}{\delta}}\sqrt{8E_J E_C}e^{-\sqrt{\frac{E_C}{8E_J}}}\,. \tag{4.11}$$

The rate depends on quasiparticle properties solely due to the normalized quasiparticle density

$$x_{qp} = \frac{1}{\Delta}\int_{\Delta}^{\infty} dE \frac{E}{\sqrt{E^2-\Delta^2}} f(E) = \int_{1}^{\infty} dx \frac{1}{\sqrt{x^2-1}} f(\Delta x)\,. \tag{4.12}$$

In equilibrium the quasiparticle distribution function is a Fermi-Dirac distribution which can be approximated with a Boltzmann function for energies close to the gap. In this limit the integral in the defining equation for the normalized density can be calculated yielding

$$x_{qp}(T) = \sqrt{\frac{\pi k_B T}{2\Delta}}e^{-\frac{\Delta}{k_B T}} \tag{4.13}$$

The density and hence the relaxation rate is exponentially suppressed at temperatures below the gap and increases with higher temperatures due to thermally excited quasiparticles. Therefore we expect the rate to increase exponentially with the temperature and the qubit is well protected against relaxation due to quasiparticles at low temperatures if the superconductors are in equilibrium. Nevertheless experimental data show excess quasiparticles even at lower temperatures which can only be understood if there are additional non-equilibrium quasiparticles present at the junction. Possible sources of these quasiparticles can be the leakage from surroundings or quasiparticles excited due to radiation [9]. The presence of non-equilibrium quasiparticles leads to a saturation of the quasiparticle density at low temperatures and hence a finite relaxation rate even at low temperatures. We numerically solve the Boltzmann equation with quasiparticle injection at energy $E_{inj} > \Delta$ and quasiparticle relaxation due to

phonon scattering to obtain the normalized quasiparticle density in the presence of non-equilibrium quasiparticles [32]. In Addition we use the Boltzmann equation in relaxation time approximation with a constant injection rate η:

$$\eta = \frac{f(E) - f^{eq}(E)}{\tau(E)} \tag{4.14}$$

and the definition for x_{qp} to obtain

$$\begin{aligned} x_{qp} = \frac{1}{\Delta}\int_{\Delta}^{\infty} dE f(E)n(E) = x_{qp}^{eq}(T) + \frac{\eta}{\Delta}\int_{\Delta}^{\infty} dE n(E)\tau(E) \\ = x_{qp}^{eq}(T) + x_{qp}^{0}\,, \end{aligned} \tag{4.15}$$

where $x_{qp}^{eq}(T)$ is defined in equation 4.13. To obtain this form for x_{qp} we assumed that the relaxation time has no temperature dependence which seems rather crude but fits well with experimental data for qubit relaxation rates although the saturation in relaxation does not necessarily arise due to non-equilibrium quasiparticles. We plot all three quasiparticle densities, the thermal equilibrium density x_{qp}^{eq}, the numerically obtained one and the one emerging from relaxation time approximation in figure 4.1a. Both densities emerging from solving Boltzmann equation show saturation. This can be understood as a balance of quasiparticle generation and relaxation, e.g. due to phonon or electron scattering. At temperatures higher than the gap quasiparticle density is dominated by thermally excited quasiparticles.

Now we can plug everything together and compare our results with real life experiments. We want to apply our results to an experiment performed by Sun et al. [33]. In their experiment they measure T_1 times for transmon qubits build from different materials in dependence of temperature. The transmons, we chose two of them, consist either of pure aluminum ($\Delta = 180\mu eV$) superconductors or oxygen doped aluminum ($\Delta = 280\mu eV$). Due to the larger gap, thermal quasiparticles are suppressed in the doped aluminum up to higher temperatures as in the transmon made of pure aluminum leading to higher T_1 times at elevated temperatures. Qubit parameters are taken from [33] and summarized in table 4.1. We compare the temperature dependence of normalized quasiparticle densities x_{qp} for both qubits obtained with the different approximations presented in this section in figure 4.1a. For high temperatures all densities coincidence with the thermal equilibrium density while at temperatures below the respective gap the thermal density drastically decreases while both densities obtained from Boltzmann equation saturate at a certain offset (x_{qp}^0 for the temperature independent relaxation time approximation). Offset values are fit parameters obtained by fitting the qubit relaxation rate (or relaxation time T_1 to be precise) to the experimental data. In figure 4.1b we fit expression 4.11 for the qubit relaxation rate to experimental data obtained in the experiment [33]. Since in the experiment

Table 4.1: Qubit parameters

Qubit	Δ [GHz]	δE [GHz]	E_J [GHz]	E_C [GHz]
Al	273	4.25	9.1	0.248
oxygen doped Al	425	5.16	11.1	0.3

the $T_1 = \Gamma_1^{-1}$ has been measured, we fit $1/\Gamma$ to the experimental data. At high temperatures the rates for both qubits (red dots pure Al, blue doped Al) well follow the rates obtained with the thermal equilibrium density. At lower temperatures both rates saturate which can very well be fitted with the quasiparticle densities for temperature independent relaxation times. We find $x_{qp}^0 = 6 \cdot 10^{-6}$ and $3.7 \cdot 10^{-6}$ for the pure and doped aluminum respectively. The dependence of the quasiparticle induced relaxation rate on the gap can clearly be seen since the T_1 time for the pure aluminum qubit with smaller gap drops at lower temperatures than the qubit with larger gap.

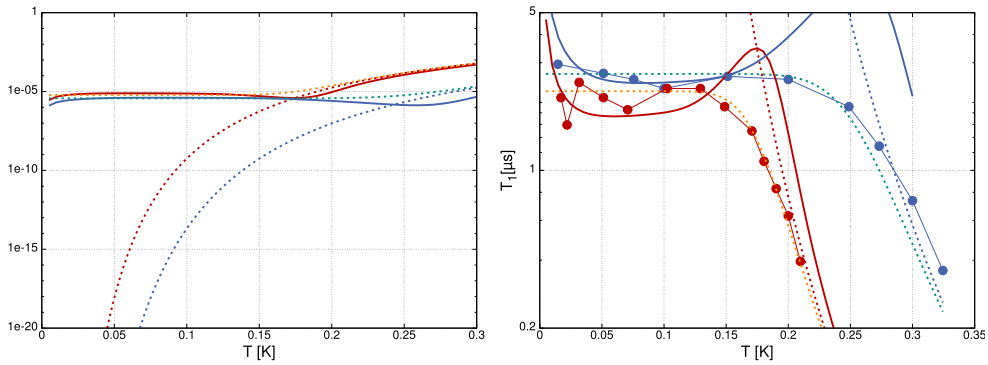

(a) normalized quasiparticle density x_{qp} **(b)** relaxation time $T_1 = \Gamma_1^{-1}$

Figure 4.1: (a) Normalized quasiparticle density. Dashed red (blue) lines represent thermal equilibrium for Al (doped Al). Solid lines are the corresponding densities from the Boltzmann equation with phonon scattering while orange (green) dashed lines emerge from equation 4.15 for Al (doped Al). (b) The corresponding relaxation times with experimental values taken from [33] (red and blue dots, lines are a guidance to the eye).

Finally we want to analyze the dependence of the qubit relaxation time on qubit parameters, namely E_J, E_C. In figures 4.2c and 4.2 we plot qubit relaxation times in dependence of the charging energy E_C and the Josephson energy E_J. The figures show that decreasing E_C as well as decreasing E_J has positive influence on the relaxation time. Of course one has to keep in mind that the transmon only works in regions with $E_J \gg E_C$. But since the increase in T_1 due to E_C is stronger than due to E_J one can easily achieve both goals, large ratio of E_J and E_C and good T_1 times. We find that the exponential factor in the relaxation rate has small influence in the parameter regime of

the qubit since on could expect exponentially suppressed relaxation times with smaller E_C but the opposite happens due to the appearance of E_C in the denominator of the square root leads to the strong increase of T_1 with decreasing charging energy.

4.1.2 Dephasing

As we showed earlier dephasing depends on different matrix elements than relaxation, namely s_{00}, s_{11}, c_{00} and c_{11}. If we take the transmon with its Hamiltonian symmetric in the phase drop across the junction the matrix elements involving the sine drop out and the dephasing rate depends only on the remaining cosine matrix elements. For this special case of a symmetric Hamiltonian the dephasing rate in golden rule/ first order approximation is well defined and due to the small matrix elements of for dephasing, see figure 4.3, orders of magnitude smaller than the relaxation rate. Therefore quasiparticle induced dephasing doesn't play an important role for transmon qubits. But since we can calculate the dephasing for a transmon qubit for all different approaches - golden rule, self-consistent and non-Markovian - we can use it to compare the different approaches with each other. The important matrix element for dephasing is

$$c^2 = \frac{1}{4}(c_{11} - c_{00})^2 = \frac{1}{4}\frac{E_C}{8E_J}e^{-\sqrt{\frac{E_C}{8E_J}}} \tag{4.16}$$

which is purely real. Hence the ratio between relaxation and dephasing matrix elements is

$$\frac{c^2}{s_{01}^2} = \frac{1}{4}\sqrt{\frac{E_C}{8E_J}}\,, \tag{4.17}$$

which fulfills $\frac{c^2}{s_{01}^2} \ll 1$ in the transmon regime. Hence we already know from equation 3.64 that dephasing will be way smaller than relaxation for the transmon. Nevertheless this statement holds only as long as the divergent part of the dephasing rate $\sim s^2$ vanishes. As soon as we have a qubit with non symmetric Hamiltonian the dephasing due to quasiparticle tunneling might become more important although matrix elements for dephasing are small.

The rates for a transmon obtained from the different approaches (gr - golden rule,

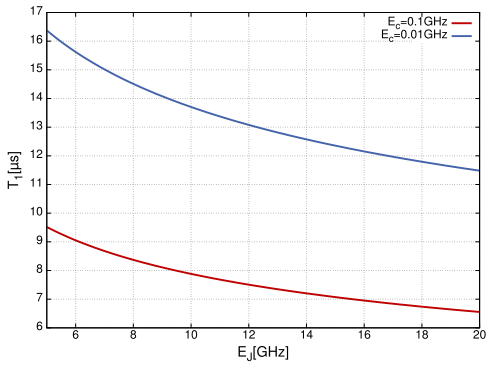

(a) T_1 time vs E_J

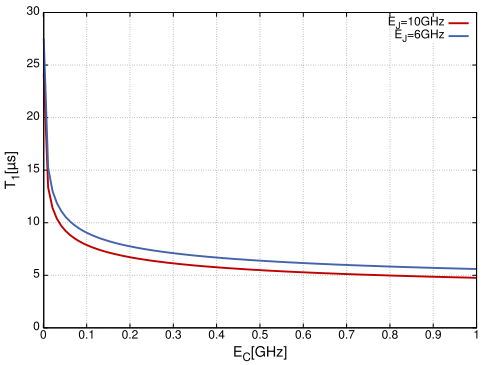

(b) T_1 time vs E_C

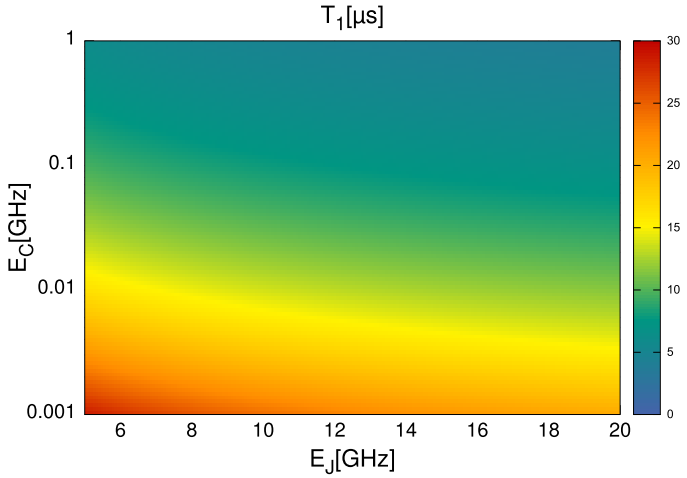

(c) T_1 for a transmon versus charging energy E_C and Josephson energy E_J. A small charging energy leads to a strong increase in the relaxation time. Larger E_J has the same but weaker effect.

Figure 4.2

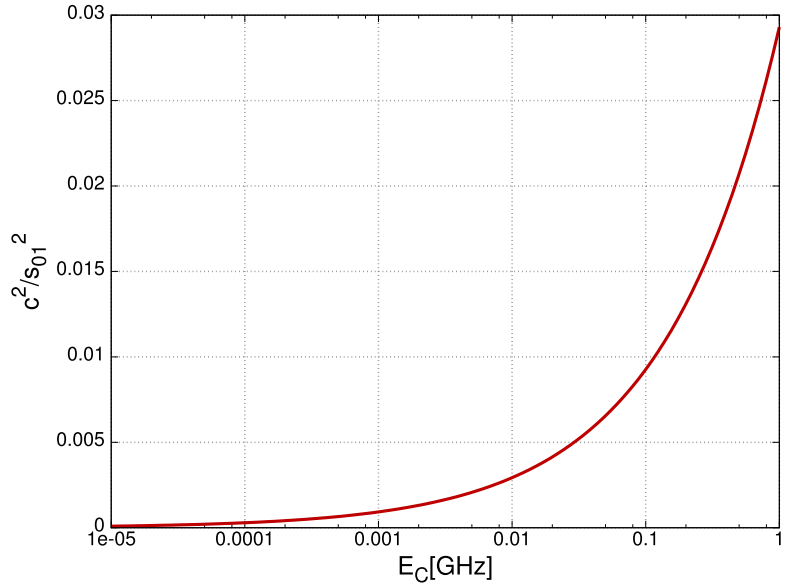

Figure 4.3: Transmon ratio c^2/s_{01}^2 between matrix elements for dephasing and relaxation, $E_J = 9.1GHz$

sc - self-consistent, nm - non Markovian) read

$$\Gamma_{2^*,gr} = 2\epsilon \int_\Delta^\infty dE(1-f(E))f(E) \tag{4.18}$$

$$\Gamma_{2^*,sc} = 2\epsilon \frac{1}{\pi} \int_\Delta^\infty \int_\Delta^\infty dEdE' \frac{EE'-\Delta^2}{EE'} n(E)n(E')f(E')(1-f(E)) \times \frac{\Gamma_{2^*,sc}}{(E-E')^2+\Gamma_{2^*,sc}^2} \tag{4.19}$$

$$J_{2^*,nm}(t-t_0) = 2\epsilon \frac{1}{\pi(1+E_J/\Delta)} \int_\Delta^\infty \int_\Delta^\infty dEdE' \frac{EE'-\Delta^2}{EE'} n(E)n(E')f(E')(1-f(E)) \times \frac{\sin^2(\frac{E-E'}{2}(t-t_0))}{(E-E')^2} \tag{4.20}$$

with $\epsilon = \frac{16E_Jc^2}{\pi\Delta} \ll 1$. We calculate the rates for a transmon with parameters as for the pure aluminum transmon from previous section numerically. For that reason we

rewrite the integrals in dimensionless variables, yielding

$$\Gamma_{2^*,gr} = 2\epsilon\Delta \int_1^\infty dx(1 - f(\Delta x))f(\Delta x) \tag{4.21}$$

$$\Gamma_{2^*,sc} = 2\epsilon\frac{1}{\pi}\int_1^\infty\int_1^\infty dxdy\frac{xy-1}{\sqrt{x^2-1}\sqrt{y^2-1}}f(\Delta x)(1-f(\Delta y)) \times\frac{\Gamma_{2^*,sc}}{(x-y)^2+\Gamma_{2^*,sc}^2/\Delta^2} \tag{4.22}$$

$$J_{2^*,nm}(t-t_0) = 2\epsilon\frac{1}{\pi(1+E_J/\Delta)}\int_1^\infty\int_1^\infty dxdy\frac{xy-1}{\sqrt{x^2-1}\sqrt{y^2-1}}f(\Delta x)(1-f(\Delta y)) \times\frac{\sin^2(\frac{x-y}{2}\Delta(t-t_0))}{(x-y)^2} \tag{4.23}$$

First we calculate the integrals for an equilibrium distribution function $f(\Delta x) = 1/(1+e^{x\Delta/k_BT})$ at a temperature of $300mK$ and compare the numerical results with the low energy approximations from chapter 3. The resulting exponents $J_{2^*,nm}(t)$, $\Gamma_{2^*,sc}\cdot t$ and $\Gamma_{2^*,gr}\cdot t$ are graphed in figure 4.4. In contrary to the predicted behavior in the

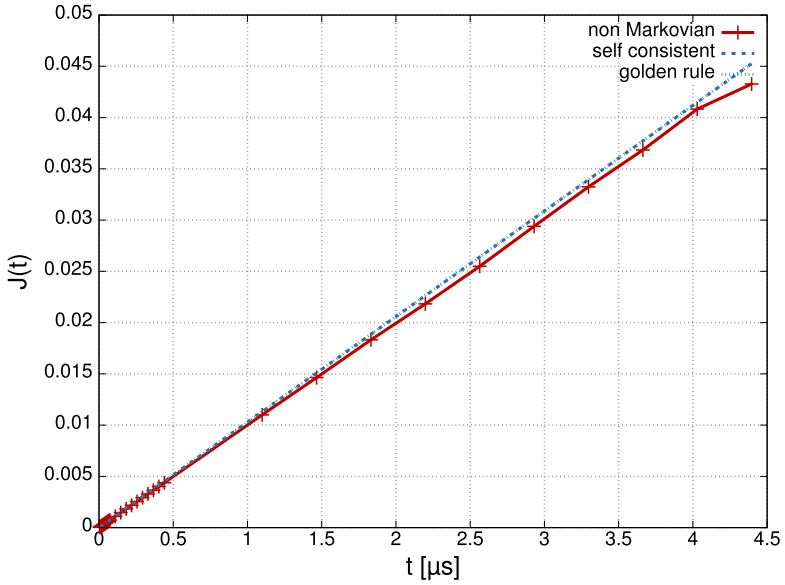

Figure 4.4: Time dependent exponents $J_{2^*,nm}(t)$ (solid red), $\Gamma_{2^*,sc}t$ (dashed blue) and $\Gamma_{2^*,gr}t$ (dotted green) for equilibrium distribution at $300mK$.

Table 4.2: Dephasing times T_{2^*} and relaxation time for the pure aluminum transmon

	T_1 $[\mu s]$	$T_{2^*,gr}$ $[\mu s]$	$T_{2^*,sc}$ $[\mu s]$	$T_{2^*,nm}$ $[\mu s]$
$T = 300mK$	0.02	97.07	97.18	96.17

low energy approximation the non Markovian rate is linear in time t (the derivation at larger t is likely to be a numerical error) and a fit with gnuplot yields $J_{2^*}(t) = 1.9046 \cdot 10^{-8} \cdot (\Delta t)$ which yields a dephasing rate $\Gamma_{2^*,nm} = 10399/s$. The self-consistent and golden rule rate are $10295.5/s$ and $10301.92/s$ respectively. Therefore all three rates are almost identical. Since we can define a non Markovian dephasing rate we can also calculate the corresponding pure dephasing times T_{2^*}. We sum up the resulting dephasing times in table 4.2. As mentioned in 3 the low energy approximation fails since the Fermi distribution is smeared out to much above the gap and we neglect to much of the integral in that approximation. In figure 4.5 we plot qubit dephasing times obtained for the pure aluminum qubit from [33] (we changed the gap to $\Delta = 150GHz$). The dephasing times emerging from the three different approaches yield the same result and reach from μs up to seconds. The dephasing times are large compared to relaxation times for the same qubit implying that pure dephasing is negligible compared to relaxation and the decoherence time $T_2 = (1/2T_1 + 1/T_{2^*})^{-1}$ is dominated solely by relaxation for a transmon. This comes not as surprise. We have seen at the beginning of this chapter, that the dephasing matrix element is small compared to the relaxation matrix element. For the transmon the dephasing rate doesn't diverge even in the golden rule approximation and hence we can expect it to be small. This might change for qubits with non-symmetric Hamiltonian which have a divergent part $s^2 \neq 0$. In this case dephasing can still play an important role and further analyzes are necessary to check this for different qubit types. The failure of the low energy approximation is obvious as it overestimates the dephasing time by orders of magnitude compared to all other rates.

4.2 Transmission Line Embedded Josephson Junction

In this section we will analyze a transmission line interrupted by a Josephson junction at an arbitrary position of the transmission line. Of course the junction gives rise to the Josephson effect and as we will show in this section one can use the whole system as a transmon qubit, provided a suitable set of system parameters has been chosen. Experimentally, the model consists of different superconducting layers: one layer, interrupted with a barrier, forming the transmission line, a feeding line at each end of the transmission line, capacitively coupled to the transmission line, and finally two layers surrounding the whole setup, referred to as 'ground plates' see figure 4.6a. The feeding lines can be used to read-out and control the transmission line (transmon

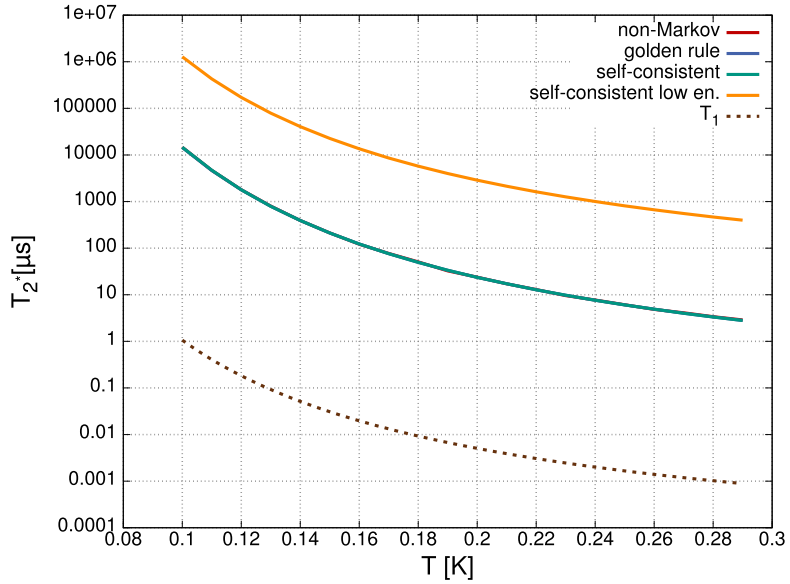

Figure 4.5: Pure dephasing times for the pure aluminum transmon with parameters taken from [33] as function of temperature. Superconducting gap is $150GHz$. The dephasing times obtained from the different approaches match perfectly with each other and have magnitudes much larger than the relaxation time T_1 (dashed line). Solely the low energy approximation for the self-consistent rate (solid orange) deviates from the rest predicting a much higher dephasing time.

qubit). In this section we closely follow [34] where this system has been analyzed in detail.

4.2.1 Basics

To derive a model for the system consisting of the transmission line, the Josephson junction and the capacities coupling the transmission line to the control lines, we divide the transmission line with total length $2d$ into small segments of length δx, where δx is much smaller than the transmission line length, $\delta x \ll 2d$ and much smaller than typical wave lengths in the system, $\delta x \ll \lambda$, where λ typically lies well within the microwave spectrum. Since typical transmission lines have a length in the range of $1cm$, the flux ϕ will vary significantly along the transmission line but with the prerequisite $\delta x \ll \lambda$, we can approximate the flux for each segment with a constant $\phi_{\alpha,i}$, where $\alpha = l/r$ is for segment i on the left/ right side of the junction, see figure 4.6b. Every segment is coupled with a capacity $C_i = c(x_i)\delta x$ to the ground plate and with inductance $L_i = l(x_i)\delta x$ to the next segment. Here, $c(x)$ and $l(x)$ are respectively the capacity and inductance per unit length, which we will assume to be constant and

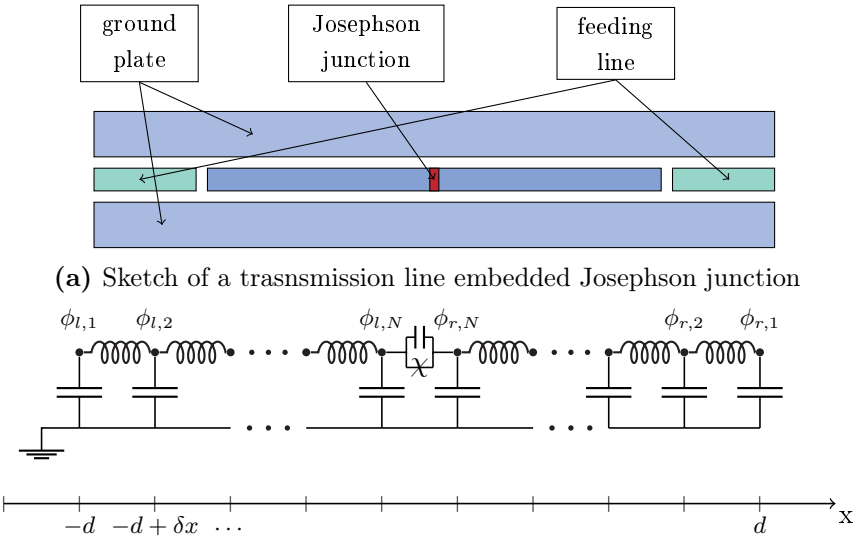

(a) Sketch of a trasnsmission line embedded Josephson junction

(b) Lumped element model

Figure 4.6: A transmission line with embedded Josephson junction

identical on both sides of the junction (a generalization is straightforward, see e.g. [34]). According to section 1.1.1, the Lagrangian for the transmission line, the junction and the coupling capacities can be written as sum of three parts [35], namely

$$\mathcal{L} = \mathcal{L}_{tl} + \mathcal{L}_{jj} + \mathcal{L}_{in} + \mathcal{L}_{out}\,. \tag{4.24}$$

Here, $\mathcal{L}_{tl}$ is the Lagrangian of the pure transmission line to the left and to the right of the junction. For each side, according to figure 4.6b, the Lagrangian is the sum of N inductively coupled LC circuits:

$$\mathcal{L}_{tl} = \sum_{\alpha=l,r}\left\{\sum_{i=1}^{N}\frac{C_i}{2}\dot{\phi}_{\alpha,i}^2 - \sum_{i=1}^{N-1}\frac{(\phi_{i+1}-\phi_i)^2}{2L_i}\right\}. \tag{4.25}$$

$\mathcal{L}_{jj}$ in eq. 4.24 describes the Josephson effect due to the junction,

$$\begin{aligned}\mathcal{L}_{jj} &= \frac{C_J}{2}\dot{\delta\phi}^2 + E_J\cos(\delta\phi/\Phi_0)\\ &= \frac{C_J}{2}\dot{\delta\phi}^2 - \frac{1}{2L_J}\delta\phi^2 - U_{nl}(\delta\phi)\,,\end{aligned} \tag{4.26}$$

$L_J^{-1} = E_J/\Phi_0^2$. We explicitly separated the Josephson term into its linear part $\sim\delta\phi^2$ which behaves just like a linear inductance with $L = L_J$ and its non-linear part

$$U_{nl}(\delta\phi) = -E_J\cos\left(\frac{\delta\phi}{\Phi_0}\right) - \frac{E_J}{2\Phi_0}\delta\phi^2\,. \tag{4.27}$$

Here $\delta\phi$ is the flux difference across the junction, $\delta\phi = \phi_{r,N} - \phi_{l,N}$. The idea behind this separation is to solve the linearized Lagrangian for its eigenmodes and than treat the non-linear part as a perturbation which can be expressed in terms of the eigenmodes of the linearized model. Therefore we will neglect the non-linear potential U_{nl} for the time being and introduce it later on as a perturbation, to analyze it's influence on system behavior. The last terms of the Lagrangian 4.24, $\mathcal{L}_{in/out}$ represent the in- and out ports of the transmission line,

$$\mathcal{L}_{in/out} = \frac{C_{in/out}}{2}(\dot{\phi}_{l/r,1} - V_{in/out})^2\,, \tag{4.28}$$

where $V_{in/out}$ are voltages applied respectively to the in and out port of the transmission line and allow for control/ read-out of transmission line states. In addition, they will provide a term similar to the gate charge n_g in the CPB/ transmon Hamiltonian 1.27 in the transmission line Hamiltonian. Now, before using Euler-Lagrange equations to derive the eofs for the transmission line system, we carry out the transition from the lumped element model to a continuum model. To do so, we express the capacity and inductance per segment with the capacity/ inductance per unit length multiplied by δx and let δx go to zero. This yields the continuum limit Lagrangian for the transmission line

$$\mathcal{L}_{tl}[\phi_l, \phi_r] = \int_{-d}^{x_j}\left[\frac{c(x)}{2}\dot{\phi}_l^2(x,t) - \frac{(\partial_x\phi_l)^2(x,t)}{2l(x)}\right]dx + \int_{x_j}^{d}\left[\frac{c(x)}{2}\dot{\phi}_r^2(x,t) - \frac{(\partial_x\phi)_r^2(x,t)}{2l(x)}\right]dx\,. \tag{4.29}$$

In latter expression, we introduced the flux fields $\phi_{l/r}$ for the left and right segment of the transmission line and the junction position x_j, which can but doesn't have to be in the middle ($x_j = 0$) of the transmission line. This freedom in changing the junction position yields another degree in freedom in system design that can be used to optimize system parameters according to the target application [34]. In the continuum limit, the Josephson and the in/ out parts of the Lagrangian read

$$\mathcal{L}_{jj} = \frac{C_J}{2}(\dot{\phi}_r(x_j) - \dot{\phi}_l(x_j))^2 - \frac{1}{2L_J}(\phi_r(x_j) - \phi_l(x_j))^2 - U_{nl}(\phi_r(x_j) - \phi_l(x_j)) \tag{4.30}$$

$$\mathcal{L}_{in/out} = \frac{C_{in/out}}{2}(\dot{\phi}_{l/r}(\mp d) - V_{in/out})^2\,, \tag{4.31}$$

yielding boundary conditions for the left and right flux field $\phi_{l/r}$ at the junction position and in/ out ports. In absence of the junction and the ports, the fields satisfy standard wave equations on either side of the junction:

$$\ddot{\phi}_{l/r}(x,t) - v^2\phi''_{l/r} = 0\,, \tag{4.32}$$

with the phase velocity $v = 1/\sqrt{lc}$. At the junction, the current arriving from the left side must be equal to the current through the junction and to the current leaving the

junction on the right side. Due to the current conservation, the fields have to obey the following boundary condition at the junction position x_j (see also 4.30):

$$\frac{1}{l}\phi_l'(x_j,t) = \frac{1}{l}\phi_r'(x_j,t) = C_J(\ddot{\phi}_r(x_j,t) - \ddot{\phi}_l(x_j,t)) + \frac{1}{L_J}(\phi_r(x_j,t) - \phi_l(x_j,t))\,. \quad (4.33)$$

If we took into account the full junction potential, the current would be given by the known Josephson relation $I \sim \sin(\delta\phi/\Phi_0)$ instead of above expression. Similar, the current at the left and right end of the transmission line must either vanish if we assume that no capacitative coupling exists or it must equal the current arising due to an AC voltage applied to the ports:

$$\ddot{\phi}_{l/r}(\mp d,t) \mp \frac{1}{C_{in/out}l}\phi_{r/l}'(\mp d,t) = \dot{V}_{in/out}(t)\,, \quad C_{in/out} \neq 0 \quad (4.34)$$

$$\phi_\alpha(\mp d,t) = 0\,, \quad \text{otherwise}\,. \quad (4.35)$$

The eof 4.32 together with boundary conditions 4.33 and respectively 4.34 or 4.35 respectively, completely describe the system dynamics. Due to the boundary conditions 4.33 and 4.34 there exists a set of eigenmodes for the system. We expand the solution for a general flux field in the basis provided by these eigenmodes

$$\phi_\alpha(x,t) = \sum_m g_{\alpha,m}(x) f_m(t) \quad (4.36)$$

where $f_m(t)$ obeys the differential equation $\ddot{f}_m(t) + \omega_m^2 f_m(t) = 0$ and $g_{\alpha,m}$ is the space dependent amplitude for mode m. The wave equation 4.32 imposes the governing differential equation for the spatial eigenmodes $g_{\alpha,m}(x)$

$$g_{\alpha,m}''(x) + k_m^2\, g_{\alpha,m}(x) = 0\,, \quad k_m = \frac{\omega_m}{v}\,, \quad (4.37)$$

which can be solved by the the ansatz [34]

$$g_m(x) = \begin{cases} \sin(k_m(x+d) - \varphi_l), & -d \le x \le x_j \\ A_m \sin(k_m(x-d) + \varphi_r), & x_j < x \le d \end{cases}\,. \quad (4.38)$$

In the ansatz, we only specify the relative amplitude A_M between the left and right side but do not provide an overall amplitude such that the modes are not normalized but will have a mode dependent mass, as we will see later. The phases φ_α are determined by the homogeneous part ($\dot{V}_\alpha = 0$) of boundary condition 4.34. They are given as

$$\tan(\varphi_\alpha) = \frac{c}{C_j}\frac{1}{k_m}\,. \quad (4.39)$$

Current conservation through the junction (see eq. 4.33) fixes the relative amplitude A_m between the left and right flux field to be

$$A_m = \frac{\cos(k_m(x_j + d) - \varphi_l)}{\cos(k_m(x_j - d) + \varphi_r)}, \tag{4.40}$$

while current current conservation between left side and junction yields a transcendental equation for the mode vector k_m similar to the transcendental equation fixing the eigenmodes for a pure transmission line:

$$\begin{aligned} k_m &= \frac{l}{L_j}(1 - \frac{k_m^2}{k_p^2}) \Big[\tan(k_m(x_j - d) + \varphi_r) - \tan(k_m(x_j + d) - \varphi_l)\Big] \\ &= \frac{l}{L_j}(1 - \frac{k_m^2}{k_p^2}) \left[\frac{\sin(-2k_m d + \varphi_r - \varphi_l)}{\cos(k_m(x_j + d) - \varphi_l)\cos(k_m(x_j - d) + \varphi_r)}\right]. \end{aligned} \tag{4.41}$$

In latter equation, we introduced the 'plasma wave vector' k_p of the Josephson junction, defined as $k_p = \omega_p/v$ with the junctions plasma frequency $\omega_p = 1/\sqrt{L_J C_J} = \sqrt{8E_{C,J}E_j}$. This transcendental equation can only be solved numerically, but a closer look reveals some information about the expected solution. The expression on the right hand side of eq. 4.41 is zero for $k_m = k_p$ suggesting that we can expect one eigenvalue to be close to the junctions plasma frequency. Assuming the influence of the phases φ_α to be small, we can expect solutions of the transcendental equation to be close to the "interesting" points of the right hand side, namely zeros and divergences. This yields two more sets of solutions, one given by the zeros of the sine in the nominator, yielding $k_m \approx \frac{m\pi}{2d}$. These solutions are nothing more than the eigenmodes of the bare transmission line with total length $2d$. These modes usually yield finite flux values at the junctions position and we can expect them to be influenced by the junction if the plasma frequency is almost in resonance with the given eigenmode. The second set of solutions provided by equation 4.41 has wave vectors close to the zeros of the cosine terms in the denominator yielding solutions of the form $k_m \approx \frac{2m+1}{2}\frac{\pi}{d \pm x_j}$, with $m \in \mathcal{N}$. These solutions recover the eigenmodes of transmission lines with length $d \pm x_j$ respectively. Since the corresponding waves always have nodes at the junction position (again, assuming the influence of φ to be relative small), the junctions influence on those modes should be small. Indeed, numerical solutions confirm the suspected spectrum for a system without coupling ($C_{in/out} = 0$), see figure 4.7. The eigenmodes of the linearized system and their first derivate with respect to x obey an orthogonality

Table 4.3: Parameters used for numerical calculations.

Parameter	Value
l	$5 \cdot 10^{-7} H/m$
c	$2 \cdot 10^{-10} F/m$
C_J	$2 \cdot 10^{-12} F/m$
d	$6 \cdot 10^{-3} m$

relation slightly different to the usual orthogonality relation for functions:

$$\begin{aligned}\langle g_m g_n \rangle = \int_{-d}^{d} c g_m(x) g_n(x) dx + C_{in} g_m(-d) g_n(-d) \\ + C_{out} g_m(d) g_n(d) + C_J \delta g_m \delta g_n = C_m \delta_{mn}\end{aligned} \tag{4.42}$$

$$\langle g'_m g'_n \rangle = \int_{-d}^{d} \frac{1}{l} g'_m(x) g'_n(x) + \frac{1}{L_J} \delta g_m \delta g_n = \omega_m^2 M_m \delta_{mn} \tag{4.43}$$

Here, δg_m is the phase drop $g_m(x_j^+) - g_m(x_j^-)$ at the junction and C_m is the effective mass of mode m which has the dimension of a capacity and we will refer to it either ass effective mass or total capacity of mode m. With these relations we are able to decouple the different eigenmodes in the linearized Lagrangian 4.24 and find

$$\mathcal{L}_{lin} = \sum_m \left\{ \frac{M_m}{2} \dot{f}_m^2 - \dot{f}_m q_{g,m} - \frac{\omega_m^2 M_m}{2} f_m^2 \right\} \tag{4.44}$$

where $q_{g,m} = (g_m(-d) C_{in} V_{in} + g_m(d) C_{out} V_{out})$ is a charge offset due to applied gate voltages similar to the CPB. From the Lagrangian we can easily derive the linearized Hamiltonian

$$\mathcal{H} = \sum_m \frac{1}{2C_m} (q_m + q_g)^2 + \frac{\omega_m^2 C_m}{2} f_m^2 \,. \tag{4.45}$$

It doesn't come as a surprise that this Hamiltonian is just a sum of decoupled harmonic oscillators with frequencies determined by the transcendental equation 4.41. The non linear part of the potential will lead to a finite coupling between different modes with a flux drop δg_m across the junction. Now, to take into account the non linear part, we expand the argument of the non linear potential in the basis provided by the eigenmodes,

$$U_{nl}(\{f_m\}) = -E_j \cos\left(\sum_m f_m \frac{\delta g_m}{\Phi_0} \right) - \frac{1}{2L_J} \left(\sum_m f_m \delta g_m \right)^2 , \tag{4.46}$$

and find the Hamiltonian of the full system, expanded in the basis of eigenmodes of the linearized model:

$$\mathcal{H} = \sum_m \left\{ \frac{1}{2C_m}(q_m + q_g)^2 + \frac{\omega_m^2 C_m}{2}\left(1 - \frac{1}{\omega_m^2 C_m L_J}\delta g_m^2\right) f_m^2 \right. \\ \left. -\frac{1}{2L_J}\sum_{n\neq m} f_m f_n \delta g_m \delta g_n \right\} - E_j \cos\left(\sum_n f_n \frac{\delta g_n}{\Phi_0}\right) . \tag{4.47}$$

The Hamiltonian reveals the influence of the non- linearity. On one hand, the eigenfrequencies experience a shift due to a phase bias $\sim \delta g_m^2$ across the junction. On the other hand, there is a coupling between different modes, where we have linear coupling $\sim (2L_J)^{-1}$ and a coupling due to to the cosine term. It becomes clear from this Hamiltonian, that coupling only exists between modes that provide a finite phase drop δg_m across the junction. Therefore it turns out to be useful to separate the modes that are not influenced by the junction from those suffering from the junctions influence. We rescale the variables for latter modes according to

$$\tilde{f}_m = f_m \delta g_m \tag{4.48}$$

$$\tilde{q}_m = \frac{q_m}{\delta g_m} \tag{4.49}$$

$$\tilde{C}_m = \frac{C_m}{\delta g_m^2} \tag{4.50}$$

and the Hamiltonian now reads

$$\mathcal{H} = H_0 + \sum_m^{\bullet} \left\{ \frac{1}{2\tilde{C}_m}(\tilde{q}_m + \tilde{q}_g)^2 + \frac{\omega_m^2 \tilde{C}_m}{2}\left(1 - \frac{1}{\omega_m^2 \tilde{C}_m L_J}\right) \tilde{f}_m^2 \right. \\ \left. -\frac{1}{2L_J}\sum_{n\neq m}^{\bullet} \tilde{f}_m \tilde{f}_n \right\} - E_j \cos\left(\sum_n^{\bullet} \frac{\tilde{f}_n}{\Phi_0}\right) , \tag{4.51}$$

where H_0 is the linear Hamiltonian of those modes that do not feel the junctions influence which we will not discuss further while $\sum_m^{\bullet}$ denotes the sum over all modes influenced by the junction. We quantize the Hamiltonian of the influenced modes by

introducing creation and annihilation operators of mode m:

$$a_m = \sqrt{\frac{\tilde{C}_m\omega_m}{2}}\left(\tilde{f}_m + i\frac{1}{\tilde{C}_m\omega_m}(\tilde{q}_m + \tilde{q}_g)\right) \tag{4.52}$$

$$a_m^\dagger = \sqrt{\frac{\tilde{C}_m\omega_m}{2}}\left(\tilde{f}_m - i\frac{1}{\tilde{C}_m\omega_m}(\tilde{q}_m + \tilde{q}_g)\right) \tag{4.53}$$

We express the Hamiltonian with the so defined ladder operators and expand the cosine up to the first non linear order ($\sim \tilde{f}^4$). To simplify the results we apply the RWA neglecting terms rotating faster than $|\omega_m - \omega_n|$. Within this approximation the Hamiltonian can be expressed with Kerr nonlinearities K_{mn} and beam splitter like interactions ζ_{lmn}, [34] (the work on the nonlinearities and so forth was done in this paper, we only sum up their results at this place):

$$\begin{aligned}\mathcal{H} = \omega'_m(a_m^\dagger a_m + \frac{1}{2}) - \sum_{m,n}\frac{1}{2}K_{mn}a_m^\dagger a_m a_m^\dagger a_m \\ - \sum_{m\neq n}\zeta_{mmn}(a_n^\dagger a_m + a_m^\dagger a_n) + \sum_{l\neq m\neq n}\zeta_{lmn}(a_l^\dagger a_l + \frac{1}{2})(a_m^\dagger a_n + a_n^\dagger a_m)\end{aligned} \tag{4.54}$$

The nonlinearity induces a frequency shift $\omega'_m = \omega_m - \sum_n K_{mn}$ while the nonlinearities are defined as

$$K_{mm} = \frac{1}{8L_j\Phi_0^2}\frac{1}{\tilde{C}_m\omega_m} = \frac{E_{C,m}}{L_J\omega_m} \tag{4.55}$$

$$K_{mn} = 2\sqrt{K_{mm}K_{nn}} \tag{4.56}$$

$$\zeta_{lmn} = (1-\delta_{lm}/2)(K_{ll}^2 K_{mm}K_{nn})^{1/4} \tag{4.57}$$

with the charging energy $E_{C,m} = e^2/2C_m$ of mode m. Here the self-Kerr coefficient K_{mm} proportional to the charging energy $E_{C,m}$ is the anharmonicity within each mode m itself, i.e. the deviation from an ideal harmonic oscillator with ladder operators $a_m^{(\dagger)}$ while the coefficients K_{mn} describe the inter-mode anharmonicity. As it becomes clear from the Kerr nonlinearity 4.55 the resonator can be made strongly nonlinear by either increasing the mode charging energies $E_{C,m}$ or decreasing the product $L_J\omega_m$ which means decreasing the Josephson energy or changing the junction position. Increasing charging energy can for example be achieved either with decreasing the transmission line length (since the total capacity of the line is the sum $C \sim 2lc + C_J + C_i + C_o$) or decreasing in/ out capacities or the Josephson junctions capacity, see figure 4.8b and 4.9b where we plot respectively transmission line capacity and detuning $\omega_{i+1} - 2\omega_i$ versus transmission line length. The detuning reaches very high values with short transmission lines. With those modifications the resonator described with the Hamiltonian 4.51

can be made so nonlinear that the transmission lines first fundamental mode lies far above Junctions plasma frequency. In this case the lowest mode of the whole system is more or less given by the plasma mode of the Josephson junction dressed by the transmission line ($\tilde{\omega}_p \approx \sqrt{8E_{C,1}E_J}$), see figure 4.8. Since in that case higher modes are comfortably far away from the first mode we can truncate the Hamiltonian to this one mode yielding the effective Hamiltonian of a transmon qubit in parallel with an additional inductance:

$$\mathcal{H} = 4E_{C,1}n^2 + \frac{E_L}{2}\varphi^2 - E_J\cos\varphi\,, \tag{4.58}$$

with the number of Cooper pairs $n = (q_1 + g_g)/2e$, the charging energy $E_{C,1}$ of the lowest system mode, the phase drop $\varphi = \tilde{f}_1/\Phi_0$ across the junction and the inductive energy$E_L = \frac{\omega_1^2}{8E_{C,1}} - E_J$. From this point we proceed in the same way as for the lumped element transmon and approximate the Hamiltonian 4.58 with an harmonic oscillator yielding

$$H = 4E_{C,1}n^2 + \frac{1}{2}\frac{\omega_1^2}{8E_{C,1}}\varphi^2 \tag{4.59}$$

with eigenfrequency ω_1. Similar to the lumped element transmon we calculate the anharmonicity of the transmission line embedded Josephson junction system in the transmon limit and find that the anharmonicity is scaled with a factor $\kappa = \sqrt{E_J/(E_L + E_J)} = \tilde{\omega}_p/\omega_1$:

$$\alpha = -\frac{E_J}{E_L + E_J}E_{C,1} = -\kappa^2 E_{C,1}\,, \tag{4.60}$$

with the plasma frequency $\tilde{\omega}_P = \sqrt{8E_{C,1}E_J}$ of the Josephson junction shunted with the total capacity of the transmission-line-junction system. Since we have $\nu \leq 1$ the anharmonicity of the in-line transmon is smaller than the anharmonicity of a corresponding lumped element transmon with total capacity $\tilde{C}_1$. But as we've seen in figure 4.8 the ratio $\omega_1/\tilde{\omega}_p$ quickly approaches one in parameter regimes where we can truncate the full Hamiltonian to the fist mode such that the anharmonicity of the in-line transmon (almost) equals the anharmonicity for a lumped element transmon with total capacity $\tilde{C}_1$. The relative anharmonicity of the in-line transmon reads

$$\alpha_{rel} = \frac{-1}{\frac{\omega_1}{\kappa^2 E_{C,1}} - 2} \approx \frac{-1}{\sqrt{8E_J/E_{C,1}} - 2} \tag{4.61}$$

which in the limit $\kappa \to 1$ equals the anharmonicity of the corresponding lumped element transmon.

4.2.2 Relaxation

We calculate relaxation rates for the in-line transmon in the harmonic oscillator approximation. The rate is similar to the rate for a corresponding transmon with plasma

frequency $\tilde{\omega}_p = \sqrt{8E_J E_{C,1}}$ scaled by the well known factor κ:

$$\Gamma_1 = \kappa \frac{2x_{qp}}{\pi} \sqrt{\frac{2+\delta_1}{\delta_1}} \tilde{\omega_p} e^{-E_{C,1}/\omega_1} \,, \tag{4.62}$$

with $\delta_1 = \frac{\omega_1}{\Delta}$. We compare the in-line transmon derived from the transmission line embedded Josephson junction with a lumped element transmon with identical Josephson junction and charging energy. The ratio between the relaxation times of both transmons is ($T_{1,tl}$ for the in-line and $T_{1,le}$ for the lumped element transmon)

$$\frac{T_{1,tl}}{T_{1,le}} = \sqrt{\frac{2+\delta_p}{2+\delta_1}\frac{\delta_1}{\delta_p}} \frac{\omega_1}{\omega_p} e^{E_{C,1}(\frac{1}{\omega_1} - \frac{1}{\omega_p})} \,, \tag{4.63}$$

while the ratio between the anharmonicity reads

$$\frac{\alpha_{1,tl}}{\alpha_{1,le}} = \frac{\omega_p^2}{\omega_1^2} \,. \tag{4.64}$$

In parameter regimes where the one-mode approximation for the transmission line system is correct, e.g. $\kappa \approx 1$, both ratios quickly approach one and lumped the in-line transmon develops to the lumped element transmon. Going away from regimes with $\kappa \approx 1$ the ratio of the relaxation times increases exponentially in the frequency difference ($\sim exp(E_{C,1}(-\frac{\omega_1 - \omega_p}{\omega_p \omega_1}))$ while the anharmonicity ratio decreases only quadratic in the ratio of the frequencies. Hence the increase in relaxation time succeeds the loss in anharmonicity and this parameter regime could be of interest for qubits protected against quasiparticle induced decoherence. On the other hand, when departing from the strong anharmonic regime, the one-mode approximation will fail at a certain point. The critical parameter proofing the validity of the one-mode approximation is the detuning $\Omega = \delta\omega_{12} - \delta\omega_{11} = \omega_2 - 2\omega_1$ between the transition from one photon in the first mode to two photons in the first mode, $\delta\omega_{11} = \omega_1$, and the transition of the photon from the first to the second mode, $\delta\omega_{12} = \omega_2 - \omega_1$. We calculate the different parameters numerically for the parameters defined in 4.3. Numerically obtained values for both ratios are graphed in figure 4.9b and detuning in figure 4.9b. As suspected both ratios quickly approach one with decreasing transmission line length while the detuning strongly increases. Here the one mode approximation is very good but at the same time nothing is gain due to in-line design. On the other hand the relaxation time ratio gets better for longer transmission lines (e.g. smaller nonlinearity) while the anharmonicity ratio gets worse. At a transmission line length about $0.01m$ the junctions plasma frequency approaches the first fundamental mode of the transmission line and the detuning has a deep drop as the first fundamental mode becomes the first mode of the entire system while the junctions plasma frequency emerges into the second mode of the system, see also figure 4.8a and 4.7a. In this region the one-mode approximation

isn't applicable anymore. Unfortunately the gain in relaxation time begins to exceed the loss in anharmonicity not until this region is reached. Therefore the transmission line length is no appropriate parameter to optimize the in-line transmon regarding quasiparticle tunneling.

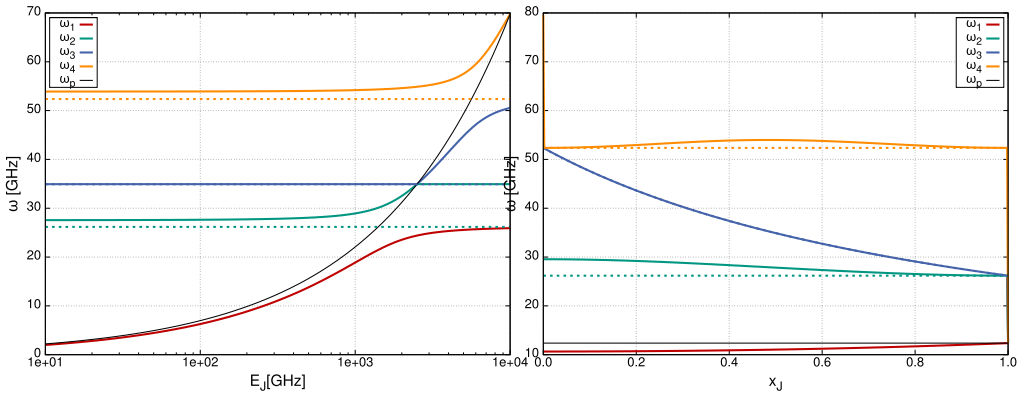

(a) Eigenfrequencies vs E_J] **(b)** Eigenfrequencies vs x_J

Figure 4.7: Lowest eingefrequencies of a transmission line with embedded Josephson junction, parameters as given in table 4.3 with $C_{in/out} = 0$. The junction position for (a) is $x_j = 0.5d$ (b) $C_{in/out} = 2 \cdot 10^{-12}F$. The numerically obtained values (solid lines) show the behavior described in the text. There exist modes close to eigenmodes of transmission liens with length $2d$ (dashed lines, modes showing anti-crossing behavior at the plasma frequency) while other modes are close to eigenmodes corresponding to a transmission line with length $(1 \pm x_j)d$ (dashed blue line for instance). While far away from the junctions plasma frequency ω_p the modes are almost unperturbed by the junction and follow the corresponding modes for the pure transmission line. In contrary when in resonance with the plasma frequency modes are strongly influenced and try to follow the plasma frequency. These modes show typical anti-crossing behavior. In (b) we see the influence of the additional design parameter x_J on the eigenmodes for the case of a huge junction with $E_J = 314GHz$ (we chose such a high value since the influence of x_J lessens with smaller E_j). For the modes close to eigenfrequencies of the pure transmission line (red and orange) the position increases the anharmonicity compared to the linear transmission line while for modes $\sim \frac{1}{1 \pm x_J}$ the influence is dramatic since they fade into the remaining modes at $x_J = 1/0$ (the dashed line for the analytical value perfectly matches the numerical obtained values).

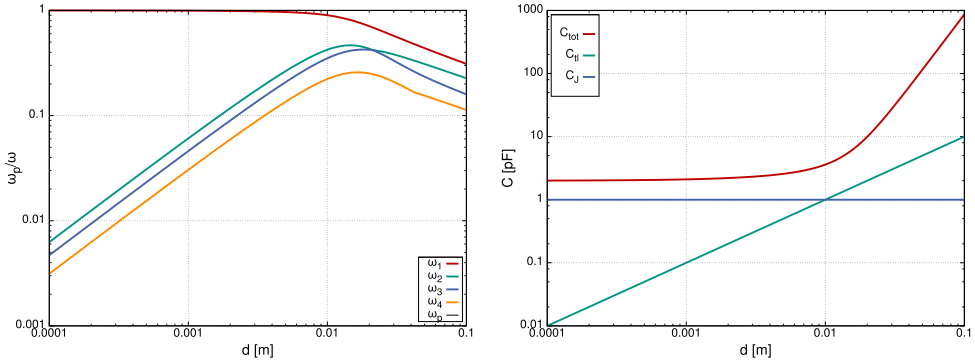

(a) $\frac{\omega_p}{\omega}$ **(b)** $\tilde{C}_1$

Figure 4.8: (a) First four eigenfrequencies of the system normalized to the dressed junction plasma frequency $\tilde{\omega}_p = \sqrt{E_{C,1}E_J}$ for varying transmission line length $L = 2d$ and junction position $x_J = 0.5$. With decreasing length the bare transmission line's eigenfrequencies lie far above the junctions plasma frequency while the ratio ω_p/ω_1 quickly approaches one and the the first eigenmode of the combined system is just the dressed plasma frequency of the junction. (b) Total capacity $\tilde{C}_1$ for the first eigenmode together with capacity C_{tl} of the bare transmission line and capacity C_J of the junction. For a short transmission line the total capacity approaches a finite value slightly larger than the junctions capacity which can be interpreted as an additional shunting capacity due to the transmission line.

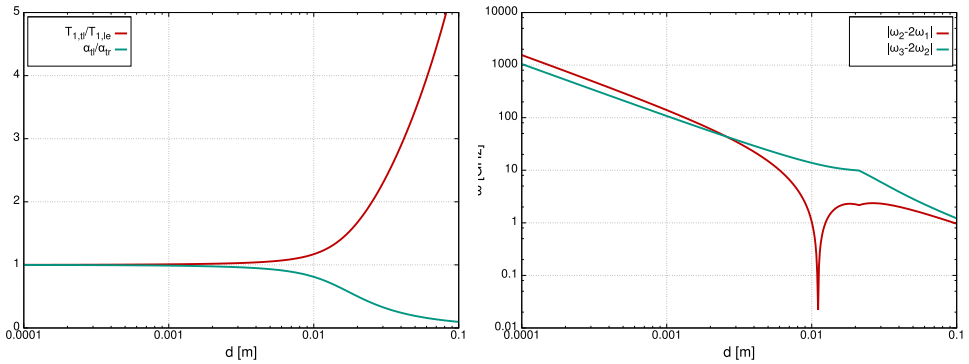

(a) $T_{1,tl}/T_{1,le}$ and α_{tl}/α_{le} **(b)** Detuning $\omega_{i+1} - 2\omega_i$

Figure 4.9: (a) Ratio between relaxation time $T_{1,tl}$ for the transmission line transmon and the lumped element transmon, $T_{1,le}$ as well as the ratio between the corresponding anharmonicity α_{tl} and α_{le}. (b) Detuning between different system eigenmodes. The system can be treated as an effective transmon only in regions with large detuning between mode ω_1 and mode ω_2 to avoid undesired transitions into the second mode of the system. In regions with large detuning (a) shows that both ratios are close to one and the difference between the lumped element and the in-line transmon are negligible.

Chapter 5
5 Conclusion

We studied qubit decoherence due to single quasiparticle tunneling through a Josephson junction where we put special focus on pure dephasing. From previous works it was known that pure dephasing rates diverge in a golden rule approximation. Hence we needed a systematic way to include higher orders of the tunneling Hamiltonian in our calculations to overcome that divergence. In chapter 2 we developed a real time diagrammatic technique to describe a quantum system coupled to several reservoirs and applied it to a qubit coupled to quasiparticle degrees of freedom via single particle tunneling. The diagrammatic technique enabled us to calculate qubit decoherence up to arbitrary orders in the tunneling Hamiltonian.

In chapter 3 we calculated different decoherence rates for a generic superconducting qubit. At first our technique developed in chapter 2 was used to calculate relaxation rates in second order of the coupling. Since this is the first non-vanishing contribution we obtained results that are equivalent with golden rule rates for qubit relaxation. We further simplified the expressions for the golden rule rates by applying the low energy approximation yielding a simple analytic form proportional to the total quasiparticle density n_{qp}. The approximation is valid for qubit energy splittings small compared to the superconducting gap but large compared to the width of the quasiparticle distribution function. In section 4.1.1 we compared our relaxation rates with experimental data for different transmon qubits. Three different models for the distribution function were used to calculate the quasi particle density: A equilibrium distribution which includes only thermally excited quasiparticles, a distribution obtained from a Boltzmann equation with constant injection rate and finally a distribution arising from a Boltzmann equation with electron-phonon relaxation and quasiparticle injection. The Fermi distribution underestimates relaxation rates at low temperatures due to exponentially suppressed particle number at low temperatures while experimental data show a saturation at low temperature. In contrast to the equilibrium distribution both distributions obtained with a Boltzmann equation inject excess quasiparticles into the system even

at low temperatures and generate a saturation of the quasiparticle density. With those distribution functions we achieved a good agreement between experiment and theory although we admit that saturation in the relaxation rate does not necessarily have to arise from excess quasiparticles.

We also applied the lowest order approximation to pure dephasing and noticed that for superconducting qubits with a Hamiltonian symmetric in the phase drop across the junction the golden rule rate converges. The resulting expression for the rate is proportional to the integral over the distribution function. But since not all qubit possess a symmetric Hamiltonian we re-normalized the second order approximation with a method similar to the self-consistent Born approximation. By substituting the free time evolution in the lowest order diagrams with the full time evolution we found a self-consistent equation for the pure dephasing rate due to quasiparticle tunneling which can be obtained from the golden rule rate by replacing the delta-function with a Lorentzian with the width given by the dephasing rate. Up to this point all rates were obtained within the Markov approximation of a memoryless bath. But since pure dephasing happens in the low frequency region of the bath spectrum this assumption does not necessarily hold and we approached qubit dephasing due to quasiparticle tunneling from a different side. With a re-definition of reservoir and tunnel Hamiltonian we were able to calculate a non-Markovian 'rate' for dephasing. The non-Markovian calculation yields a time dependence which is not per se a exponential decay with an exponent linear in time.

We compared the three different dephasing rates for a transmon in section 4.1.2. For these calculations we use a Fermi distribution for the quasiparticles. The non-Markovian rate, though non linear in t on first sight, reveals linear behavior for the transmon and all three rates, golden rule, self-consistent and non-Markovian turned out to be equivalent in the case of a transmon and equilibrium quasiparticles. The resulting dephasing time T_{2^*} is much larger than the relaxation time for the same qubit and hence is negligible in the decoherence time T_2. This statement holds for all qubits with a Hamiltonian symmetric in the phase across the junction since for all these qubits the part of dephasing rate giving rise to the initially mentioned divergence vanishes and the dephasing rate is dominated by the small qubit matrix element for dephasing. For a qubit that does not belong to this class the behavior might be different and dephasing due to quasiparticles might become comparable to relaxation.

Finally we studied a Josephson junction embedded in a transmission line in section 4.2. We introduced a linearized model for the system, solved for the eigenmodes of the linear model and expressed the non-linear part due to the junction in the basis of the eigenmodes. It turned out that one eigenfrequency of the system always is close to the junctions plasma frequency while the remaining modes are close to eigenmodes of the bare junction. We found a range of parameters where the first mode of the full system is given by the junctions plasma frequency dressed by the transmission line while at the same time the first fundamental mode of the bare transmission line

lies comfortable far above the lowest lying mode. In this strongly anharmonic case we recovered the Hamiltonian for a transmon with a additional inductance due to the transmission line. We analyzed this in-line transmon in regard of anharmonicity and robustness against quasiparticle induced relaxation. In the parameter range we analyzed the in-line transmon did not show an advantage compared to a standard lumped element transmon.

Bibliography

[1] G. Lindblad. On the generators of quantum dynamical semigroups. *Communications in Mathematical Physics*, 48(2):119–130, 1976. ISSN 0010-3616. doi: 10.1007/BF01608499. URL http://dx.doi.org/10.1007/BF01608499.
(Cited on page xi.)

[2] Jelena Stajic. The future of quantum information processing. *Science*, 339(6124): 1163, 2013. doi: 10.1126/science.339.6124.1163. URL http://www.sciencemag.org/content/339/6124/1163.short.
(Cited on pages xi and 2.)

[3] Peter W. Shor. Polynomial-time algorithms for prime factorization and discrete logarithms on a quantum computer. *SIAM J.Sci.Statist.Comput. 26 (1997) 1484*, January 1996. URL http://arxiv.org/abs/quant-ph/9508027v2.
(Cited on page xi.)

[4] David P. DiVincenzo. The physical implementation of quantum computation. *Fortschritte der Physik*, 48(9-11):771–783, 2000. ISSN 1521-3978. doi: 10.1002/1521-3978(200009)48:9/11<771::AID-PROP771>3.0.CO;2-E. URL http://dx.doi.org/10.1002/1521-3978(200009)48:9/11<771::AID-PROP771>3.0.CO;2-E.
(Cited on page xi.)

[5] Lieven M. K. Vandersypen, Matthias Steffen, Gregory Breyta, Costantino S. Yannoni, Mark H. Sherwood, and Isaac L. Chuang. Experimental realization of shor's quantum factoring algorithm using nuclear magnetic resonance. *Nature*, 414(6866):883–887, December 2001. ISSN 0028-0836. URL http://dx.doi.org/10.1038/414883a.
(Cited on page xi.)

[6] Juha Leppäkangas and Michael Marthaler. Fragility of flux qubits against quasiparticle tunneling. *Physical Review B*, 85(14):144503, April 2012. doi: 10.1103/PhysRevB.85.144503. URL http://dx.doi.org/10.1103/PhysRevB.85.144503.
(Cited on pages xiii and 65.)

[7] Roman Lutchyn, Leonid Glazman, and Anatoly Larkin. Quasiparticle decay rate of josephson charge qubit oscillations. *Physical Review B*, 72(1):014517, July

2005. doi: 10.1103/PhysRevB.72.014517. URL `http://dx.doi.org/10.1103/PhysRevB.72.014517`.
(Cited on page xiii.)

[8] M. Lenander, H. Wang, Radoslaw C. Bialczak, Erik Lucero, Matteo Mariantoni, M. Neeley, A. D. O'Connell, D. Sank, M. Weides, J. Wenner, T. Yamamoto, Y. Yin, J. Zhao, A. N. Cleland, and John M. Martinis. Measurement of energy decay in superconducting qubits from nonequilibrium quasiparticles. *Phys. Rev. B*, 84:024501, Jul 2011. doi: 10.1103/PhysRevB.84.024501. URL `http://link.aps.org/doi/10.1103/PhysRevB.84.024501`.
(Cited on page xiii.)

[9] R. Barends, J. Wenner, M. Lenander, Y. Chen, R. C. Bialczak, J. Kelly, E. Lucero, P. O'Malley, M. Mariantoni, D. Sank, H. Wang, T. C. White, Y. Yin, J. Zhao, A. N. Cleland, John M. Martinis, and J. J. A. Baselmans. Minimizing quasiparticle generation from stray infrared light in superconducting quantum circuits. *Applied Physics Letters*, 99(11):113507, 2011. doi: 10.1063/1.3638063. URL `http://link.aip.org/link/?APL/99/113507/1`.
(Cited on pages xiii and 71.)

[10] J. Wenner, Yi Yin, Erik Lucero, R. Barends, Yu Chen, B. Chiaro, J. Kelly, M. Lenander, Matteo Mariantoni, A. Megrant, and et al. Excitation of superconducting qubits from hot nonequilibrium quasiparticles. *Physical Review Letters*, 110(15):150502, April 2013. doi: 10.1103/PhysRevLett.110.150502. URL `http://dx.doi.org/10.1103/PhysRevLett.110.150502`.
(Cited on pages xiii and 53.)

[11] John M. Martinis, M. Ansmann, and J. Aumentado. Energy decay in josephson qubits from non-equilibrium quasiparticles. *ArXiv e-prints*, August 2009. URL `http://arxiv.org/abs/0904.2171v2`.
(Cited on pages xiii and 53.)

[12] R. Barends, S. van Vliet, J. Baselmans, S. Yates, J. Gao, and T. Klapwijk. Enhancement of quasiparticle recombination in ta and al superconductors by implantation of magnetic and nonmagnetic atoms. *Physical Review B*, 79(2):020509, January 2009. doi: 10.1103/PhysRevB.79.020509. URL `http://dx.doi.org/10.1103/PhysRevB.79.020509`.
(Cited on pages xiii and 53.)

[13] G. Catelani, S. E. Nigg, S. M. Girvin, R. J. Schoelkopf, and L. I. Glazman. Decoherence of superconducting qubits caused by quasiparticle tunneling. *Physical Review B*, 86(18):184514, November 2012. doi: 10.1103/PhysRevB.86.184514.

URL http://dx.doi.org/10.1103/PhysRevB.86.184514.
(Cited on pages xiii, 57, and 58.)

[14] Yuriy Makhlin, Gerd Schön, and Alexander Shnirman. Quantum-state engineering with josephson-junction devices. *Reviews of Modern Physics*, 73(2):357–400, May 2001. doi: 10.1103/RevModPhys.73.357. URL http://dx.doi.org/10.1103/RevModPhys.73.357.
(Cited on page 2.)

[15] John Clarke and Frank K. Wilhelm. Superconducting quantum bits. *Nature*, 453 (7198):1031–1042, June 2008. ISSN 0028-0836. URL http://dx.doi.org/10.1038/nature07128.
(Cited on page 2.)

[16] G. Schön and A. Shnirman. Festkörper qubits. *Physik Journal*, pages 51–56, November 2005.
(Cited on page 2.)

[17] M.H. Devoret. Quantum fluctuations in electrical circuits. In *Les Houches Session LXIII, Quantum Fluctuations*, pages 351–386, 1995.
(Cited on page 2.)

[18] B.D. Josephson. Possible new effects in superconductive tunnelling. *Physics Letters*, 1(7):251 – 253, 1962. ISSN 0031-9163. doi: http://dx.doi.org/10.1016/0031-9163(62)91369-0. URL http://www.sciencedirect.com/science/article/pii/0031916362913690.
(Cited on page 7.)

[19] P. W. Anderson and J. M. Rowell. Probable observation of the josephson superconducting tunneling effect. *Phys. Rev. Lett.*, 10:230–232, Mar 1963. doi: 10.1103/PhysRevLett.10.230. URL http://link.aps.org/doi/10.1103/PhysRevLett.10.230.
(Cited on page 7.)

[20] J. M. Martinis and K. Osborne. Superconducting qubits and the physics of josephson junctions. *eprint arXiv:cond-mat/0402415*, February 2004.
(Cited on pages 8 and 18.)

[21] M. H. Devoret, A. Wallraff, and J. M. Martinis. Superconducting qubits: A short review. *eprint arXiv:cond-mat/0411174*, November 2004.
(Cited on pages 9 and 12.)

[22] Jens Koch, Terri Yu, Jay Gambetta, A. Houck, D. Schuster, J. Majer, Alexandre Blais, M. Devoret, S. Girvin, and R. Schoelkopf. Charge-insensitive qubit design

derived from the cooper pair box. *Physical Review A*, 76(4):042319, October 2007. doi: 10.1103/PhysRevA.76.042319. URL http://dx.doi.org/10.1103/PhysRevA.76.042319.
(Cited on pages 9, 69, and 70.)

[23] Leon N. Cooper. Bound electron pairs in a degenerate fermi gas. *Phys. Rev.*, 104: 1189–1190, Nov 1956. doi: 10.1103/PhysRev.104.1189. URL http://link.aps.org/doi/10.1103/PhysRev.104.1189.
(Cited on page 13.)

[24] J. Bardeen, L. Cooper, and J. Schrieffer. Microscopic theory of superconductivity. *Physical Review*, 106(1):162–164, April 1957. doi: 10.1103/PhysRev.106.162. URL http://dx.doi.org/10.1103/PhysRev.106.162.
(Cited on page 13.)

[25] J. Bardeen, L. N. Cooper, and J. R. Schrieffer. Theory of superconductivity. *Physical Review*, 108(5):1175–1204, December 1957. doi: 10.1103/PhysRev.108.1175. URL http://dx.doi.org/10.1103/PhysRev.108.1175.
(Cited on page 13.)

[26] G. Lindblad. On the generators of quantum dynamical semigroups. *Communications in Mathematical Physics*, 48(2):119–130, 1976. ISSN 0010-3616. doi: 10.1007/BF01608499. URL http://dx.doi.org/10.1007/BF01608499.
(Cited on page 26.)

[27] Michael Marthaler. *Study of Quantum Electrodynamics in Superconducting Devices*. PhD thesis, Fakultät für Physik, Universität Karlsruhe, June 2009. URL http://www.tfp.uni-karlsruhe.de/Publications/Pub2009/PhDMarthaler.pdf.
(Cited on page 26.)

[28] A Palacios-Laloy, F Mallet, F Nguyen, F Ong, P Bertet, D Vion, and D Esteve. Spectral measurement of the thermal excitation of a superconducting qubit. *Physica Scripta*, T137:014015, December 2009. doi: 10.1088/0031-8949/2009/T137/014015. URL http://dx.doi.org/10.1088/0031-8949/2009/T137/014015.
(Cited on page 47.)

[29] D. Ristè, C. C. Bultink, M. J. Tiggelman, R. N. Schouten, K. W. Lehnert, and L. DiCarlo. Millisecond charge-parity fluctuations and induced decoherence in a superconducting transmon qubit. *Nature Communications*, 4:1913, May 2013. doi: 10.1038/ncomms2936. URL http://dx.doi.org/10.1038/ncomms2936.
(Cited on page 47.)

[30] Yuriy Makhlin, Gerd Schön, and Alexander Shnirman. Dissipation in josephson qubits. In R. Fazio, V.F. Gantmakher, and Y. Imry, editors, *New Directions in Mesoscopic Physics (Towards Nanoscience)*, volume 125 of *NATO Science Series*, pages 197–224. Springer Netherlands, 2003. ISBN 978-1-4020-1665-3. doi: 10.1007/978-94-007-1021-4_8. URL `http://dx.doi.org/10.1007/978-94-007-1021-4_8`.
(Cited on page 60.)

[31] G. Barone and G. Paterna. *Physics and Applications of the Josephson Effect*. 1982.
(Cited on page 65.)

[32] Andreas Heimes. Personal communication.
(Cited on page 72.)

[33] L. Sun, L. DiCarlo, M. D. Reed, G. Catelani, Lev S. Bishop, D. I. Schuster, B. R. Johnson, Ge A. Yang, L. Frunzio, L. Glazman, and et al. Measurements of quasiparticle tunneling dynamics in a band-gap-engineered transmon qubit. *Physical Review Letters*, 108(23):230509, June 2012. doi: 10.1103/PhysRevLett.108.230509. URL `http://dx.doi.org/10.1103/PhysRevLett.108.230509`.
(Cited on pages 72, 73, 78, and 79.)

[34] J. Bourassa, F. Beaudoin, Jay M. Gambetta, and A. Blais. Josephson-junction-embedded transmission-line resonators: From kerr medium to in-line transmon. *Physical Review A*, 86(1):013814, July 2012. doi: 10.1103/PhysRevA.86.013814. URL `http://dx.doi.org/10.1103/PhysRevA.86.013814`.
(Cited on pages 79, 80, 81, 82, and 86.)

[35] M Leib, F Deppe, A Marx, R Gross, and M J Hartmann. Networks of nonlinear superconducting transmission line resonators. *New Journal of Physics*, 14(7):075024, 2012. URL `http://stacks.iop.org/1367-2630/14/i=7/a=075024`.
(Cited on page 80.)

Danksagung

An dieser Stelle möchte ich mich bei verschiedenen Personen bedanken, die es mir ermöglicht haben, diese Arbeit zu vollenden.Michael Marthaler für ein Jahr Betreu-

ung, teilweise sogar mit tatkräftiger Unterstützung des wissenschaftlichen Nachwuchses. Meinen Arbeits- und Bürokollegen für die tolle ZeitEinen besonderen Dank an

Andreas 'The Ear' Heimes für viele interessante Gespräche und Hilfestellungen, wenn es mal wieder nicht weiterging.Und natürlich meine Eltern, die mir das alles ermöglicht

haben.

Danke!